WL-TR-92-3088

DYNAMICS AND ROBUST CONTROL OF SAMPLED DATA SYSTEMS FOR LARGE SPACE STRUCTURES

Volume 1: Optimal Linear Quadratic Regulator Digital Control of a Free-Free Orbiting Platform

Peter M. Bainum
Aprille Joy Ericsson
Xing Quangqian

Department of Mechanical Engineering
School of Engineering
Howard University
2300 Sixth Street, NW
Washington, D.C. 20059

November 1992

Final Report for the Period September 1989 - September 1991

FLIGHT DYNAMICS DIRECTORATE
Wright Laboratory
Air Force Materiel Command
Wright-Patterson Air Force Base, Ohio 45433-6553

NOTICE

When Government drawings, specifications, or other data are used for any purpose other than in connection with a definitely related Government procurement operation, the United States Government thereby incurs no responsibility or any obligation whatsoever. The fact that the Government may have formulated or in any way supplied the said drawings, specifications, or other data, is not to be regarded by implication, or otherwise as in any manner, as licensing the holder or any other person or corporation; or as conveying any rights or permission to manufacture, use, or sell any patented invention that may in any way be related thereto.

This report is releasable to the National Technical Information Service (NTIS). At NTIS, it will be available to the general public, including foreign nations.

This technical report has been reviewed and is approved for publication.

VIPPERLA B. VENKAYYA
Project Engineer
Design & Analysis Methods Section

NELSON D. WOLF, Technical Manager
Design & Analysis Methods Section
Analysis & Optimization Branch

DAVID K. MILLER, Lt Col, USAF
Chief, Analysis & Optimization Branch
Structures Division

"If your address has changed, if you wish to be removed from our mailing list, or if the addressee is no longer employed by your organization please notify WL/FIBRA, Wright-Patterson AFB OH 45433-6553 to help us maintain a current mailing list".

Copies of this report should not be returned unless return is required by security considerations, contractual obligations, or notice on a specific doucment.

REPORT DOCUMENTATION PAGE

Form Approved
OMB No. 0704-0188

1. AGENCY USE ONLY (Leave blank)	2. REPORT DATE	3. REPORT TYPE AND DATES COVERED
	Nov. 1992	Final Report: Sept. 1989 - Sept. 1991

4. TITLE AND SUBTITLE Dynamics and Robust Control of Sampled Data Systems for Large Space Structures - Volume 1: Optimal Linear Quadratic Regulator Digital Control of a Free-Free Orbiting Platform.

5. FUNDING NUMBERS
Prog Element: 62201F
Proj: 2401
Task: 02
WU: 93
Contr: F33615-89-C-3225

6. AUTHOR(S)
Peter M. Bainum
Aprille Joy Ericsson
Xing Quang-qian

7. PERFORMING ORGANIZATION NAME(S) AND ADDRESS(ES)
Howard University
Department of Mechanical Engineering
2300 6th. Street, N.W.
Washington, D.C. 20059

8. PERFORMING ORGANIZATION REPORT NUMBER

9. SPONSORING MONITORING AGENCY NAME(S) AND ADDRESS(ES)
V.B. Venkayya (513-255-7191)
Flight Dynamics Directorate (WL/FIBRA)
Wright Laboratory
Air Force Materiel Command
Wright-Patterson Air Force Base, Ohio 45433-6553

10. SPONSORING MONITORING AGENCY REPORT NUMBER
WL-TR-92-3088

11. SUPPLEMENTARY NOTES

12a. DISTRIBUTION AVAILABILITY STATEMENT
Approved for public release; distribution is unlimited

12b. DISTRIBUTION CODE

13. ABSTRACT (Maximum 200 words)

The objective of this research is to develop practical design procedures that can be used in conjunction with optimal digital controllers for future orbiting large space structural systems. In practice, the observational data used to verify the orientation and shape of large flexible systems will, in general, be collected on a sampled basis (discrete-time data system). The system is assumed to be completely observable and deterministic. Systems which will be designed to control both the overall orientation as well as the shape of some of the subsystems (such as antenna mesh form) must function in the discrete-time domain The aim of this research is to develop methods that can be used to design linear quadratic regulator (LQR) controllers for orbiting large flexible systems. The digital control of an orbiting thin square plate system is analyzed in this volume of the final report.

14. SUBJECT TERMS	15. NUMBER OF PAGES
Digital control; large space structures; observable and deterministic system; linear quadratic regulator technique.	177
	16. PRICE CODE

17. SECURITY CLASSIFICATION OF REPORT	18. SECURITY CLASSIFICATION OF THIS PAGE	19. SECURITY CLASSIFICATION OF ABSTRACT	20. LIMITATION OF ABSTRACT
Unclassified	Unclassified	Unclassified	UL

SUMMARY

A mathematical model to predict the dynamics of a flexible orbiting platform is developed. The platform is idealized as a large thin homogeneous square plate, made up of a continuous distribution of mass points in a plane. By considering the internal and external forces acting on each generic mass point, the equations for the rigid body motions, as well as the elastic degrees of freedom are developed. It assumed that the elastic motion is limited to small amplitudes and that the center of mass follows a circular orbit. For small amplitude flexural motion, the rigid body and elastic modes are modeled to the first order, thus linearizing the equations of motion for control law synthesis.

Under the assumption that the linear system is completely observable, the optimal control laws are developed for the case where the observational data is collected on a sampled basis, i.e., a discrete time data system.

The attitude and shape control can be achieved by placing point thrust actuators perpendicular to the main surface and the edge of the plate. Their effects on the motion are modeled to the first order. Controllability for the system is verified for two sets of actuator locations. An application of the linear quadratic regulator technique in a discrete-time domain yields the optimum control law feedback gains.

A comparison of the performance of the different sets of actuator locations results in the best choice of actuator positioning. Parametric studies are conducted to show the effect of varying the state penalty matrix, control penalty matrix, and the sampling period on the transient performance of the system.

PREFACE

This research symbolizes the work performed during the period September 1989 to August 1991 on WL Contract No. F33615-89C-3225. In concurrence with the completion of this research work a master's thesis was submitted to Howard University for the author, Aprille Joy Ericsson. The first volume of this contract report is based on this thesis. The second volume will be forth coming.

Special appreciation is extended to Dr. V.B. Venkayya, WL/FIBRA Principal Project Engineer who directed this effort and helped provide support. Also the author thanks Capt. Bruce Synder, and Mr. Duane Veley who were also project engineers for this research. They provided helpful comments and constructive criticism.

ACKNOWLEDGEMENTS

The author wishes to express her appreciation to her advisor, Dr. Peter Bainum and co-advisor, Prof. Xing Quangqian for their patience and guidance throughout this research. The author would also like to extend her appreciation to Dr. Robert Reiss for also serving on the thesis committee and his contribution of knowledge in the area of material mechanics.

The author is indebted to Dr. Johnetta Davis, the Graduate School of Arts and Sciences, Dr. James Johnson, Dr. Taft Broome, and NASA/HU Large Space Structures Institute for their encouragement and their initial financial support of this research. She would also like to thank Dr. Irving Jones for his technical advice in the area of structural dynamics and permission to have full use of the Computer Learning and Design Center facilities.

TABLE OF CONTENTS

LIST OF FIGURES

LIST OF TABLES

CHAPTER 1 - INTRODUCTION

The Solar System is our extended home. Through the use of space technology mankind's expansion outward from Earth to other worlds becomes feasible. The opportunity to stimulate individual initiative and free enterprise in space will surface through the development of new lands. Historically, when the power of the human intellect combines with abundant energy and rich material resources wealth is created. On the space frontier, new wealth can be created to benefit the entire human community by combining the energy of the Sun with materials left in space during the formulation of the Solar System. Mankind's reach will extend in science, industry, and the settlement of space with the correct combinations of: vigor and continuity, the elements of scientific research, technological advances, the discovery and development of new resources in space and the provisions of essential industries and systems . Government investments will generate, in value, financial returns many times its initial cost to the benefit of all.

To meet the challenge of the space frontier, the National Commission on Space, has proposed a step by step program to open the inner Solar System for: exploration, basic and applied research, resource development, and human operations.[1] With the advent of the Space Shuttle as a

reliable, affordable transportation system, the preliminary steps of acquiring a network of outposts in space can be undertaken. By following a systematic program -with minimum risk and funding- a progressive path for future space activities can occur. This program's structure will be in accordance with the inner Solar System's natural characteristics: energy, distance, signal delay time, and availability of resources.

An outpost actually consists of one or several large platforms with connecting appendages, i.e., solar panels, radar dishes, habitation modules, skylabs, etc.. There are major differences between satellites and large platforms; size and capabilities are two such differences. Large platforms are well defined by Cuneo and Williams, ' as a system which provides basic services to a changing set of activities. '[2] The capability of service -either updating payloads, or performing repairs, or replacing degraded modules, and/or replacing consumables- is probably the most common aspect attributed to platforms. The primary purposes of a platform is to provide shared support for multiple payloads and to provide connectivity. The reasons for platforms, are to obtain: (1) the economies of scale which come from shared support, and (2) the new and improved services which come from connectivity.[3]

The forementioned network of outposts would have several different locations: low earth orbit (LEO); geostationary orbit (GEO); lunar (surface and/or orbit); Mars and its asteroids. The outposts of interest for this thesis will be located in LEO, approximately 250 nautical miles from the Earth's surface. Low earth orbits are those just beyond the Earth's atmosphere and are the easiest to reach from Earth. This orbit provides both a close proximity orbital view of Earth and a window for observation of the Universe. Freedom from strong gravitational effects allows experiments that would be impossible to conduct on Earth's surface and facilitates the construction of large structures of low mass. Earth provides a sheltering skirt of magnetic field that protects us from solar flare radiation.

Planetary landings are costly in terms of propellant requirements for the descent, but the access of surface materials becomes an invaluable resource. When lifting payloads into orbit, away from Earth's gravitational field, we expend energy; to overcome the Earth's gravitational clutch, the rockets must attain speeds to lift a payload free of Earth's pull. We must expend the same amount of energy necessary to haul that same payload influenced by the full force of gravity to a height of 4,000 miles. To reach a nearer goal of low Earth orbit -where rockets and their payloads achieve a balancing act, while skimming above

Earth's atmosphere- we must spend about half as much energy, equivalent to climbing a mountain 2,000 miles high.[1] Once in 'free space', away from planets and moons, large distances can be traveled with modest expenditures of energy. Other gains from working in an orbiting space environment include: full-time solar energy, which is valuable for industrial processing, and microgravity, which is advantageous for building large space structures, i.e. Space Station, Variable-G Research Facility, and a Mars Interplanetary Vehicle. Once these facilities are built, research data can be accumulated to understand how the absence of gravity affects the fabrication of faultless materials, physical conditions, and motor skills of humans.[4,5]

Early industrial production in space may be best achieved by transporting raw materials from the Moon or Earth to orbiting platforms processing and fabricating finished products via robotic factories powered by continuous solar energy.

The first space enterprise to reach economic viability was satellite communications. Once in orbit, communication satellites lock into geostationary position and relay electronic messages, telephone calls, electronic mail, and television broadcasts. Future developments in space-based

communications and information systems will revolutionize our daily lives.[6] The proposed deployment of large plate or dish shape orbiting structures will make it possible to equip a car, boat, or airplane with a receiver and a display to pinpoint its exact location by satellite, allowing the provision of navigation, collision warning, fleet dispatch, emergency location, and two-way communication via satellite. These services can even be provided to small hand-held terminals powered by penlight batteries.

Currently in early stages of development is the remote sensing from low Earth orbiting satellites and/or structures. From the vantage point of space they enhance the ability to observe and produce specialized maps, that help facilitate the management of crops and mineral resources as well as forecast potentially destructive phenomena to forests, fisheries, pollution, and water resources.

One highly prospective space enterprise would -if technically and economically feasible- satisfy all of the ideal conditions. This enterprise would provide energy for Earth from orbiting structures that are intercepting solar energy.[7] The Soviet Union has already announced the goal of building the first solar powered satellite to supply energy to the Earth in the 1990's. To capture such a market would have substantial impact on the world's energy problem.[1]

Using the capabilities of the Space Shuttle many future missions have been proposed based on the deployment of large space structures. Most of the satellites that have been launched so far consist of a massive central rigid body, with characteristic dimensions of the order of a few meters, attached to light rigid or flexible appendages usually characterized by dimensions of not more than tens of meters. The natural frequencies associated with such flexible parts are normally several orders of magnitude greater than the orbital frequency and the frequencies of the rigid body rotational motions. In contrast to the existing satellite systems, the proposed large space systems' entire structure will be considered flexible. With the inherent size and necessary low weight to area ratio, the structural frequencies in the range of 1/100 Hertz or less may be considered in the study of the dynamics and control of these systems. For these proposed missions the operational considerations define stringent accuracy limits (possibly of the order of millimeters for a typical structure of 100 m) on the shape control of these structures.[8] To satisfy these requirements and others, both shape and orientation of the orbiting system should be controllable.

Often the optimal control laws for these future systems are developed under the assumption that the state vector is observed directly or the state information can be estimated

on a continuous basis. However, for future applications the observational data will often be collected on a sampled basis, creating a discrete time data system. The amount of information collected may be reduced and the format of data input may be acquired more conveniently. The case presented here will have the characteristics of being completely observable, with an addressed deterministic system (i.e., no random noise nor sensor system dynamics will be considered).

It will be useful, and timely, to study the control problem of large flexible orbiting space structural systems with discrete-time observational data. The development of modern control theory and technology provides a strong tool for solving this kind of engineering problem. The LQR regulator technique is that strong tool for synthesizing linear system control laws.[9] The LQR strategy can provide acceptable control performance once the state and control penalty matrices are properly selected. It does not restrict the number of actuators to be equal to the number of degrees of freedom in the system. Although, the LQR method has been developed and widely applied, it is still not an easy task to apply it to the engineering design for the control of large space structural systems, especially for systems with sampled data input.[10] There are still many specific problems to be investigated. This present work represents an initial effort toward understanding the dynamics and control

of large flexible structures in a discrete time domain.

By using a continuum approach, Santini, developed a mathematical formulation for predicting the motion of a general orbiting flexible body.[11] The formulation is based on the following assumptions that: (1) the elastic deformations are in the linear ranges so that the displacements can be expressed as superpositions of the various modes; and (2) the linear characteristic dimensions of the structure are assumed much smaller than the orbital radius. The effects of higher harmonics in the Earth's gravitational potential are included. However, the formulation has a slight drawback in that the elastic modal shapes are expressed only in terms of Cartesian components. This can be remedied by redeveloping the formulation using vector calculus, which was done by Kumar.[8]

For simple structures, such as beams, plates, and shallow spheres moving in orbit, modified versions of Santini's formulation allow the development of the translational, rotational, and elastic equations of motion. In order to gain insight into the dynamics and control of the proposed large flexible platform system, the formulation and manipulation of the equations of motion for a free-free beam were studied.[12,13] Of particular interest was a beam which, in equilibrium, has its longitudinal axis aligned

along the vertical.

Assuming the center of mass follows a circular orbit and the pitch and the flexural deformations occur only within the orbital plane, it is seen that the pitch motion does not influence the elastic motion. The pitch and the elastic modes are decoupled for large values of the square of the ratio of the structural modal frequency to the orbital angular rate.[14] For small values of this ratio the elastic motion is governed by Hill's 3-term equation which can be approximated by a Mathieu equation. Using a Mathieu stability chart, the resulting stability was considered.[15] For small amplitude flexural motion, the rigid body and elastic modes were modeled to the first order, thus linearizing the equations of motion.[16] A parametric analysis of the controllability of the motion of the beam about a nominal orientation for a discretized system was reviewed.[17] Extensions were made to the LQR formulation and were applied to a thin flexible orbiting plate in a continuous time domain.[18]

Many large space structures proposed for future space applications can be approximated by the basic structural forms of a thin plate or a shallow spherical shell. The ability to accurately determine the frequencies and mode shapes is essential for the analysis and control of large

orbiting structures. Methods of describing free and forced vibrations of plates and shallow shells have been formulated by many investigators. A comparative study of several different methods was reviewed for a free-free aluminum square plate.[19]

An extension to the comparative study of reference 19 has been accomplished in this thesis to include an additional technique, GTSTRUDL. GTSTRUDL is a structural design language that incorporates the finite element method. With this additional technique the final product is now a comparison of four different frequency and mode shape approximation methods.[20,21] The methods compared were:

1) the approximate frequencies and mode shapes of a rectangular plate derived from the formulation by Warburton [22,23];
2) the analytical results for a square plate were calculated from a method by Lemke[24];
3) the frequencies and mode shapes were computed using a finite element program, STRUDL, written at M.I.T. [25]; and
4) the frequencies and mode shapes were computed using GTSTRUDL, an update version of STRUDL written at Georgia Tech [20].

It was found that GTSTRUDL obtained better results than STRUDL and produced accurate results for specific finite

element (see Table 1) input grid point (node) locations, whereas, the Warburton and Lemke methods could only afford approximate answers.[21]

Attitude and shape control are assumed to be realized in this investigation by placing point thrust actuators in a symmetrical pattern perpendicular to the main surface and the edge of the plate.[26] The placement of the actuators on the main surface help control the shape deformation and the torque about two of the principal axes. The placement of the actuators along the edge of the plate help control the torque about the third axis. Care is taken not to place the actuators on the nodal lines associated with the first and second transverse vibrational modes or on the nodal circle associated with the third mode. The actuator's effects on the rigid body and elastic modes are modeled to the first order. In this thesis it will be assumed that the system is completely observable.

The control laws for the system will be applied to obtain the optimal control feedback gains based on an application of the linear regulator problem for a discrete time-data system.[9,10] The implementation of the LQR procedure will be accomplished by using the ORACLS software routines.[27]

A system may be completely controllable in a continuous-time domain, but once it is discretized, controllability is not guaranteed. To insure the controllability of a discretized data system, the sampling period theorem will be applied for proper selection of the sampling period. The theorem mandates the eigenvalues of the closed loop system must satisfy certain conditions.[10,17] For signal reconstruction, the sampling period, ΔT, should be as small as possible, but if the sampling time is too small, the computational requirements may exceed the computer speed.[17]

Under normal operation, the onboard computer estimation and control must finish processing all the input data during one sampling period, ΔT, i.e., the prediction of the state variables which will be used for the controller must be available before the beginning of the next sampling sequence. Thus the sampling period should be more than the minimum computational time required by the onboard microcomputer for the simulation of each step in the estimation and control process. The choice of sampling time is also constrained by the performance of the transient response, i.e., overshoot characteristics, settling time, steady state RMS errors.

CHAPTER 2 - DEVELOPMENT OF EQUATIONS OF MOTION FOR A FLEXIBLE ORBITING BODY

2.1 - Assumptions

In order to achieve a low mass to area ratio many of the proposed large space structures have been designed in the form of lattice or truss structures. A finite element analysis of such an orbiting structure would require a large computing capability and may be expensive. A preliminary insight into the dynamics of the system can be obtained by representing the structure as a large thin plate.

Early analyses of space structures were based on aluminum or aluminum alloys; since then advances in technology have made composite graphite a feasible alternative. When comparing the two materials, graphite displays two advantages, flexibility and weight, thus, making graphite the optimum material.

The material property values adopted for reinforced composite graphite here are: Young's Modulus, E, 40×10^6 lb/in^2; Poisson's ratio, υ,0.3; and density, ρ, 5.42×10^{-2} lb/in^3.[28] The structure's dimensions are assumed as; width and length, ℓ, 100 m; and thickness, t, 0.01 m. It assumed is to travel in a circular orbit at an altitude, h, 250 n.miles, while maintaining a constant angular velocity, ω_c,

0.0011162 rad/sec.

The equations of motion are derived using a Newton-Euler formulation. The principal assumptions made for this development are:

(1) the mass is idealized as a continuous distribution of mass points in a plane;

(2) the structural properties are uniformly distributed;

(3) the material of the body is isotropic;

(4) the structure is deformed in such a manner that it experiences only small strains (within the linear range);

(5) the elastic displacements are small as compared with the characteristic linear dimensions of the body;

(6) the elastic deformations in the plane of the plate are much smaller in comparison to the deformations normal to the plate;

(7) the first three elastic modes will be considered, since normally only a few elastic modes contribute significantly to the vibrational motion of the structure;

(8) the system is considered closed, i.e., no mass transfer across the system boundaries; and

(9) there are no geometrical constraints on the motion.

2.2 - Coordinate Frames

Initially the equations of motion are derived for a flexible orbiting body of arbitrary shape.[11] Figure (1) shows a flexible orbiting body with various symbols and coordinate frames.

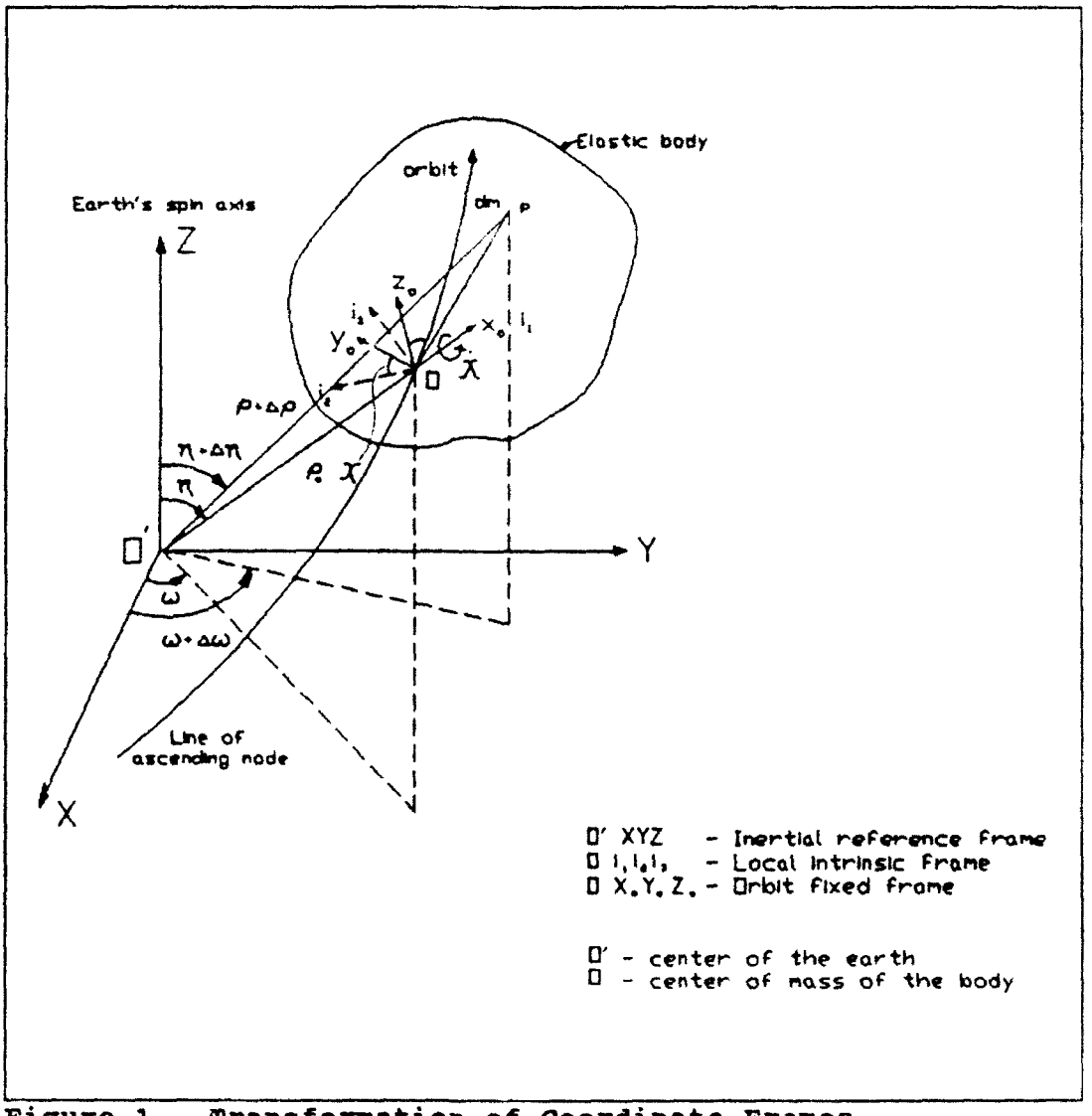

Figure 1. Transformation of Coordinate Frames

τ_o: O'XYZ is an earth centered inertial reference frame (τ_o) with O'Z along the earth's spin axis and O'X along the ascending node.

τ_1: $Oi_1i_2i_3$ is the local intrinsic frame (τ_1) centered at the center of mass of the body O, with Oi_1 along the local vertical and Oi_2 perpendicular to the plane ZO'O.

τ_2: $OX_oY_oZ_o$ is an orbit fixed reference frame (τ_2) centered at the center of mass of the body O, with OX_o along the local vertical and OY_o along the orbit normal opposite to the orbit angular momentum vector.

τ_3: Oxyz defines the principal axes of inertia (τ_3) of the body in the undeformed state (not shown in figure).

The above reference frames are related to each other as follows:

$$\begin{bmatrix} i_1 \\ i_2 \\ i_3 \end{bmatrix} = T_1 \begin{bmatrix} X \\ Y \\ Z \end{bmatrix} \quad (1a) \qquad ; \qquad \begin{bmatrix} X_o \\ Y_o \\ Z_o \end{bmatrix} = T_2 \begin{bmatrix} i_1 \\ i_2 \\ i_3 \end{bmatrix} \quad (2a) \qquad ; \qquad \begin{bmatrix} X \\ Y \\ Z \end{bmatrix} = T_3 \begin{bmatrix} X_o \\ Y_o \\ Z_o \end{bmatrix} \quad (3a)$$

$$\tau_1 = T_1 \tau_o \quad (1b) \qquad \tau_2 = T_2 \tau_1 \quad (2b) \qquad \tau_3 = T_3 \tau_2 \quad (3b)$$

The various transformation matrices are[11]:

$$T_1 = \begin{bmatrix} \sin\eta\cos\omega & \sin\eta\sin\omega & \cos\eta \\ \cos\eta\cos\omega & \cos\eta\sin\omega & -\sin\eta \\ -\sin\omega & \cos\omega & 0 \end{bmatrix} \tag{4}$$

T_1 represents the transformation from the inertial frame to the intrinsic frame.

$$T_2 = \begin{bmatrix} 1 & 0 & 0 \\ 0 & \cos\chi & \sin\chi \\ 0 & -\sin\chi & \cos\chi \end{bmatrix} \tag{5}$$

T_2 represents the transformation from the intrinsic frame to the orbit fixed frame.

$$T_3 = \begin{bmatrix} \cos\phi\cos\theta & (\sin\phi\cos\psi+\cos\phi\sin\theta\sin\psi) & (\sin\phi\sin\psi-\cos\phi\sin\theta\cos\psi) \\ -\sin\phi\cos\theta & (\cos\phi\cos\psi-\sin\phi\sin\theta\sin\psi) & (\cos\phi\sin\psi+\sin\phi\sin\theta\cos\psi) \\ \sin\theta & -\cos\theta\sin\psi & \cos\theta\cos\psi \end{bmatrix} \tag{6}$$

T_3 represents the transformation from the orbit frame to the body frame according to the sequence (1) ψ-yaw; (2) θ-pitch; and (3) ϕ-roll, respectively. The body angular velocity components ω_x, ω_y, and ω_z are then related to the Euler angular rates $\dot{\phi}$, $\dot{\theta}$, and $\dot{\psi}$ as follows:

$$\omega_x = \dot{\theta}\sin\phi + \dot{\psi}\cos\phi\cos\theta - \omega_c(\sin\phi\cos\psi + \cos\phi\sin\theta\sin\psi) \tag{7}$$

$$\omega_y = \dot{\theta}\cos\phi - \dot{\psi}\sin\phi\cos\theta - \omega_c(\cos\phi\cos\psi - \sin\phi\sin\theta\sin\psi) \tag{8}$$

$$\omega_z = \dot{\psi}\sin\theta + \dot{\phi} + \omega_c(\cos\theta\sin\psi) \tag{9}$$

2.3 - Gravitation

The gravitational potential at any point can be expressed in its most general form[8,11,12]:

$$V(\rho,\eta,\omega) = \left(\frac{\nu a^2}{\rho}\right) + \nu a \sum_{s=1}^{\infty} \left(\frac{a}{\rho}\right)^{s+1} \Omega_s(\eta,\omega) \qquad (10)$$

where,

$$\Omega(\eta,\omega) = \sum_{m=0}^{s} K_{sm}\left[P_s^{(m)}(\eta)\cos(m\omega + \phi_{sm})\right] \qquad (11)$$

$P_s^{(m)}(\eta)$ represents the $m^{\underline{th}}$ associated Legendre function of order s; K_{sm} and ϕ_{sm} are constants obtained through analysis of the satellite orbital motion; ρ represents the distance from the point to the center of the earth; and η and ω represent the colatitude and the longitude, respectively, of the point.

For the gravitational force per unit mass at the body's center of gravity, G:[8,11]

$$F_g(\rho,\eta,\omega) = \overline{\nabla} V\big|_G = \begin{bmatrix} \dfrac{\partial V}{\partial \rho} \\ \dfrac{\partial V}{\rho \partial \eta} \\ \dfrac{\partial V}{\rho \sin\eta \partial \omega} \end{bmatrix}_G \qquad (12)$$

For a point at a distance $\bar{r}$ from G, neglecting small quantities of the order $|\bar{r}|/\rho$, the gravity force, F(x):

$$F(x) = F_G + B^* (T_3 T_2)^{-1} \bar{r} \tag{13}$$

Substitution of the matrix operator, B^*, leads to:

$$F(x) = F_G + \frac{\nu a^2}{\rho^3}\left[B^{(o)} + \sum_{s=1}^{\infty} K_s \left(\frac{a}{\rho}\right)^s B^{(s)}\right](T_3 T_2)^{-1}\bar{r} \tag{14}$$

where $B^{(o)}$ and $B^{(s)}$ are defined as:

$$B^{(o)} = \begin{bmatrix} 2 & 0 & 0 \\ 0 & -1 & 0 \\ 0 & 0 & -1 \end{bmatrix} \tag{15}$$

$$B^{(s)} = \begin{bmatrix} (s+1)(s+2)\Omega_s & -(s+2)\Omega'_s & (s+2)\dfrac{\ddot{\Omega}_s}{\sin\eta} \\ -(s+2)\Omega'_s & [\Omega''_s - (s+1)\Omega_s] & \left(\dfrac{\ddot{\Omega}_s}{\sin\eta}\right)' \\ -(s+2)\dfrac{\ddot{\Omega}_s}{\sin\eta} & \left(\dfrac{\ddot{\Omega}_s}{\sin\eta}\right)' & \Omega'_s \cot\eta - \Omega_s\left(s+1+\dfrac{m^2}{\sin^2\eta}\right) \end{bmatrix} \tag{16}$$

where, $(\,)' = \dfrac{\partial(\,)}{\partial\eta}$; $\dot{(\,)} = \dfrac{\partial(\,)}{\partial\omega}$

Reprojecting on the body fixed axes results in;

$$f(x) = T_3 T_2 F_G + \frac{\nu a^2}{\rho^3}\left[M^{(o)} + \sum_{s=1}^{\infty} K_s \left(\frac{a}{\rho}\right)^s M^{(s)}\right]\bar{r} \tag{17}$$

$M^{(o)}$ and $M^{(s)}$ are symmetric matrices, where the following definition of $M^{()}$ represents both matrices,

$$M^{()} = T_3\, T_2\, B^{()}\, (T_3 T_2)^{-1} \tag{18}$$

$$M^{(o)} = \begin{bmatrix} 3\cos^2\phi\cos^2\theta - 1 & -3\sin\phi\cos\phi\cos^2\theta & 3\cos\phi\cos\theta\sin\theta \\ -3\sin\phi\cos\phi\cos^2\theta & 3\sin^2\phi\cos^2\theta - 1 & -3\sin\phi\cos\theta\sin\theta \\ 3\cos\phi\cos\theta\sin\theta & -3\sin\phi\cos\theta\sin\theta & 3\sin^2\theta - 1 \end{bmatrix} \tag{19}$$

$$(M^{(s)})_{ij} = \sum_{n=1}^{3}\sum_{k=1}^{3} t_{ni}\, t_{kj}\, B_{nk}^{(s)} \tag{20}$$

where t_{mn} is the (mn) element of the $(T_3T_2)^{-1}$ matrix and $B_{mn}^{(s)}$ is the (mn) element of the $B^{(s)}$ matrix.

2.4 - Equations of Motion

The position of a general point with respect to the body fixed frame, τ_3, is given by

$$\vec{r} = \vec{r}_o + \vec{q} \tag{21}$$

where $\vec{r}_o$ represents the position vector of the body with respect to O in the undeformed state, $\vec{r}_o = \xi_x\hat{i} + \xi_y\hat{j} + \xi_z\hat{k}$; and $\vec{q}$ represents the elastic displacement of the body. Therefore,

$$\vec{r} = \vec{q} \quad (22a) \quad \text{and} \quad \vec{r} = \vec{q} \quad (22b) \tag{22}$$

For small amplitude elastic displacements, $\vec{q}$ can be represented as a superposition of various modal contributions:

$$\vec{q} = \sum_{n=1}^{\infty} A_n(t)\,\vec{\Phi}^{(n)}(\vec{r}_o) \tag{23}$$

where $A_n(t)$ represents the n^{th} modal amplitude; and $\vec{\Phi}^{(n)}$ represents the eigenmodes of vibration, $\vec{\Phi}^{(n)}=\Phi^{(n)}_x\hat{i}+\Phi^{(n)}_y\hat{j}+\Phi^{(n)}_z\hat{k}$. Substitution of Eqn. (23) into Eqn. (17) forms:

$$f = T_3T_2F_G + \frac{\nu a^2}{\rho^3}\left[M^{(o)} + \sum_{s=1}^{\infty} K_s\left(\frac{a}{\rho}\right)^s M^{(s)}\right]\left[\vec{r}_o + \sum_{n=1}^{\infty} A_n\vec{\Phi}^{(n)}\right] \tag{24}$$

The linear operator $\mathcal{L}[\vec{q}]$ transforms small structural displacements, $\vec{q}$, to the structural forces acting on the generic point of the body. The mode shape, $\vec{\Phi}^{(n)}(\vec{r}_o)$, is associated with the natural frequency, ω_n and satisfies the following orthonormality condition:

$$\int \vec{\Phi}^{(n)}\cdot\vec{\Phi}^{(n)}\,dm = \delta_{mn}M_n \tag{25}$$

where M_n represents the generalized mass in the nth mode. The linear operator of $\mathcal{L}[\vec{\Phi}^{(n)}]$ becomes:

$$\mathcal{L}[\vec{\Phi}^{(n)}] = -\omega_n^2\vec{\Phi}^{(n)}\,dm \tag{26}$$

Therefore,

$$\mathcal{L}[\ddot{q}(\vec{r}_o, t)]\, dm = [-\sum_{n=1}^{\infty} \omega_n^2 A_n(t)\, \Phi^{(n)}]\, dm \qquad (27)$$

To satisfy the laws of conservation, an unconstrained body's elastic modes must be orthogonal to the rigid body modes:

Conservation of Linear Momentum-Translational Orthogonality

$$\int_{vol} \Phi^{(n)}\, dm = 0 \qquad (28)$$

Conservation of Angular Momentum-Rotational Orthogonality

$$\int_{vol} \vec{r}_o \times \Phi^{(n)}\, dm = \int_{vol} \begin{bmatrix} 0 & -r_3 & r_2 \\ r_3 & 0 & -r_1 \\ -r_2 & r_1 & 0 \end{bmatrix} \Phi^{(n)}(\vec{r}_o)\, dm = 0 \qquad (29)$$

If the body is constrained against translational and rotation of the undeformed center of mass, the corresponding modes are called "fixed modes". For fixed modes Eqns. (26) and (27) do not hold. For fixed modes the center of mass in the deformed state no longer coincides with the origin of the body frame. Only for the free modes does $\int \vec{r}\, dm = 0$.

2.4.1 - Equations of Rotational Motion

Returning to the development of the local equations, the equation of motion for an elemental mass, dm, whose instantaneous position vector from the center of mass of the body is $\vec{r}$, can be written as:

$$\mathcal{L}[\vec{q}] + \vec{f}\,dm + \vec{E} = \vec{a}\,dm \qquad (30)$$

where $\vec{f}$ represents the gravitational force per unit mass; $\vec{E}$ represents the external forces (other than gravitational).

Rewriting the inertial acceleration of a differential mass as a contribution of terms as seen by an observer in the rotating body fixed system of coordinates, r_3, it can be seen that the general force equation for a rotating body is:

$$\vec{a}\,dm = dm\,\vec{a}_{cm} + dm[\ddot{\vec{r}} + 2\vec{\omega}\times\dot{\vec{r}} + \dot{\vec{\omega}}\times\vec{r} + \vec{\omega}\times(\vec{\omega}\times\vec{r})] \qquad (31)$$

where $\vec{\omega}$ represents the angular velocity, $\vec{\omega}=\omega_x\hat{i}+\omega_y\hat{j}+\omega_z\hat{k}$.

The equations of rotational motion of the body are obtained by taking the moments of all the external, internal, and inertial forces acting on the body. After equating Eqns. (30) and (31) and taking the moments:

$$\int \vec{r}\times[\vec{a}_{cm} + \ddot{\vec{r}} + 2\vec{\omega}\times\dot{\vec{r}} + \dot{\vec{\omega}}\times\vec{r} + \vec{\omega}\times(\vec{\omega}\times\vec{r})]\,\rho\,dv = \int \vec{r}\times\left[\frac{\mathcal{L}[\vec{q}]}{dm} + \vec{f} + \frac{\vec{E}}{dm}\right] dm \qquad (32)$$

The various terms of Eqn. (32) can be evaluated using vector calculus. Assuming $|\vec{q}/\vec{r}| << 1$, only the 1st order terms in $\vec{q}$ are retained. Through the substitution of the values of the integrals into Eqn. (32) and rearrangement of terms, one can obtain the following form for the rotational equations of motion:[8,11,12]

$$\{I_x\dot{\omega}_x+(I_z-I_y)\omega_y\omega_z\}\hat{i}+\{I_y\dot{\omega}_y+(I_x-I_z)\omega_x\omega_z\}\hat{j}+$$
$$\{I_z\dot{\omega}_z+(I_y-I_x)\omega_x\omega_y\}\hat{k}+\sum_{n=1}^{\infty}\vec{Q}^{(n)}+\vec{C}+\sum_{n=1}^{\infty}\vec{D}^{(n)}=\vec{G}_I+\sum_{n=1}^{\infty}\vec{G}^{(n)} \qquad (33)$$

The terms, I_x, I_y, and I_z, are the principal moments of inertia of the body in the undeformed state. The terms, $\vec{Q}^{(n)}$, reflect the inertia torque associated with the elastic deformations, where $\vec{Q}^{(n)}=Q_x^{(n)}\hat{i}+Q_y^{(n)}\hat{j}+Q_z^{(n)}\hat{k}$

$$\sum_{n=1}^{\infty}\vec{Q}^{(n)}=\int_{vol}[\vec{r}_o\times\ddot{\vec{q}}+2\vec{r}_o\times(\omega\times\dot{\vec{q}})+\vec{r}_o\times(\dot{\omega}\times\vec{q})+\ddot{\vec{q}}\times(\dot{\omega}\times\vec{r}_o)+$$
$$-(\vec{r}_o\cdot\vec{\omega})(\vec{\omega}\times\vec{q})-(\vec{q}\cdot\vec{\omega})(\vec{\omega}\times\vec{r}_o)\,dm \qquad (34)$$

$$Q_x^{(n)}=\ddot{A}_n(H_{yz}^{(n)}-H_{zy}^{(n)})+2\dot{A}_n[(H_{yy}^{(n)}+H_{zz}^{(n)})\omega_x-H_{yx}^{(n)}\omega_y-H_{zx}^{(n)}\omega_z]+$$
$$A_n[2(H_{yy}^{(n)}+H_{zz}^{(n)})\dot{\omega}_x-(H_{xy}^{(n)}+H_{yx}^{(n)})\dot{\omega}_y-(H_{zx}^{(n)}+H_{xz}^{(n)})\dot{\omega}_z+$$
$$-2\omega_y\omega_z(H_{zz}^{(n)}-H_{yy}^{(n)})-\omega_x\omega_y(H_{xz}^{(n)}+H_{zx}^{(n)})+$$
$$\omega_x\omega_z(H_{xy}^{(n)}+H_{yx}^{(n)})+(\omega_z^2-\omega_y^2)(H_{yz}^{(n)}+H_{zy}^{(n)})] \qquad (35)$$

$Q_y^{(n)}$ and $Q_z^{(n)}$ are obtained by the cyclic permutation of x, y, z in the expression for $Q_x^{(n)}$, where $H_{\alpha\beta}^{(n)}$ is defined as,

$$H_{\alpha\beta}^{(n)}=\int_{vol}\xi_\alpha\Phi_\beta^{(n)}\,dm \qquad (36)$$

The term, $\vec{C}$, represents the external momentum caused by external forces other than gravitational, where $\vec{e}$ is the external force per unit mass.

$$\vec{C}=\int\vec{r}\times\vec{e}\,dm \qquad (37)$$

The terms, $\vec{D}^{(n)}$, account for the difference in position between the actual center of mass and the center of mass of the undeformed body. For the case of free modes $\vec{D}^{(n)}= 0$.

$$\sum_{n-1}^{\infty} \vec{D}^{(n)} = \int \vec{q}\, dm \times (\vec{a}_{cm} - \vec{f}_o) + \sum_{n-1}^{\infty} \omega_n^2 A_n \int \vec{r}_o \times \Phi^{(n)}\, dm \qquad (38)$$

The term, $\vec{G}_r$, corresponds to the gravitational torque on a rigid body,

$$\vec{G}_r = \int_{vol} \vec{r}_o \times M \vec{r}_o\, dm \qquad (39)$$

$$\vec{G}_r = (I_z - I_y) M_{23} \hat{i} + (I_x - I_z) M_{31} \hat{j} + (I_y - I_x) M_{12} \hat{k} \qquad (40)$$

where M_{ij} is an element of the M matrix which is defined as

$$M = M^{(o)} + \sum_{s-1}^{\infty} K_s (a/\rho)^s M^{(s)}$$

The terms, $\vec{G}^{(n)}$, correspond to the gravitational torque due to elastic deformations, where $\vec{G}^{(n)} = G_x^{(n)} \hat{i} + G_y^{(n)} \hat{j} + G_z^{(n)} \hat{k}$.

$$\sum_{n-1}^{\infty} \vec{G}^{(n)} = \int_{vol} [\vec{r}_o \times M \vec{q} + \vec{q} \times M \vec{r}_o]\, dm \qquad (41)$$

$$G_x^{(n)} = A_n [(M_{33} - M_{22}) (H_{yz}^{(n)} + H_{zy}^{(n)}) - M_{21} (H_{xz}^{(n)} + H_{zx}^{(n)}) + M_{31} (H_{xy}^{(n)} + H_{yx}^{(n)}) + 2M_{23} (H_{yy}^{(n)} - H_{zz}^{(n)})] \qquad (42)$$

$G_y^{(n)}$ and $G_z^{(n)}$ components are obtained by the cyclic permutation of x, y, z in the expression of $G_x^{(n)}$.

2.4.2 - Generic Mode Equation

The generic mode equation is obtained by taking the modal components of all internal, external, and inertial forces acting on the body[8,11,12].

$$\int_{vol} \vec{\Phi}^{(n)} \cdot [\vec{a}_{cm} + \ddot{\vec{r}} + 2\vec{\omega} \times \dot{\vec{r}} + \dot{\vec{\omega}} \times \vec{r} + \vec{\omega} \times (\vec{\omega} \times \vec{r})] \rho dv - \int_{vol} \vec{\Phi}^{(n)} \cdot [\mathcal{L}[\vec{q}]/\rho + \vec{f} + \vec{e}] \rho dv \tag{43}$$

The various terms appearing in Eqn. (43) can be expanded. With the substitution of the various integrals and rearrangement of the terms, the following generic modal equation results:

$$\ddot{A}_n + \omega_n^2 A_n + \varphi_n / M_n + \sum_{m=1}^{\bar{m}} \varphi_{mn} / M_n = [g_n + \sum_{m=1}^{\bar{m}} g_{mn} + E_n + D_n'] / M_n \tag{44}$$

$$\varphi^{(n)} = \int_{vol} [\vec{\Phi}^{(n)} \cdot \dot{\vec{\omega}} \times \vec{r}_o + \vec{\Phi}^{(n)} \cdot \vec{\omega} \times (\vec{\omega} \times \vec{r}_o)] dm \tag{45}$$

$$\begin{aligned} \varphi^{(n)} = {} & \dot{\omega}_x (H_{yz}^{(n)} - H_{zy}^{(n)}) + \dot{\omega}_y (H_{zx}^{(n)} - H_{xz}^{(n)}) + \dot{\omega}_z (H_{xy}^{(n)} - H_{yx}^{(n)}) + \\ & \omega_x \omega_y (H_{xy}^{(n)} + H_{yx}^{(n)}) + \omega_y \omega_z (H_{yz}^{(n)} + H_{zy}^{(n)}) + \omega_z \omega_x (H_{zx}^{(n)} + H_{xz}^{(n)}) + \\ & - \omega_x^2 (H_{yy}^{(n)} + H_{zz}^{(n)}) - \omega_y^2 (H_{xx}^{(n)} + H_{zz}^{(n)}) - \omega_z^2 (H_{xx}^{(n)} + H_{yy}^{(n)}) \end{aligned} \tag{46}$$

The term, $\varphi^{(n)}$, represents the influence (or force) of the rotational motion of the body on the $n^{\underline{th}}$ elastic mode due to inertia.

$$\sum_{m=1}^{\bar{m}} \varphi_{mn} = \int [2\vec{\Phi}^{(n)} \cdot \vec{\omega} \times \dot{\vec{q}} + \vec{\Phi}^{(n)} \cdot \dot{\vec{\omega}} \times \vec{q} + \vec{\Phi}^{(n)} \cdot \vec{\omega} \times (\vec{\omega} \times \vec{q})] \rho dv \tag{47}$$

$$\varphi_{mn} = 2\dot{A}_m[\omega_x(L_{yz}^{(mn)} - L_{zy}^{(mn)}) + \omega_y(L_{zx}^{(mn)} - L_{xz}^{(mn)}) + \omega_z(L_{xy}^{(mn)} - L_{yx}^{(n)})] +$$
$$A_m[\dot{\omega}_x(L_{yz}^{(mn)} - L_{zy}^{(mn)}) + \dot{\omega}_y(L_{zx}^{(mn)} - L_{xz}^{(mn)}) + \dot{\omega}_z(L_{xy}^{(mn)} - L_{yx}^{(mn)}) +$$
$$\omega_x\omega_y(L_{xy}^{(mn)} + L_{yx}^{(mn)}) + \omega_y\omega_z(L_{yz}^{(mn)} + L_{zy}^{(mn)}) + \omega_z\omega_x(L_{zx}^{(mn)} + L_{xz}^{(mn)}) +$$
$$-\omega_x^2(L_{yy}^{(mn)} + L_{zz}^{(mn)}) - \omega_y^2(L_{zz}^{(mn)} + L_{xx}^{(mn)}) - \omega_z^2(L_{xx}^{(mn)} + L_{yy}^{(mn)})] \quad (48)$$

The terms, φ_{mn}, represent the influence of the other elastic modes on the $n^{\underline{th}}$ elastic mode due to inertia, where $L_{\alpha\beta}^{(mn)}$ is defined as,

$$L_{\alpha\beta}^{(mn)} = \int_{vol} \Phi_\alpha^{(m)} \cdot \Phi_\beta^{(n)} \, dm \quad (49)$$

The term, g_n, is the gravitational force acting on the $n^{\underline{th}}$ mode due to the rigid body motion.

$$g_n = \int_{vol} \Phi^{(n)} \cdot M\bar{r}_o \rho \, dv - \sum_\alpha \sum_\beta H_{\alpha\beta}^{(n)} M_{\alpha\beta} \quad (50)$$

The terms, g_{mn}, represent the gravitational force acting on the $n^{\underline{th}}$ mode due to the elastic motion on the $m^{\underline{th}}$ mode.

$$\sum_{m=1}^{\infty} g_{mn} = \int_{vol} \Phi^{(n)} M\bar{q} \, dm - A_m \sum_\alpha \sum_\beta L_{\alpha\beta}^{(mn)} M_{\alpha\beta} \quad (51)$$

The term, E_n, is the external force component acting on the $n^{\underline{th}}$ mode.

$$E_n = \int_{vol} \Phi^{(n)} \cdot \bar{e} \, dm \quad (52)$$

The term, D'_n, represents the term corresponding to the displacement of the center of mass due to the elastic motion. For unconstrained motion D'_n vanishes.

$$D_i' = \int_{vol} \Phi^{(n)} \, dm \cdot (\vec{a}_{cm} - \vec{f}_g) \qquad (53)$$

2.4.3 - Equations of Translational Motion

The equations of translational motion of the body in orbit are obtained by integrating the summation of Eqns. (30) and (31).

$$\int_{vol} [\vec{a}_{cm} + \ddot{\vec{r}} + 2\vec{\omega} \times \dot{\vec{r}} + \dot{\vec{\omega}} \times \vec{r} + \vec{\omega} \times (\vec{\omega} \times \vec{r})] \rho dv = \int_{vol} [\mathcal{L}[\vec{q}]/\rho + \vec{f} + \vec{e}] \rho dv \qquad (54)$$

Noting $\int \vec{r} \rho dv = 0$, one can obtain the translational equation of motion.

$$\vec{a}_{cm} + \vec{f}_g + \vec{D} = \vec{E}/m \qquad (55)$$

where $\vec{a}_{cm}$ is the inertial acceleration of the center of mass; $\vec{f}_g$ is the intensity of the gravitational force at the center of mass of the body (force/mass); m is the mass of the body; $\vec{E}$ is the resultant of the external forces; and

$$\vec{D} = 1/m \int_{vol} [\ddot{\vec{q}} + 2\vec{\omega} \times \dot{\vec{q}} + \dot{\vec{\omega}} \times \vec{q} + \vec{\omega} \times (\vec{\omega} \times \vec{q}) - \mathcal{L}[\vec{q}]/\rho - M\vec{q}] \rho dv \qquad (56)$$

For the free-free mode shapes -unconstrained mode shapes- $\vec{D}=0$.

Because of the size of the structure considered in this work, (i.e., (100 m)) one may neglect the effect of elastic motion on the orbital motion of the center of mass. In this thesis, the equations of orbital motion are not considered

for further analysis. It is assumed that the orbital position of the center of mass can be readily computed using techniques of orbital mechanics.

In summary, the motion of an arbitrary flexible body in orbit is described by Eqns. (33), (44), and (54). Consideration of the effects of gravity gradient -including higher order harmonics- has been included in the derivation of these equations. Equations (33) and (54) are vector equations which describe the dynamics of the rigid rotational and rigid translational motions, respectively. Equation (44) is a scalar equation which describes the elastic motion of the body in its n^{th} elastic mode. With the calculation of the natural frequency and modal shape functions, the equations of motion of a particular system can be derived.

2.5 - Motion of a Thin Flexible Plate in Orbit

One class of structures, which has been proposed for use in many future space applications, has the basic form of a thin flat plate. Included among the proposed applications are: solar energy collection, communications, and scientific data based orbiting platforms. A brief development of a mathematical model for the attitude motion and elastic motion for a large, yet thin, flexible, flat plate in orbit is presented in this section. The equations presented here for the plate's motion are the result of simplification of the general set of equations that describe the motion of an arbitrary flexible body in orbit (previously presented in Section 2.4).

By taking into consideration assumption (9), one can further simplify the development of the equations of rotational motion. Assumption (9) leads to $H^{(n)}_{\alpha\beta}=H^{(n)}_{\beta\alpha}$, where for all α and β, $H^{(n)}_{\alpha\beta}=0$, similarly, $\bar{D}_n=D'_{(n)}=0$. With a rearrangement of terms and the separation of the rotational equation of motion into its vector components, Eqn. (33) can be developed to yield the following set of rotational equations of motion for the elastic plate in orbit.[8,13]

$$
\begin{aligned}
I_x\dot{\omega}_x-(I_y-I_z)\,\omega_y\omega_z &= -C_x+G_{rx} && (57a)\\
I_y\dot{\omega}_y-(I_z-I_x)\,\omega_z\omega_x &= -C_y+G_{ry} && (57b)\\
I_z\dot{\omega}_z-(I_x-I_y)\,\omega_x\omega_y &= -C_z+G_{rz} && (57c)
\end{aligned}
\qquad (57)
$$

The general equation for elastic motion is listed below.

$$\ddot{A}_n + \omega_n^2 A_n + \varphi_{n}/M_n + \sum_{m=1}^{\infty} \varphi_{mn}/M_n = [Q_n + \sum_{m=1}^{\infty} g_{mn} + E_n + D_n'] / M_n \qquad (58)$$

This paper will present three different nominal orientations of the platform in orbit; attitude and shape control will be achieved for each. They are:

Case (1) the platform following the local horizontal with its larger surface normal to the local vertical, see Figure 2.1;

Case (2) the platform following the local vertical with its larger surface perpendicular to the plane of the orbit, see Figure 2.2; and

Case (3) the platform following the local vertical with its larger surface perpendicular to the orbit normal, see Figure 2.3.

It can be shown that for gravitational stability the plate's axis of minimum moment of inertia should be nominally oriented along the local vertical. However, in many applications it is required that the major surface of the plate be pointed towards the earth. Therefore, fo· the plate orientation of Case (1) a complete development of the equations will be presented. For the two other orientations, Case (2) and Case (3), the final form of the equations of motion will be shown.

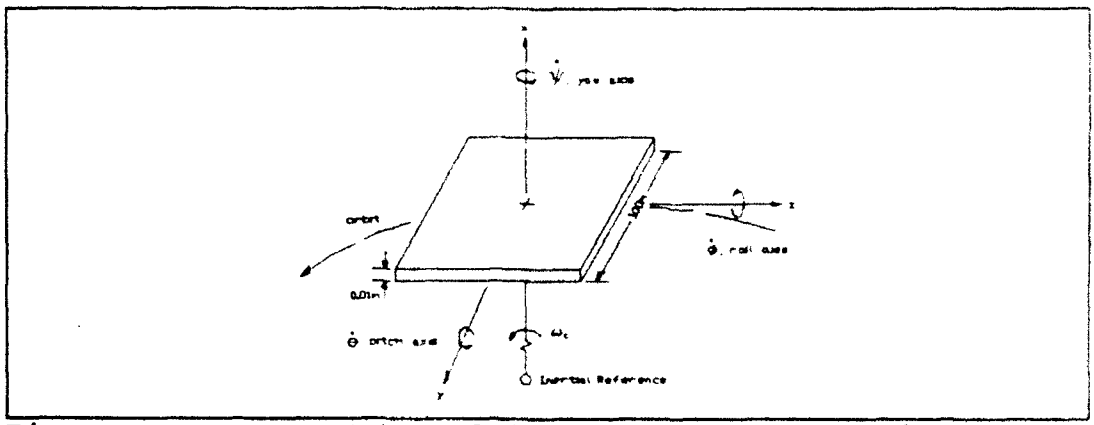

Figure 2.1. Case (1) - Platform along local horizontal

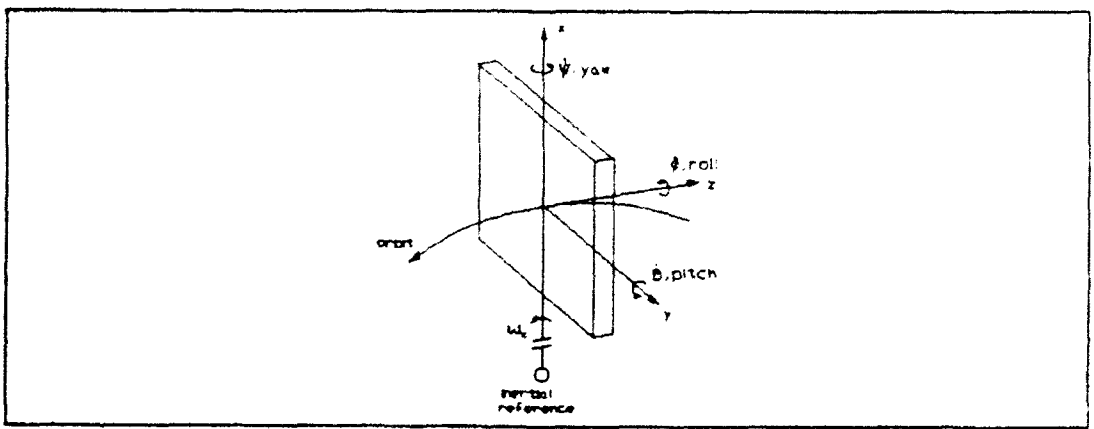

Figure 2.2. Case(2) - Platform following local vertical with major surface normal to the orbit plane

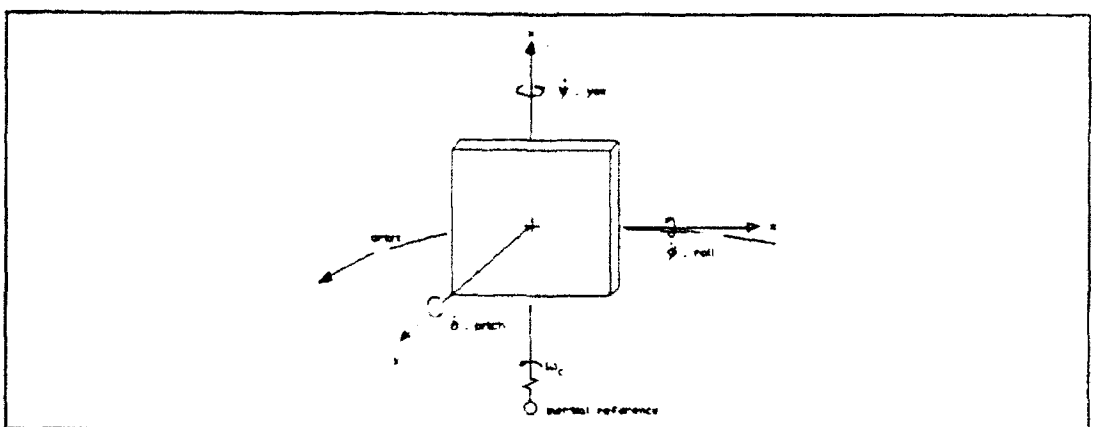

Figure 2.3. Case (3) Platform following local vertical with major surface in the orbit plane

2.5.1 - Plate Normal Nominally Along the Local Vertical

Case (1)

From the equations of motion, Eqns. (57a,b,c), and (58) can be written,[8]

$$\begin{aligned}
\textit{Yaw:} \quad & \dot{\omega}_x + \left[\frac{(I_z - I_y)}{I_x}\right]\omega_y\omega_z = \frac{(G_{rx} + C_x)}{I_x} && (59a)\\
\textit{Pitch:} \quad & \dot{\omega}_y + \left[\frac{(I_x - I_z)}{I_y}\right]\omega_x\omega_z = \frac{(G_{ry} + C_y)}{I_y} && (59b)\\
\textit{Roll:} \quad & \dot{\omega}_z + \left[\frac{(I_y - I_x)}{I_z}\right]\omega_y\omega_x = \frac{(G_{rz} + C_z)}{I_z} && (59c)
\end{aligned} \qquad \textbf{(59)}$$

$$\underset{Mode}{\textit{Generic}}: \quad \ddot{A}_n + \omega_n^2 A_n + [\varphi_n + \sum_{m=1}^{\bar{m}} \varphi_{mn}]/M_n = [g_n + \sum_{m=1}^{\bar{m}} g_{mn} + E_n]/M_n \qquad \textbf{(60)}$$

For Case (1) the plate is oriented with its normal following the local vertical, its axis is aligned with the outward direction of the local vertical (see Fig. 2.1). Under the nominal motion the Euler angles, ψ, ϕ, and θ, are defined according to the sequence given after Eqn. (6). From the previously shown transformations, the Euler angular rates are related to the body rates as derived in Eqns. (7), (8), and (9). In order to examine the stability of the system Eqns. (59) can be linearized by assuming small amplitude pitch, roll, and yaw displacements and also small values of their respective time derivatives. With this in mind the angular rates become:

$$\omega_x = \dot{\psi} - \omega_c\phi \quad \rightarrow \quad \dot{\omega}_x = \ddot{\psi} - \omega_c\dot{\phi} \tag{61}$$

$$\omega_y = \dot{\theta} - \omega_c \quad \rightarrow \quad \dot{\omega}_y = \ddot{\theta} \tag{62}$$

$$\omega_z = \dot{\phi} + \omega_c\psi \quad \rightarrow \quad \dot{\omega}_z = \ddot{\phi} + \omega_c\dot{\psi} \tag{63}$$

As a result of the previous assumptions, (2), (3), (6), (7) and (9), further simplifications of the equations of motion are in order. Assumption (6) leads to $\vec{\Phi}^{(n)}(\vec{r}_o) = \Phi^{(n)}(\hat{n}) = \Phi^{(n)}{}_x\hat{i}$, where $\hat{n}$ is unit normal vector to the plate. As previously stated, by assumption (9), $H^{(n)}{}_{\alpha\beta} = H^{(n)}{}_{\beta\alpha}$ and $H^{(n)}{}_{\alpha\beta} = 0$, and $\vec{D}_n = \vec{D}'_{(n)} = 0$. In addition, $L^{(mn)}{}_{\alpha\beta} = \delta_{mn}\delta'{}_{\beta\alpha}M_n$ where,

$$\delta_{mn} = Kronecker\ delta \quad \delta_{\alpha\beta} = \begin{cases} 0 & \alpha \neq \beta \\ 1 & \alpha = \beta \end{cases} \tag{64}$$

Hence,

$$\vec{Q}^{(n)} = 0; \quad \vec{G}^{(n)} = 0; \quad \varphi_n = 0; \quad g_n = 0 \tag{65}$$

$$\varphi_{mn} = -(\omega_y^2 + \omega_z^2) L_{xx} A_m = -(\omega_y^2 + \omega_z^2)\delta_{mn} M_n A_m \tag{66}$$

$$g_{mn} = A_m L_{xx} M_{11} = A_m M_{11} \delta_{mn} M_n \tag{67}$$

$$G_{rx} = (I_z - I_y) M_{23} \; ; \quad G_{ry} = (I_x - I_z) M_{31} \; ; \quad G_{rz} = (I_x - I_z) M_{12} \tag{68}$$

Assumptions of a spherical symmetric gravitational field and circular orbit and neglecting the higher order terms, $(M^{(s)})$, of the M matrix results in the following simplification of M_{12}, M_{23}, and M_{31},

$$\nu a^2/\rho^3 = \omega_c^2 \quad \rightarrow$$

$$M_{12} = -3\omega_c^2 \sin\phi\cos\phi\cos^2\theta \tag{69}$$

$$M_{23} = -3\omega_c^2 \sin\phi\cos\theta\sin\theta \tag{70}$$

$$M_{31} = 3\omega_c^2 \cos\phi\cos\theta\sin\theta \tag{71}$$

With the use of the above simplifications -for this case- the yaw, roll, pitch, and the generic mode equations, respectively, become,

$$\ddot{\psi} - \omega_c\dot{\phi} + \frac{(I_z-I_y)}{I_x}[\dot{\theta}\dot{\phi} - \omega_c(\dot{\phi}-\dot{\theta}\psi) - \omega_c^2\psi] - \frac{C_x}{I_x} - \frac{(I_z-I_y)}{I_x}\omega_c^2[3\sin\phi\cos\theta\sin\theta] \tag{72}$$

$$\ddot{\phi} + \omega_c\dot{\psi} + \frac{(I_y-I_x)}{I_z}[\dot{\theta}\psi - \omega_c(\dot{\psi}+\dot{\theta}\phi) + \omega_c^2\phi] - \frac{C_z}{I_z} - \frac{(I_y-I_x)}{I_z}\omega_c^2[3\sin\phi\cos\phi\cos^2\theta] \tag{73}$$

$$\ddot{\theta} + \frac{(I_x-I_z)}{I_y}[\psi\dot{\phi} + \omega_c(\dot{\psi}\psi-\dot{\phi}\phi) - \omega_c^2\psi\phi] - \frac{C_y}{I_y} + \frac{(I_x-I_z)}{I_y}\omega_c^2[3\cos\phi\cos\theta\sin\theta] \tag{74}$$

$$\ddot{A}_n + [\omega_n^2 - (\omega_y^2+\omega_z^2) - M_{11}]A_n = E_n/M_n \tag{75}$$

where M_{11} is defined as

$$M_{11} = \omega_c^2[3\cos^2\phi\cos^2\theta - 1] \tag{76}$$

The equations of rotational motion can be simplified further with the elimination of higher order nonlinear terms involving the products of two angles or angular rates or products of an angle with an angular rate, and assuming the rigid body angular oscillations are small, i.e., $\psi,\phi,\theta<<1$. The resulting equations are presented below:

$$\ddot{\psi} - \omega_c\dot{\phi}\left[\frac{I_z-I_y}{I_x}+1\right] - \omega_c^2\psi\left[\frac{I_z-I_y}{I_x}\right] - \frac{C_x}{I_x} \tag{77}$$

$$\ddot{\phi} + \omega_c\dot{\psi}\left[1-\frac{I_y-I_x}{I_z}\right] + \omega_c^2\left[\frac{I_y-I_x}{I_z}\right]4\phi - \frac{C_z}{I_z} \tag{78}$$

$$\ddot{\theta} - \left[\frac{I_x-I_z}{I_y}\right](3\omega_c^2\theta) - C_y/I_y \tag{79}$$

At this point, further development of the generic mode equation may proceed with the substitution of the appropriate terms. This leads to

$$\ddot{A}_n + [\omega_n^2 - (\dot{\theta}^2 - 2\omega_c\dot{\theta} + \omega_c^2 + \dot{\phi}^2 + 2\omega_c\psi\dot{\phi} + \omega_c^2\psi^2) - \omega_c^2(3\cos^2\phi\cos^2\theta - 1)]A_n - E_n/M_n \tag{80}$$

Assuming the Euler angle displacements and time derivatives and the transverse elastic deformation amplitudes and time derivatives are small, with the removal of nonlinear terms Eqn. (80) simplifies further to,

$$\ddot{A}_n + [\omega_n^2 - 3\omega_c^2]A_n - E_n/M_n \tag{81}$$

Based on the preceding assumptions the following linearized equations of motion are obtained in a dimensionless form:

$$\tau = \omega_c t \quad ; \quad Z_n = A_n/\ell \quad ; \quad \phi' = d\phi/d\tau \quad ; \quad etc.$$

$$\textit{Yaw:} \qquad \psi'' - \Omega_x \psi - (1+\Omega_x)\phi' - (C_x + T_x)/I_x\omega_c^2 \qquad (82)$$

$$\textit{Roll:} \qquad \phi'' + 4\Omega_z\phi + (1-\Omega_z)\psi' - (C_z + T_z)/I_z\omega_c^2 \qquad (83)$$

$$\textit{Pitch:} \qquad \theta'' - 3\Omega_y\theta - (C_y + T_y)/I_y\omega_c^2 \quad . \qquad (84)$$

$$\frac{\textit{Elastic}}{\textit{modes}}: \qquad Z_n'' + (\Omega_n^2 - 3)Z_n - E_n/M_n\omega_c^2\ell \quad . \qquad (85)$$

where Ω_i is defined as,

$$\Omega_x = (I_z - I_y)/I_x \; ; \; \Omega_y = (I_x - I_z)/I_y \; ; \; \Omega_z = (I_y - I_x)/I_z \; ; \; \Omega_n = \omega_n/\omega_c \; ;$$

$\vec{T}$ represents the torque produced by the actuators, and $\vec{E}_r$ represents the generic force on the $r^{\underline{th}}$ mode.

Assumption (7) should be noted here, i.e., only the first three modes are considered. The following observations can be made from Eqns. (77-80) regarding the motion of a flat plate:

a) Uncontrolled rigid body motion is independent of the uncontrolled elastic motion of the plate.
b) The uncontrolled elastic modes are coupled to the rigid body motion through both inertia and gravity.
c) To first order, gravity can not excite the elastic

modes.

d) There is no intercoupling between the uncontrolled elastic modes either through inertia or gravity.

For Case (1), $I_x=2I_y=2I_z$, the rotational equations of motion become,

$$\psi'' - \phi' = (C_x + T_x)/I_x\omega_c^2 \tag{86}$$

$$\phi'' - 4\phi + 2\psi' = (C_z + T_z)/I_z\omega_c^2 \tag{87}$$

$$\theta'' - 3\theta = (C_y + T_y)/I_y\omega_c^2 \tag{88}$$

Since there are no inputs from the elastic terms in Eqns. (82-84) the uncontrolled rigid body rotational modes are not influenced by the elastic motion of the plate. However, the elastic modes are coupled to the rigid body rotational modes through higher order nonlinear terms as shown in Eqns. (77-80). Further, for this orientation of the plate $\Omega_y>0$, the pitch motion is unstable in the absence of external restoring torques, C_y (note the term, $-3\Omega_y$ in Eqn.(84)). For the class of large space structures considered, passive control has been analyzed, (see Kumar, ref. 8), but for this thesis active control will be applied. Through the application of the LQR problem with discretized input data and point actuators located on the plate's surface, active control will be implemented.

2.5.2 - Plate Normal Nominally Along the Local Horizontal

Case (2)

Assumption (6) in this case leads to $\vec{\Phi}^{(n)}(\vec{r}_o) = \Phi^{(n)}(\hat{n}) = \Phi^{(n)}{}_z\hat{K}$. Similar to Case (1), one can show that for this orientation:

$$\vec{Q}^{(n)} = 0; \quad \vec{G}^{(n)} = 0; \quad \varphi_n = 0; \quad g_n = 0; \quad \vec{D}^{(n)} = 0; \quad D_n = 0;$$
$$\varphi_{mn} = -(\omega_x^2 + \omega_y^2)\,\delta_{mn} M_n A_m; \quad \text{and,} \quad g_{mn} = A_m M_{33}\,\delta_{mn} M_n$$

in Eqns. (33) and (44). Thus, for Case (2) the equations of rotational motion are exactly the same as Eqns. (82-84), with the exception that the relationship between the principal moments of inertia I_x, I_y, and I_z, differs, $I_z = 2I_x = 2I_y$. Hence, the Yaw, Roll, and Pitch equations of motion become, respectively,

$$\psi'' - \psi + 2\phi' = (C_x + T_x)/I_x\omega_c^2 \tag{89}$$

$$\phi'' - \psi' = (C_z + T_z)/I_z\omega_c^2 \tag{90}$$

$$\theta'' + 3\theta = (C_y + T_y)/I_y\omega_c^2 \tag{91}$$

The equations of elastic motion are based on Eqn. (60), together with the above assumptions there results,

$$\ddot{A}_n + [\omega_n^2 - (\omega_x^2 + \omega_y^2) - M_{33}]\,A_n = E_n/M_n \tag{92}$$

where $M_{33} = \omega_c^2(3\sin^2\theta-1)$. Removing angular crossterms and restricting the higher order terms of the angles yields,

$$\ddot{A}_n + [\omega_n^2 - \omega_c^2(\phi^2 + 3\theta^2) + 2\omega_c\dot{\theta} - (\dot{\psi}^2 + \dot{\theta}^2)]A_n = E_n/M_n \qquad (93)$$

For small amplitude angles and elastic motions, the non-dimensionalized the generic mode equation can be written,

$$Z_n'' + \Omega_n^2 Z_n = E_n/M_n\omega_c^2\ell \qquad (94)$$

Notice for small pitch amplitude, Eqn. (93) can be reduced to a Mathieu type equation.[8] The roll and yaw motions are gyroscopically coupled to each other and they are not influenced by either the pitch or elastic modes within the linear range.

2.5.3 - Plate Normal Nominally Along the Orbit Normal Case (3)

In this last case, assumption (6) leads to $\vec{\Phi}^{(n)}(\vec{r}_o) = \Phi^{(n)}(\hat{n}) = \Phi^{(n)}{}_y\hat{j}$. Following the steps of the derivation of the two previous Cases, (1) and (2), one will arrive with the same equations of rotational motion as Eqns. (82), (83), and (84), with the difference that the principal moments of inertia I_x, I_y, and I_z, -for Case (3)- have the relationship $I_y = 2I_x = 2I_z$. Hence, the rotational equations of motion become:

$$\psi'' + \psi = (C_x + T_x) / I_x \omega_c^2 \tag{95}$$

$$\phi'' + 4\phi = (C_z + T_z) / I_z \omega_c^2 \tag{96}$$

$$\theta'' = (C_y + T_y) / I_y \omega_c^2 \tag{97}$$

The equations of elastic motion are now,

$$\ddot{A}_n + [\omega_n^2 - (\omega_z^2 + \omega_x^2) - M_{22}] A_n = E_n / M_n \tag{98}$$

where $M_{22} = \omega_c^2(3\sin^2\phi\cos^2\theta - 1)$. Cancellation of the angular crossterms and restriction of the motion to only small amplitudinal pitch motion produces,

$$\ddot{A}_n + [\omega_n^2 - \omega_c^2(4\phi^2 + \psi^2 - 1) - (\dot{\phi}^2 + \dot{\psi}^2)] A_n = E_n / M_n \tag{99}$$

Removing higher order and nonlinear terms, plus non-dimensionalizing the amplitude leads to,

$$Z_n'' + (\Omega_n^2 + 1) Z_n = E_n / M_n \omega_c^2 \ell \tag{100}$$

In this final case, roll, pitch, yaw, and the generic modes are decoupled from each other. Notice without any external influences the generic modes, yaw, and pitch motion exhibit simple harmonic motion while the pitch rate increases linearly with time for a given initial pitch rate.

CHAPTER 3 - DETERMINATION OF MODAL FREQUENCIES AND MODE SHAPES FOR A THIN FLEXIBLE FREE-FREE PLATE

The ability to accurately determine the frequencies and mode shapes is essential for the analysis and control of large space structures in orbit. Four different methods have been analyzed:[21]

1) The approximate frequencies and mode shapes of a rectangular plate are obtained from a Rayleigh-Ritz formulation by Warburton;[22,23]
2) The analytical results for a square plate are derived from the Rayleigh-Ritz method by Lemke;[24]
3) The frequencies and mode shapes are computed using the finite element program, STRUDL, developed at Massachusetts Institute of Technology;[25] and
4) The rigid body modes and the mode deflection are calculated with an updated version of STRUDL, GTSTRUDL, developed at Georgia Institute of Technology.[20]

A tabulation of the numerical results for a free-free thin aluminum square plate with the length and width of 100.0 m, thickness of 0.01 m, Young's Modulus of 0.7441 x 10^{10} kg/m^2, Poisson's ratio of 0.33, and mass density of 2768.0 kg/m^3.[19]

3.1 - Formulation by Warburton

An application of the Rayleigh Method allows the derivation of an approximate frequency formula.[22,23] The plate vibrational equation in the cartesian coordinate system (x,y) is used as a basic equation, with the length and width of the plate taken along the x and y directions, respectively, and is given as,

$$\frac{\partial^4 w}{\partial x^4} + 2\frac{\partial^4 w}{\partial x^2 \partial y^2} + \frac{\partial^4 w}{\partial y^4} + \frac{12\rho(1-\nu^2)}{Egh^2}\frac{\partial^2 w}{\partial t^2} = 0 \qquad (101)$$

where ρ, υ, and E are the weight density, Poisson's ratio, and Young's modulus of the plate material, respectively; h is the plate thickness; and g is the acceleration due to gravity. The displacement, w, is a sinusoidal function, which at any point (x,y) at any time t, is given by,

$$w = W\sin\omega t = A\theta(x)\phi(y)\sin\omega t \qquad (102)$$

where $\theta(x)$ and $\phi(y)$ are beam functions orthogonal to each other and are used to approximate the plate's behavior; and ω is the vibrational circular frequency.[22] The appropriate free-free beam functions, $\theta(x)$, are defined as,

$$\theta(x) = 1 \quad for\ m = 0 \qquad (103a)$$

$$\theta(x) = 1 - \frac{2x}{a} \quad for\ m = 1 \qquad (103b)$$

$$\theta(x) = \cos\gamma\left(\frac{x}{a} - \frac{1}{2}\right) + k\cosh\gamma\left(\frac{x}{a} - \frac{1}{2}\right) \quad for\ m = 2,4,6,\ldots \qquad (103c)$$

$$\theta(x) = \sin\gamma'\left(\frac{x}{a} - \frac{1}{2}\right) + k'\sinh\gamma'\left(\frac{x}{a} - \frac{1}{2}\right) \quad for\ m = 3,5,7,\ldots \qquad (103d)$$

(103)

where,

$$k = -\frac{\sin\frac{1}{2}\gamma}{\sinh\frac{1}{2}\gamma} \quad and \quad \tan\frac{1}{2}\gamma + \tanh\frac{1}{2}\gamma = 0 \quad (104a)$$

$$k' = \frac{\sin\frac{1}{2}\gamma'}{\sinh\frac{1}{2}\gamma'} \quad and \quad \tan\frac{1}{2}\gamma' - \tanh\frac{1}{2}\gamma' = 0 \quad (104b) \qquad (104)$$

The corresponding expressions for $\phi(y)$ can be obtained by substituting y, b, ϵ, and c for x, a, γ, and k, respectively. After calculating $\theta(x)$ and $\phi(y)$, the frequency expressions for a rectangular plate are derived as[23]:

$$\lambda^2 = \frac{\rho a^4 (2\pi f)^2 12(1-\nu^2)}{\pi^4 E g h^2} \qquad (105)$$

$$\lambda^2 = G_x^4 + G_y^4\frac{a^4}{b^4} + 2\frac{a^2}{b^2}\left[\nu H_x H_y + (1-\nu) J_x J_y\right] \qquad (106)$$

where λ is a non-dimensional factor, proportional to the frequency; a and b are the length and width of the plate; and G_x, H_x, J_x, G_y, H_y, and J_y are functions associated with the number of nodal lines (m and n, parallel to x and y) and the boundary conditions. From Eqn. (105), the frequency is obtained as:

$$f = \frac{\lambda h \pi}{a^2}\left[\frac{Eg}{48\rho(1-\nu^2)}\right]^{1/2} \qquad (107)$$

This frequency expression is valid for thin rectangular plates; for square plates it must be modified. For square plates, the combinations of (m,n)±(n,m) describe the types of existing modes (see Fig. 3.1-3.10); for these cases λ in Eqn. (107) must be modified.

Modes (m,0)±(0,m), for m = 2,4,6...

$$\lambda^2 = (m-\frac{1}{2})^4 \pm 2\nu(m-\frac{1}{2})^2\frac{8}{\pi^2} \tag{108}$$

Modes (m,1)±(1,m), for m = 3,5,7...

$$\lambda^2 = (m-\frac{1}{2})^4 \pm 2(1-\nu)(m-\frac{1}{2})^2\left[1+\frac{\nu}{(M-\frac{1}{2})\pi}\right]\frac{12}{\pi^2} \pm 2\nu(m-\frac{1}{2})^2\frac{24}{\pi^2}\left[1-\frac{2}{(m-\frac{1}{2})\pi}\right]^2 \pm 2(1-\nu)\frac{192}{\pi^4} \tag{109}$$

For any mode of vibration the nodal pattern is defined by m and n -the number of nodal lines in the x and y directions- respectively. The mode shapes are obtained by using the corresponding modal frequencies in the beam functions and then evaluating the product, $\theta(x)\cdot\phi(y)$, numerically.

Using Warburton's results, Eqns. (108) and (109) and the expressions for $\theta(x)$ and $\phi(y)$, frequencies and mode shapes are calculated for different combinations of the number of nodal lines, m and n, starting with combinations of m=0 and n=1, through m=3 and n=3. The first three

combinations of nodal line numbers, (0,0), (1,0), and (0,1), represent rigid body motion. The combination of m=1 and n=1 produce the first fundamental flexural frequency. The corresponding mode shape for the plate is obtained by multiplying the beam functions $\theta(x)$ and $\phi(y)$, for the mode characterized by m=1 and n=1 (see Fig. 3.1). Since the plate is approximated by sets of orthogonal beam functions in the x and y direction, the nodal pattern is also obtained by plotting the nodal points of these beams for their first several modes. The next two higher frequencies are obtained by combinations of m=0 and n=2, but the nodal patterns can not be visualized. This is because the frequencies are of a special type resulting from a combination of the (2,0) and (0,2) plate modes. When the mode corresponding to (2,0) (Fig. 3.2) is superimposed with -(0,2), (Fig. 3.3), the mode shape depicted in Figure 3.4 results. By imposing the (2,0) and (0,2) combinations, the third mode shape (Fig.3.5) is obtained. The combinations of nodal patterns m=1 and n=2, give identical frequencies for the fourth and fifth mode and the corresponding shape (Fig. 3.6) is as expected. The following higher two frequencies are also identical and are the results of combinations from the (3,0) and (0,3) nodal pattern lines (Fig. 3.7). The eighth frequency is obtained from m=2 and n=2 and the mode shape obtained is shown in Figure 3.8. The higher frequencies are obtained in a similar manner. The ninth and tenth modes are the special type

resulting from combinations of (3,1) and (1,3), (see Figs. 3.9 and 3.10) and the next higher frequencies are combinations of (3,2) (2,3), and (3,3) nodal lines, respectively. The calculated modal frequencies and nodal patterns are shown in Table 1.[19]

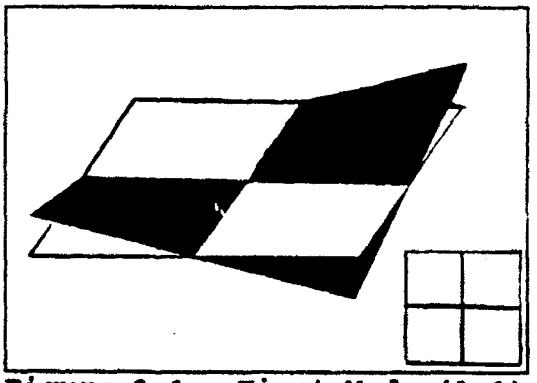

Figure 3.1. First Mode (1,1)

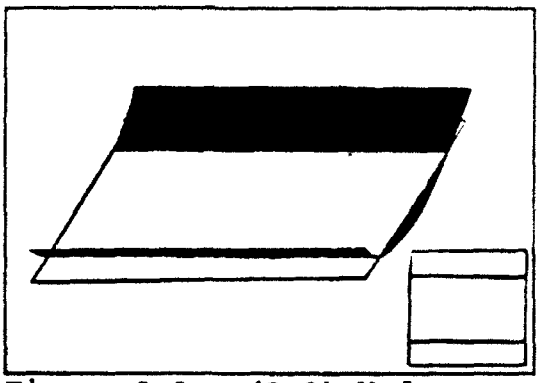

Figure 3.2. (2,0) Mode

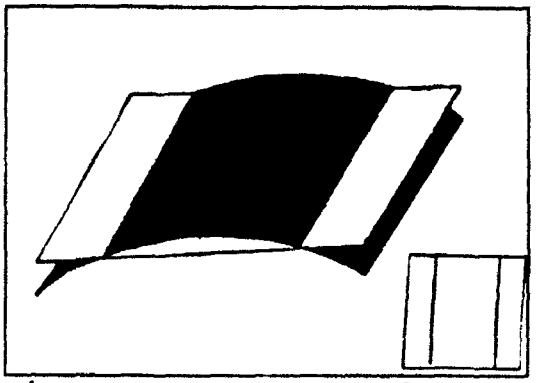

Figure 3.3. (0,2) Mode

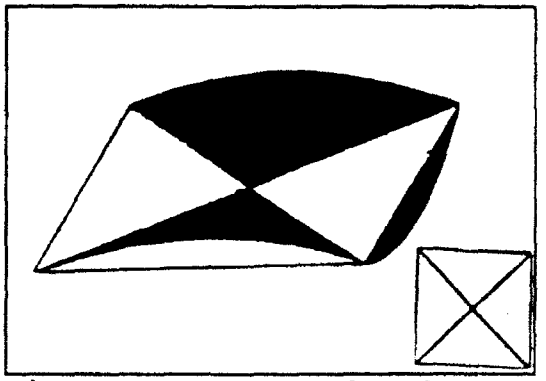

Figure 3.4. Second Mode (2,0)-(0,2)

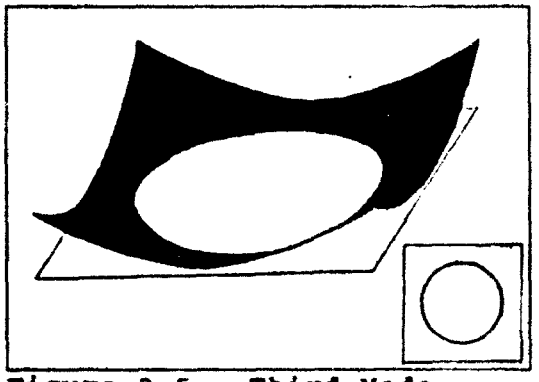

Figure 3.5. Third Mode (2,0)+(0,2)

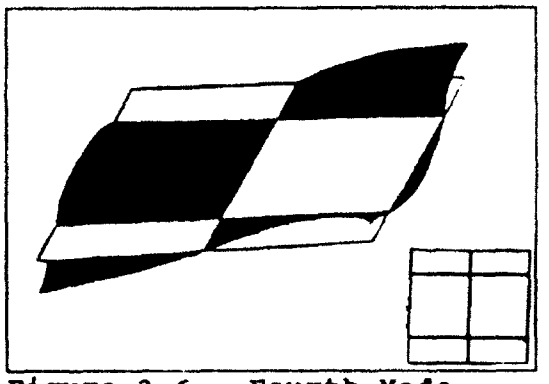

Figure 3.6. Fourth Mode (2,1)

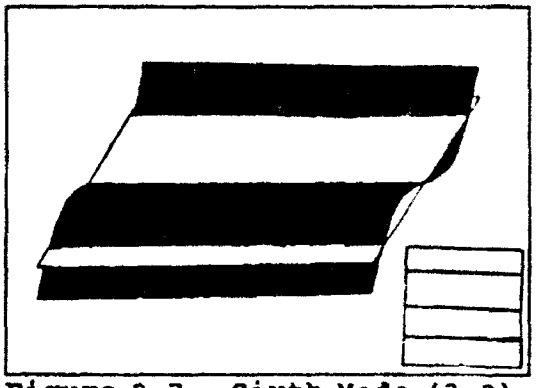

Figure 3.7. Sixth Mode (3,0)

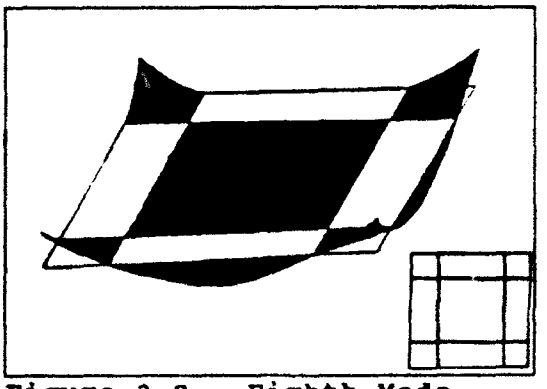

Figure 3.8. Eighth Mode (2,2)

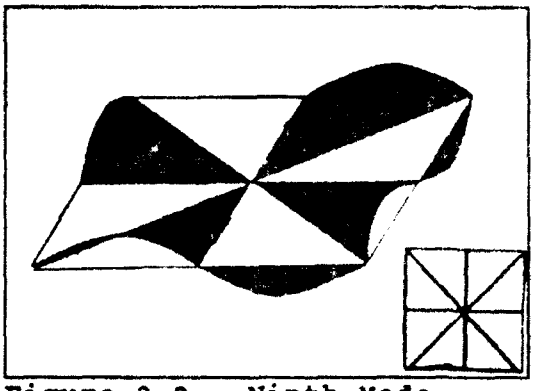

Figure 3.9. Ninth Mode (1,3)-(3,1)

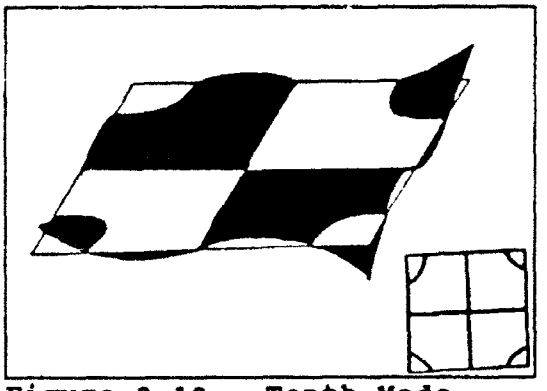

Figure 3.10. Tenth Mode (1,3)+(3,1)

3.2 - Formulation by Lemke

The analytical results for a square plate are derived from a method of Lemke, which also uses the Rayleigh-Ritz method.[24] The displacement function w, can be expressed as a sinusoidal function (at any point (x,y) and time t),

$$w = W\sin\omega t \tag{110}$$

where ω is the circular frequency ($\omega=2\pi f$). The amplitude W, can be expressed by,

$$W(\bar{x},\bar{y}) = \sum A_{mn} X_m(\bar{x})\, Y_n(\bar{y}) \tag{111}$$

where $X_m(\bar{x})$ and $Y_n(\bar{y})$ are the free-free beam functions expressed in terms of a normalized (i.e., $\bar{x}=x/a$, where $a=\ell$) xy coordinate system having the origin at the plate center;

$$X_m(\bar{x}) = \frac{\cosh k_m \cos k_m\bar{x} + \cos k_m \cosh k_m\bar{x}}{\sqrt{\cosh^2 k_m + \cos^2 k_m}} \quad (m \text{ even}); \tag{112}$$

$$X_m(\bar{x}) = \frac{\sinh k_m \sin k_m\bar{x} + \sin k_m \sinh k_m\bar{x}}{\sqrt{\sinh^2 k_m - \sin^2 k_m}} \quad (m \text{ odd}); \tag{113}$$

$Y_n(\bar{y})$ is obtained by replacing $\bar{x}$ by $\bar{y}$ and m by n, in Eqns. (112) and (113). The values k_m are the roots of the characteristic equations, that are,

$$\tan k_m + \tanh k_m = 0 \quad (m \text{ even}) \tag{114}$$

$$\tan k_m - \tanh k_m = 0 \quad (m \text{ odd}) \tag{115}$$

These equations result from the spatial boundary conditions. For a rectangular plate the potential energy due to bending is given by,

$$U = \frac{1}{2}\frac{Eh^3}{12(1-\nu^2)}\int_0^a\int_0^b\left[\left(\frac{\partial^2 w}{\partial x^2}\right)^2 + 2\nu\left(\frac{\partial^2 w}{\partial x^2}\right)\left(\frac{\partial^2 w}{\partial y^2}\right) + \left(\frac{\partial^2 w}{\partial y^2}\right)^2 + 2(1-\nu)\left(\frac{\partial^2 w}{\partial x \partial y}\right)^2\right]dx\,dy \tag{116}$$

where ν, E, and h, are the Poisson's ratio, Young's modulus and the thickness of the plate material, respectively. The kinetic energy is represented as,

$$T = \frac{1}{2}\frac{\rho h}{g}\int_0^a\int_0^b\left(\frac{\partial w}{\partial t}\right)^2 dx\,dy \tag{117}$$

where ρ is the density of the plate material, and g is the acceleration due to gravity. Thus,

$$U_{max} = \frac{1}{2}\frac{Eh^3}{12(1-\nu^2)}\int_0^a\int_0^b\left[\left(\frac{\partial^2 W}{\partial x^2}\right)^2 + 2\nu\left(\frac{\partial^2 W}{\partial x^2}\right)\left(\frac{\partial^2 W}{\partial y^2}\right) + \left(\frac{\partial^2 W}{\partial y^2}\right)^2 + 2(1-\nu)\left(\frac{\partial^2 W}{\partial x \partial y}\right)^2\right]dx\,dy \tag{118}$$

$$T_{max} = \frac{1}{2}\frac{\rho h \omega^2}{g}\int_0^a\int_0^b W^2\,dx\,dy \tag{119}$$

where U_{max} is the maximum potential energy due to bending, and T_{max} is the maximum kinetic energy due to bending. By setting $U_{max} = T_{max}$, it can be shown,

$$\omega^2 = \frac{U_{max}}{\frac{\rho h}{2g}\int_0^a\int_0^b W^2\,dx\,dy} \tag{120}$$

The coefficients A_{mn}, in Eqn. (111) are determined to produce ω^2 in Eqn. (120) -a minimum. Lemke obtained the coefficients A_{mn}, by taking six or more terms in the series, Eqn. (111), and using four different values of Poisson's ratio. Expressions for six mode shapes and frequencies along with the coefficients A_{mn}, are tabulated in reference 24. As an example the expression incorporating 15 terms for the first mode is given here:

$$W(\bar{x},\bar{y}) = \bar{X}_1\bar{Y}_1 + 0.0325(\bar{X}_1\bar{Y}_3 + \bar{X}_3\bar{Y}_1) - 0.005\bar{X}_3\bar{Y}_3 - 0.00257(\bar{X}_1\bar{Y}_5 + \bar{X}_5\bar{Y}_1) + 0.00121(\bar{X}_3\bar{Y}_5 + \bar{X}_5\bar{Y}_3) - 0.000365\bar{X}_5\bar{Y}_5 + \ldots$$

$$\textit{and}\quad \omega = \frac{13.086}{a^2}\sqrt{\frac{Eh^3}{12\rho(1-\nu^2)}} \quad \textit{for}\ \nu = 0.343$$

Frequencies and mode shapes for the first six modes were obtained using the Lemke method (see Table 1).[19]

3.3 - STRUDL, Structural Design Language

A computer program implemented was STRUDL (Structural Design Language).[25] It was developed by the Civil Engineering Department of the Massachusetts Institute of Technology and installed on Howard University's mainframe computer (IBM 3090). STRUDL has the capability to apply the finite element method to determine the mode shapes and the natural frequencies of vibration. Necessary computer input by the user is the specification of the structure's material properties, dimensions, and the types and total number of finite elements representing the structure.

For a rectangular plate, the finite elements can be specified as rectangular elements; the number of elements into which the plate is divided depends on the accuracy required. In the finite element method, the discretization of the number of degrees of freedom requires the introduction of simplifying assumptions in the element formulation, which represents an important source of error in the results. As a consequence, finite element results are dependent upon the number of elements used in the model. Thus, even when consistent element formulations insure convergence of the results as the number of elements is increased, finite element models cannot be arbitrarily designed.[25] Generally, the accuracy of the results will

improve when the structure is modeled with a higher number of elements. However, computational errors due to truncation and round-off errors may predominate as the order of the elements increases beyond a limit. Further, hardware calculation limitations can restrict the number of elements into which a structure is divided, thus, limiting the ability to obtain better results.

For the modes specified, STRUDL calculates the deflections at each element's corners; from the deflections the modal shapes can be determined. For each mode, a set of frequencies is also generated. Results obtained from STRUDL are available in Table 1.[19]

3.4 - GTSTRUDL, Georgia Tech Structural Design Language

GTSTRUDL is an updated version of STRUDL developed at Georgia Institute of Technology.[20] Similar to STRUDL, GTSTRUDL, uses the finite element method to determine the modal shapes and the vibrational frequencies. The structure's material properties and its dimensions are necessary initial inputs. In addition, the number of elements into which the structure is divided and the type of element must be specified by the user. For this thesis's structure, a thin flat square plate, the 'BPR' element - bending plate rectangular with square dimensions- was chosen.[20,29] This element only considers the deflections normal to the major surface and the in-plane rotations at the nodes, resulting in three degrees of freedom at each of the four nodes (see Figure 4).

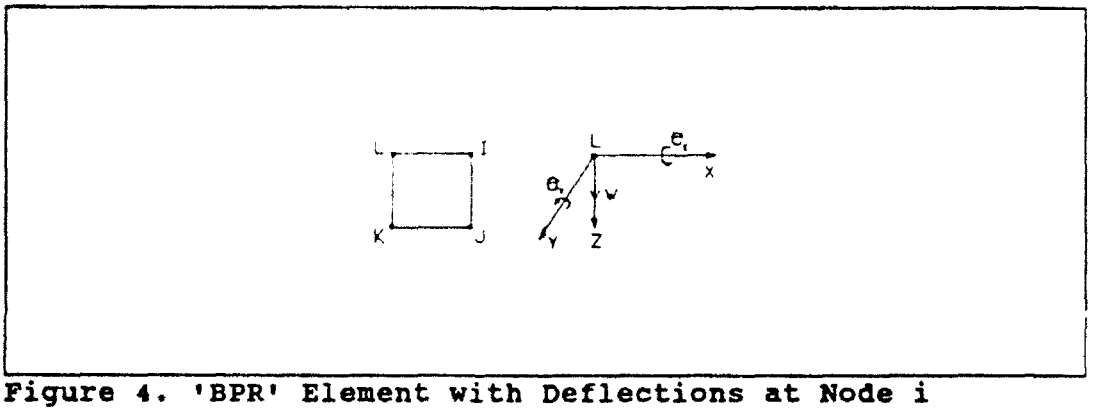

Figure 4. 'BPR' Element with Deflections at Node i

3.4.1 - Displacement Function

The corresponding displacement function, w, for the 'BPR' element, contains 12 parameters of α,

$$w = \alpha_1 + \alpha_2 x_i + \alpha_3 y_i + \alpha_4 x_i^2 + \alpha_5 x_i y_i + \alpha_6 y_i^2 + \alpha_7 x_i^3 + \alpha_8 x_i^2 y_i + \alpha_9 x_i y_i^2 + \alpha_{10} y_i^3 + \alpha_{11} x_i^3 y_i + \alpha_{12} x_i y_i^3 \quad (121)$$

The in-plane rotations, θ_x and θ_y, are related to the displacement function as follows:

$$(\theta_x)_i = \frac{\partial w_i}{\partial y} \; ; \qquad (\theta_y)_i = \frac{-\partial w_i}{\partial x} \quad (122)$$

The transition matrix, A, relates the α coefficients to the deflection vector, a, at the node, i, as follows:

$$\{a_i\} = [A_i]\{\alpha\} \; ; \qquad \{a\} = [A]^e\{\alpha\} \quad (123)$$

$$\begin{Bmatrix} w_i \\ (\theta_x)_i \\ (\theta_y)_i \end{Bmatrix} = \begin{bmatrix} 1 & x_i & y_i & x_i^2 & x_iy_i & y_i^2 & x_i^3 & x_i^2y_i & x_iy_i^2 & y_i^3 & x_i^3y_i & x_iy_i^3 \\ 0 & 0 & 1 & 0 & x_i & 2y_i & 0 & x_i^2 & 2x_iy_i & 3y_i^2 & x_i^3 & x_iy_i^2 \\ 0 & -1 & 0 & -2x_i & -y_i & 0 & -3x_i^2 & -2x_iy_i & -y_i^2 & 0 & -3x_i^2y_i & -y_i^3 \end{bmatrix} \begin{Bmatrix} \alpha_1 \\ \alpha_2 \\ \alpha_3 \\ \vdots \\ \alpha_{12} \end{Bmatrix} \quad (124)$$

where $[A]^e = [A_i, A_j, A_k, A_l]^T$

3.4.2 - The Mass Matrix, [M]

In addition, the user must specify the mass type: consistent or lumped. When specified, the computer will internally generate the mass matrix. A lumped mass approach will produce a composition consisting of a diagonal mass

matrix, whose elements correspond to each grid point's (node) mass. By evenly dividing the structure's mass by the number of elements, and then dividing that elemental mass into four, each node is assigned some mass. If a node is shared by additional elements, its mass is the total sum of each partitioned mass. The total mass at each node becomes:

a) the mass of the nodes at the corners, m_c,

$m_c = M_t \div (\#\ \text{of elements} \times 4)$;

b) the mass of the nodes along the sides, m_s,

$m_s = M_t \div (\#\ \text{of elements} \times 2)$; and

c) the mass of the nodes inside the boundaries, m_{ib},

$m_{ib} = M_t \div (\#\ \text{of elements})$.

3.4.3 - The Stiffness Matrix, [K]

The user may input the system's stiffness matrix or it may be generated by the computer, the latter option was chosen for this thesis. To begin the formulation of the stiffness matrix, the stress (σ) and strain (ϵ) relationship becomes useful.

$$\{\sigma\} = \begin{Bmatrix} M_x \\ M_y \\ M_z \end{Bmatrix} = [D]\{\varepsilon\} = \frac{Eh^3}{12(1-\nu^2)} \begin{bmatrix} 1 & \nu & 0 \\ \nu & 1 & 0 \\ 0 & 0 & \frac{1-\nu}{2} \end{bmatrix} \begin{Bmatrix} \frac{\partial^2 w}{\partial x^2} \\ \frac{\partial^2 w}{\partial y^2} \\ -\frac{2\partial^2 w}{\partial x \partial y} \end{Bmatrix} A \qquad (125)$$

The generalized strain displacement matrix, [B], gives the strains at any point within the element due to unit values of nodal displacements.[30]

$$\{\varepsilon\} = [B]\{a\} = [H][A]^{-1}\{a\} \quad where \quad [B] = [H][A]^{-1} \tag{126}$$

$$\{\varepsilon\} = [H]\{\alpha\} = [B][A]\{\alpha\} \tag{127}$$

From Hooke's Law,

$$\Pi = \frac{D}{2}\iint_R \left\{ (\nabla^2 W)^2 + 2(1-\nu)\left[\left(\frac{\partial^2 W}{\partial x \partial y} \right)^2 + \left(\frac{\partial^2 W}{\partial x^2} \right)\left(\frac{\partial^2 W}{\partial y^2} \right) \right] \right\} dx\,dy - \{a\}^T\{q\} \tag{128}$$

Taking the variation, where $\delta^{(1)}\Pi=0$, results in

$$\iint_R \left[M_x \delta\left(-\frac{\partial^2 W}{\partial x^2} \right) + M_y \delta\left(-\frac{\partial^2 W}{\partial y^2} \right) + M_{xy} \delta\left(-2\frac{\partial^2 W}{\partial x \partial y} \right) \right] dx\,dy - \{\delta a\}^T\{q\} = 0 \tag{129}$$

After substituting in the variation of the stress-strain, (also known as internal virtual work) the following is obtained,

$$\iint_R \{\delta\varepsilon\}^T\{\sigma\}\,dx\,dy - \{\delta a\}^T\{q\} = 0 \tag{130}$$

Remembering the relationship $\{\delta\varepsilon\}^T = \{\delta a\}^T[B]^T$ and substituting into Eqn. (130), results in:

$$\iint_R \{\delta a\}^T[B]^T[D][\varepsilon]\,dx\,dy - \{\delta a\}^T\{q\} = 0 \tag{131}$$

$$\{\delta a\}^T\left[\iint_R [B]^T[D][B]\{a\}\,dx\,dy - \{q\}\right] = \{\delta a\}^T([K]\{a\} - \{q\}) = 0 \quad (132)$$

where $\{\delta a\}^T$ is arbitrary, and the stiffness matrix, [K], is defined as,

$$[K] = \iint_R [B]^T[D][B]\,dx\,dy \quad \therefore \quad [K]\{a\} = \{q\} \quad (133)$$

where the nodal force vector, {q}, is defined as,

$$\{q\} = \iint p(x,y)\,[N]^T dx\,dy \; ; \quad (134)$$

and the interpolation matrix, [N], is represented by the relationship,

$$[N] = [J]\,[A]^{-1} \quad (135)$$

where the matrix, [J], is defined as,

$$[J] = \left[1,\ x_1,\ y_1,\ x_1^2,\ x_1y_1,\ y_1^2,\ x_1^3,\ x_1^2y_1,\ x_1y_1^2,\ y_1^3,\ x_1^3y_1,\ x_1y_1^3\right] \quad (136)$$

For a complete listing of the stiffness matrix individual elements refer to Appendix A.

3.4.4 - Development of The Basic Dynamic Matrix Equation

D'Alembert's principal incorporated with the principal of virtual work (with inertia as a body force distributed) can be expressed as[31]:

$$-\iiint_V \rho\{\delta u\}^T\{\ddot{u}\}\,dv + \iiint_V \{\delta u\}^T\{b\}\,dv + \iint_S \{\delta u\}^T\{T\}\,dA - \iiint_V [\delta\varepsilon]^T\{\sigma\}\,dv = \delta U \quad (137)$$

where (T) and (U) are the kinetic and potential energy, and (u) represents the displacement field $\{u\}=\{u, v, w\}^T$, which can be expressed in terms of the nodal displacements, (a), and the interpolation function, [N], as follows,

$$\{u\} = [N]\{a\} \tag{138}$$

Substitution of [N] and (a) leads to:

$$\{u\} = [J][A]^{-1}[A]\{\alpha\} = [J]\{\alpha\} \tag{139}$$

Using the interpolation functions expressed in terms of the spatial coordinates (in the static form) and considering nodal displacements, (a), as functions of time, discretizing the domain, and making the various substitutions of Eqns. (123), (133), (138), and (139) into Eqn.(135), forms,[31]

$$\begin{aligned} &-\iiint_V \rho\{\delta a\}^T[N]^T[N]\{\ddot{a}\}\,dv+\iiint_V\{\delta a\}^T[N]^T\{b\}\,dv+\iint_s\{\delta a\}^T[N]^T\{T\}\,dA \\ &-\iiint_V[\delta a]^T[N]^T[J]\,[N]\{\dot{a}\}\,dv-\iiint_V\{\delta a\}^T[B]^T[D]\,[B]\{a\}\,dv \end{aligned} \tag{140}$$

where,

$$\textit{Mass Matrix}: [M] = \iiint_V \rho[N]^T[N]\,dv \tag{141}$$

$$\textit{Damping Matrix}: [C] = \iiint_V [N]^T[J]\,[N]\,dv \tag{142}$$

$$\textit{Stiffness Matrix}: [K] = \iiint_V [B]^T[D]\,[B]\,dv \tag{143}$$

$$\textit{Force Vector} : \{q\} = \iiint_V [N]^T \{b\}\, dv + \iint_S [N]^T \{T\}\, dA \qquad (144)$$

Equation (144) now becomes,

$$\{\delta a\}\,(-[M]\{\ddot{a}\} + \{q\} - [C]\{\dot{a}\}) = \{\delta a\}^T [K]\{a\} \qquad (145)$$

After rearrangement of terms, the basic dynamic matrix equation is formed:

$$[M]\{\ddot{a}\} + [C]\{\dot{a}\} + [K]\{a\} = \{q\} \qquad (146)$$

3.4.5 - Natural Frequency Formulation for Free Vibrational Motion

Consider the free vibrational - undamped harmonic - motion system, (i.e., no damping and no external forces) and notice the damping matrix and the force vector are null. Thus,

$$[M]\{\ddot{a}\} + [K]\{a\} = 0 \qquad (147)$$

The global equation for free vibration is

$$\{a\} = \{\bar{a}\}\, e^{i\omega t} \qquad (148)$$

where $\{\bar{a}\}$ is the modal vector of constant amplitude; and ω is the natural frequency. Substituting the global equation into the dynamic equation results in,

$$([K] - \omega^2 [M])\{\bar{a}\} = 0 \qquad (149)$$

Equation (149) is in the form of a basic eigenvalue-eigenvector problem. For a non-trivial solution, the determinant of the coefficients of $\{\tilde{a}\}$ must be equal to zero.

$$|[K] - \omega^2 [M]| = 0 \tag{150}$$

Once the characteristic equation is found, the roots may be obtained by solving for the eigenvalues $-\omega^2-$ of the $n^{\underline{th}}$ mode, the natural frequency, ω_n. For each natural frequency generated, an eigenvector is calculated; these provide the natural mode shapes. To ensure that the solutions are linearly independent, each eigenvector must satisfy the orthogonality condition:

$$\{\tilde{a}\}_i^T [M] \{\tilde{a}\}_j = 0 \qquad for\ i \neq j \tag{151}$$

Rewriting Eqn. (147) leads to:

$$[K] \{\tilde{a}\} - \omega^2 [M] \{\tilde{a}\} \rightarrow [K] \{\tilde{a}\}_i - \omega_i^2 [M] \{\tilde{a}\}_i \tag{152}$$

After multiplication by $\{\tilde{a}\}^T_j$ and $\{\tilde{a}\}^T_i$ and subtraction, there results,

$$\{\tilde{a}\}_j^T [K] \{\tilde{a}\}_i - \{\tilde{a}\}_i^T [K] \{\tilde{a}\}_j = \omega_i^2 \{\tilde{a}\}_j^T [M] \{\tilde{a}\}_i - \omega_j^2 \{\tilde{a}\}_i^T [M] \{\tilde{a}\}_j \tag{153}$$

It is remembered that [K] and [M] are symmetric, therefore,

$$(\omega_i^2 - \omega_j^2) \{\tilde{a}\}_j^T [M] \{\tilde{a}\}_i = 0 \tag{154}$$

Since,

$$(\omega_i^2 - \omega_j^2) \neq 0 \quad then \quad \{\tilde{a}\}_j^T [M] \{\tilde{a}\}_i = 0 \tag{155}$$

When orthogonality is satisfied the roots are said to be distinct. An orthogonality check was performed by GTSTRUDL for each eigenvector solution. It basically determines whether the normalized spectral matrix (diagonalized eigenvalues) adequately represents the original spectral matrix.

It frequently happens in complex systems that the frequencies are "closely spaced" frequencies, that is, cases in which ω_i and ω_{i+1} differ by only 1% or so. It occasionally happens that a system has a repeated frequency, that is, $\omega_i=\omega_{i+1}=\cdots=\omega_{i+p-1}$. A theorem of linear algebra states that if the eigenvalue is repeated "p" times, there will be "p" linearly independent eigenvectors associated with this repeated eigenvalue.[32] Since it is necessary that these eigenvectors be orthogonal to each other, it is possible to choose the eigenvectors such that they will, in fact, satisfy the orthogonality relationships of Eqns. (154) and (155), even though $\omega_i=\omega_j$.

Table 1

Modal Frequencies and Nodal Patterns Obtained by Four Different Methods for an Aluminum Square Plate

	GTSTRUDL				STRUDL			Warburton		Lemke	
#	Modal Frequencies (cps)				Modal Frequencies (cps)			Frequencies		Frequencies	
NOE	16	36	64	Final	16	36	64	(cps)	NP	(cps)	NP
1	.003004	.003163	.003222	.00335	.003315	.003314	.003358	.003471		.003287	
2	.004007	.004399	.004567	.00465	.004776	.004839	.004856	.004846		.004831	
3	.005236	.005678	.005854	.00613	.006221	.006221	.006207	.006175		.006175	
4	.006955	.007771	.008103	.00838	.008632	.008690	.008692	.009000		.015744	
5	.006955	.007771	.008103	.00838	.008632	.008690	.008692	.009000		.017167	
6	.011650	.013410	.014119	.01450	.016000	.015960	.015790	.015420		.019440	
7	.011650	.013410	.014119	.01450	.016000	.015960	.015790	.015420			
8	.011900	.013695	.014536	.01546	.016180	.016150	.016070	.016560			
9			.015380		.017270	.017500	.017460	.017150			
10					.020220	.020310	.020050	.020800			
11					.026430	.026930	.027000	.027260			
12					.026430	.026930	.027000	.027260			
13					.030290	.031620	.031040	.039410			

#-Mode Number, NOE-Number of Elements, Final-Final Convergent Value, NP-Nodal Pattern

Table 2

GTSTRUDL Generated Frequencies and Nodal Patterns with Calculated Modal Mass for Composite Graphite Square Plate

#	Modal Frequencies (rad/sec)								
NOE	9	16	25	36	49	64	144	Final	NP
1	0.046934	0.050378	0.052081	0.053033	0.053616	0.053997	0.054695	0.0547	
2	0.060389	0.067033	0.07104	0.073554	0.075205	0.076337	0.078521	0.0786	
3	0.077307	0.085352	0.089886	0.092611	0.094352	0.095523	0.099731	0.0978	
4	0.101453	0.116159	0.124581	0.129684	0.132955	0.135158	0.139316	0.1393	
5	0.101453	0.116159	0.124581	0.129684	0.132955	0.135158	0.139316	0.1393	
6	0.158895	0.19 382	0.210642	0.220609	0.227476	0.232332	0.242031	0.2425	
7	0.17206	0.19579	0.210642	0.220609	0.227476	0.232332	0.242031	0.2425	
8	0.17206	0.19579	0.215541	0.228453	0.236716	0.242265	0.252681	0.2527	
9			0.225431	0.239665	0.249647	0.256784	0.271207	0.2713	
#	Modal Mass (mass sec^2/in)						Final		
M1	151.492	134.796	128.156	124.857	123.134	121.46	x386(in/sec^2)=4470lbs		
M2	380.736	230.83	226.954	238.059	192.059	175.89	x386(in/sec^2)=6474lbs		
M3	199.273	198.521	131.786	122.634	114.325	111.24	x386(in/sec^2)=4094lbs		

Young's Modulus=40x10^{6}lb/in^2, Poisson's ratio=0.3, Density=0.0542 lb/in^3

#-Mode Number, NOE-Number of Elements, Final-Final Convergent Value, NP-Nodal Pattern

3.5 - Comparison of the Various Methods of Determining the Natural Frequencies

To compare each method a tabulation of each technique's numerical results for a free-free thin aluminum plate appears in Table 1. The natural frequency values calculated by GTSTRUDL are, on an average, 3.96% smaller than the natural frequency values calculated by the other techniques. The shape patterns obtained by the methods GTSTRUDL, STRUDL, and Warburton were exactly the same, whereas, Lemke's patterns were slightly different. After this comparison was made, it was decided GTSTRUDL would be used for the following various reasons:

a) computation time - the time to compute the values is almost limited to the actual time it takes to enter the structure's program file; it also controlled by the number of elements in the system, i.e., the more elements, the larger the stiffness, the longer it takes to compute the eigenvalues. Even with these limitations it still takes GTSTRUDL much less time to compute the eigenvalues than with any other method.

b) convenience - there are two ways in which the GTSTRUDL method is more convenient than the other methods:

   i) The first one is that the actual printed results are much easier to obtain and use than the Warburton and Lemke formulations, i.e., if it is necessary to obtain a modal deflection at any particular point, GTSTRUDL

readily lists the normalized eigenvector at each node (grid point); an interpolation or graphical representation can be easily applied for any points in between the grid points.

ii) The second way is that the GTSTRUDL version, J, is available on Howard University's School of Engineering's Vax 750 & 780 system; STRUDL is available on Howard University's IBM 3090 mainframe. The STRUDL that is available on the mainframe is a very early version of the structural design language; the version of GTSTRUDL available on the VAX is a more recent copy of GTSTRUDL than the STRUDL. Also, the IBM 3090 mainframe computer system is not as user friendly as the Vax 750 & 780 computer systems.

A listing of the GTSTRUDL commands and the program implemented on the VAX 750 appear in Appendix B.

CHAPTER 4 - DEVELOPMENT OF THE STATE SPACE EQUATIONS

Feedback control engineering may be regarded as the conscious, intentional use of the mechanism of feedback to control the behavior of a dynamic process. This aspect of control system engineering is generally called control 'theory'; whereas, the state-space method is considered to be the cornerstone of modern control theory.[33] The advantage of using state-space methods, instead of the frequency-domain approach, is the characterization of the processes of interest by differential equations instead of transfer functions.

In the state-space approach, all the differential equations in the mathematical model of a system are first order equations; only the dynamic variables and their first derivatives (with respect to time) appear in the differential equations. The dynamic variables that appear in the system of first-order equations are called the state variables. The external inputs are called the control variables.

This chapter will encompass the development of the system's constant state and control influence matrices, [A] and [B], respectively, and their relationship to the system's state and control vectors, {X} and {U},

respectively. Once the matrices and vectors are formed, they will be put together to form the general state space equation.[33]

$$\{\dot{X}\} = [A]\{X\} + [B]\{U\} \tag{156}$$

In a linear system the output vector, {Y}, is assumed to be a linear combination of the state and the input,

$$\{Y\} = [C]\{X\} + [D]\{U\} \tag{157}$$

For our system the output is assumed to be completely observable and only a function of the state variables, thus,

$$\{Y\} = [C]\{X\} \tag{158}$$

where [C] is an identity matrix.

Before a complete formulation of the state-space equation can be accomplished, two factors in the completion process must be discussed: actuator placement and modal mass.

4.1 - Discussion of the Actuator Placement

When considering actuator placement, there are two points to consider: (1) orientation control, i.e, providing the most effective control torque; and (2) deformation control, i.e., providing the most efficient actuator force effort to control the shape of the system.

Orientation control is implemented by the control torque vector, $\vec{T}_p$; its mathematical model is represented by the vector cross product of the actuator position vector and the actuator force vector. To acquire the maximum torque in any direction one may either increase the force of each actuator and/or increase the torque arm. Increasing the force that contributes to the control effort may result in an undesirable increase in the energy required. An increased torque arm can be realized by placing the actuators at some maximum distance from the origin; this is plausible as long as these placement positions do not fall on the modal nodal lines (the zero deflection lines of the modal patterns).

This leads to the second consideration, deformation control. Placement of an actuator on a modal nodal line must be avoided. An actuator placed on a nodal line of a particular mode will have no effect in contributing to the deformation control of that mode. Noting that each mode has a nodal line pattern, it is important to accurately determine each mode's pattern shape (see Table 2).

The nodal lines of the first two modes for a thin square plate are easy to locate; unfortunately, the third mode's nodal circle is more difficult. With the use of GTSTRUDL-144 BPR element data, the third mode's eigenvectors -for the nodes located on the midway line of the plate's

major surface~ were plotted. By viewing the plot, (see Figure 5), as a cross-sectional cut midway through the plate, the determination of the nodal circle associated with the third mode can be accurately located.

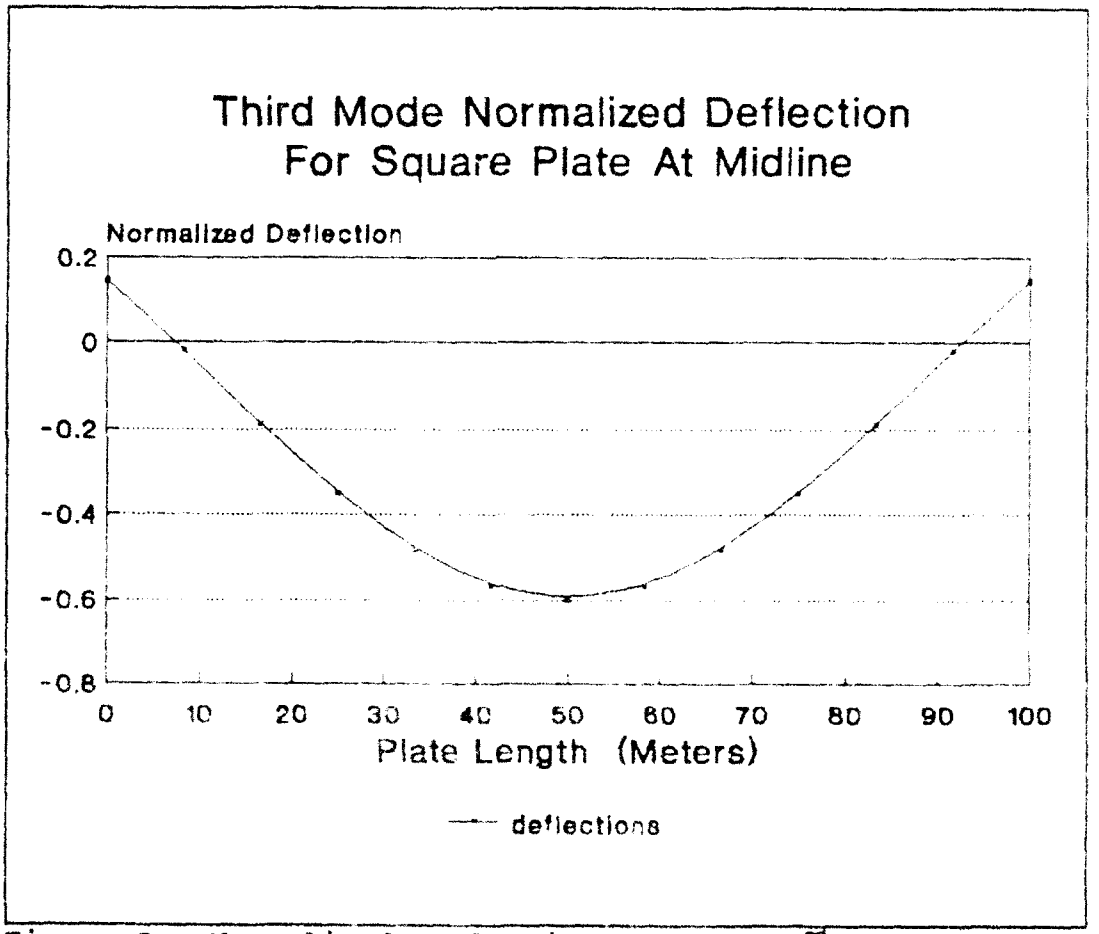

Figure 5. Normalized Deflection Plot for 3rd Mode's Cross-Sectional View

Once the nodal line pattern's were acquired for the first three mode's, a second plot, (see Figure 6), was drawn indicating 3 possible placements of the actuators (i.e., 1,1',1'', etc.). Note, in previous references [18,19] two different sets of actuator positions were studied; these proved to be less effective because of their placement on nodal lines (see Figure 7). Two sets of actuator positions, A & A' have been chosen for this thesis (see Figure 8). Six actuators are assumed to be placed in a symmetrical pattern with both force axis directions perpendicular to the major surface and along the edge of the plate.[26] The first four actuators are assumed to be placed normal to the major surface; they help control the shape deformation and the torque about the two major axes in the plane of the plate. The other two actuators, 5 and 6, are placed along the edge of the plate; they provide control for torque about the third axis, normal to the major surface.

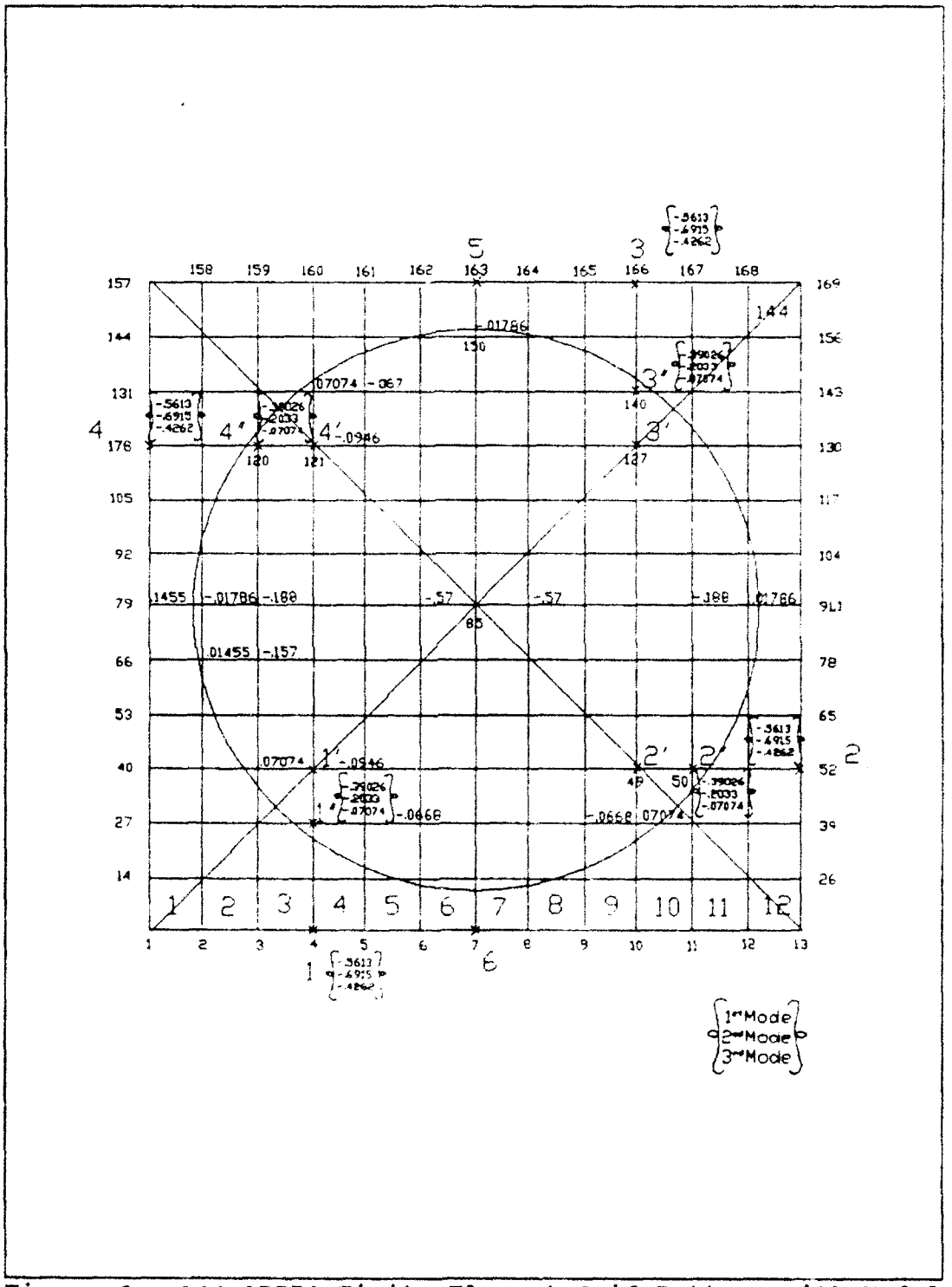

Figure 6. 144 'BPR' Finite Element Grid Pattern with Nodal Deflections for Three Different Sets of Actuator Positions

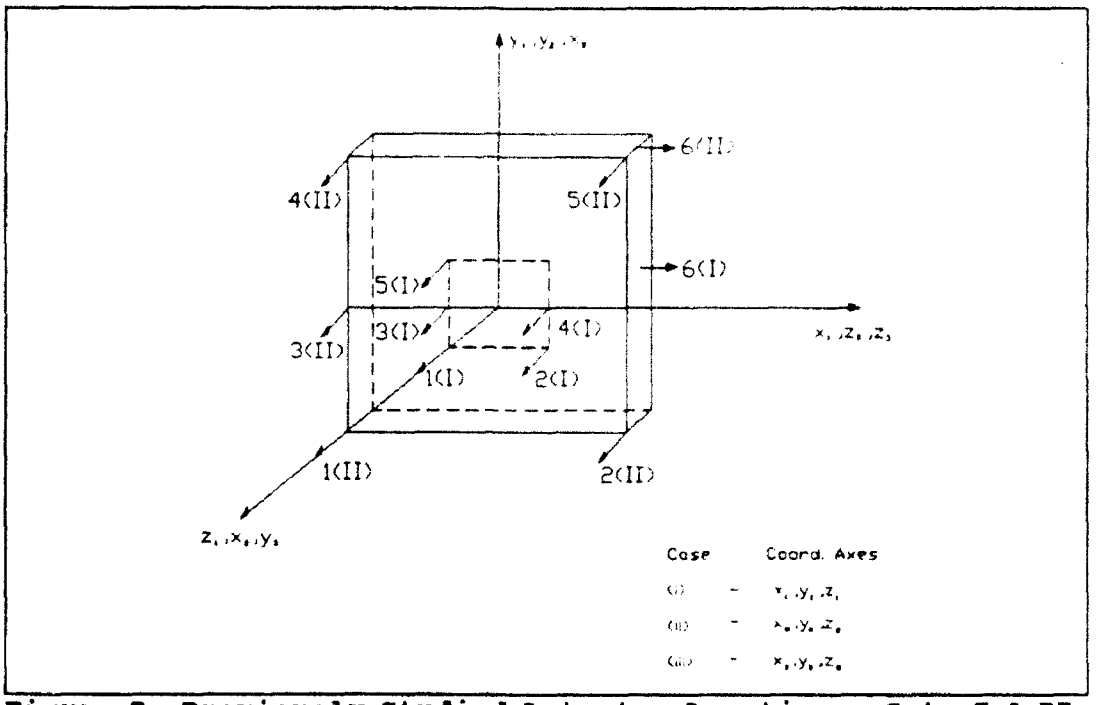

Figure 7. Previously Studied Actuator Locations, Sets I & II

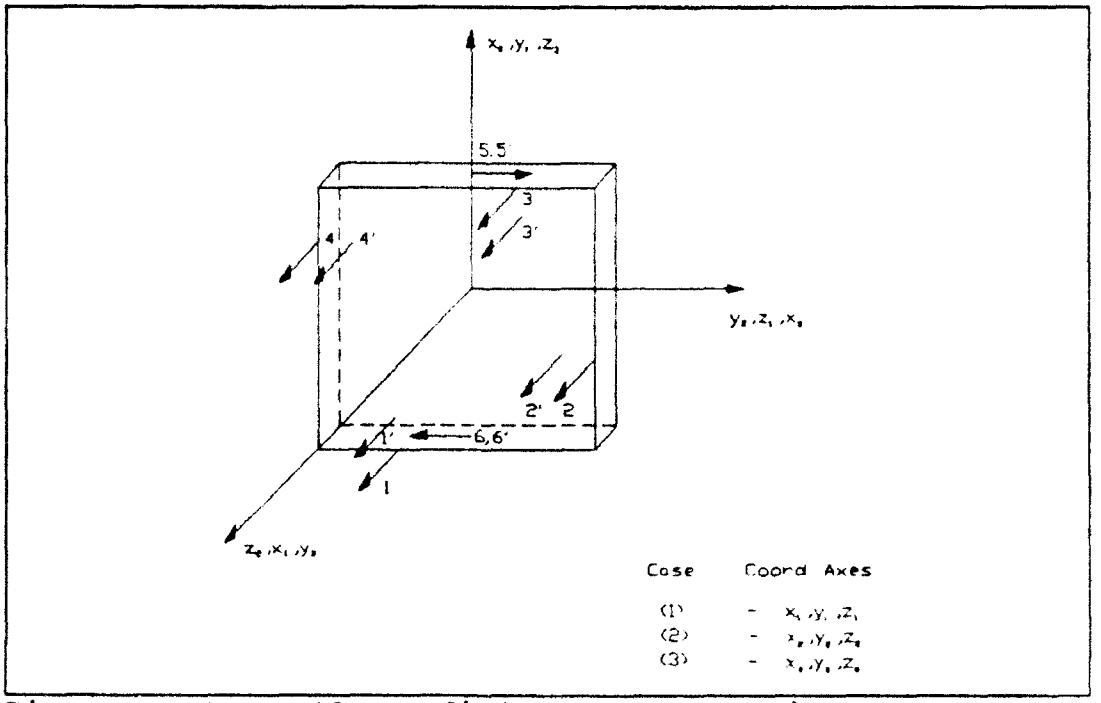

Figure 8. Currently Studied Actuator Locations, Sets A & A'

4.2 - Calculation of the Modal Mass

To calculate the modal mass values, a formulation presented by Hurty and Rubenstien was followed.[34] Using the equation of the form:

$$M_r = \sum_{n=1}^{n.o.e.} \Phi_r^{(n)\,T} M^{(n)} \Phi_r^{(n)} \qquad (159)$$

where r represents the mode number; n represents the gridpoint node; n.o.e. represents the total number of elements; M, represents the mass; and $\vec{\Phi}$ represents the normalized deflection of the grid point (node).

The modal masses were calculated and plotted for the plate modeled by different numbers of assumed finite elements. Figure 9 shows the variation of the modal mass as a function of the number of finite elements assumed to represent the system. The final convergent value was used for the modal mass. The calculated modal masses for the first three modes are, M_1=20,278.65 kg, M_2=29,366,14 kg, and M_3=18572.34 kg.

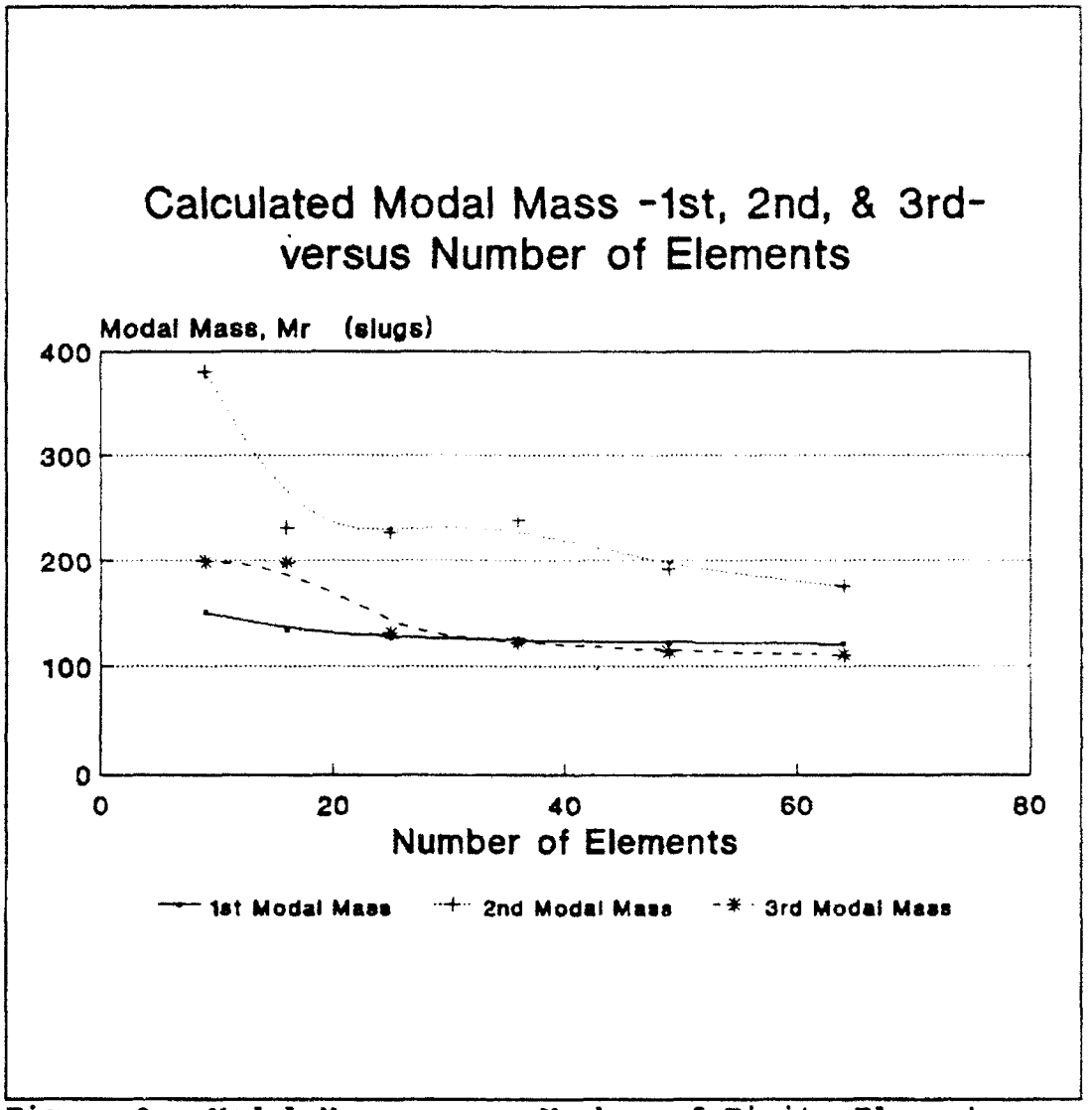

Figure 9. Modal Mass versus Number of Finite Elements

4.3 - Formulation of the System's State Vector and Matrix

With the assumption that the system can be modeled by three rigid-body rotational modes and the first three generic modes, assignment of the correct dynamic variables to the state vector follows. The state vector for this system:

$$\{X\} = [x_1, x_2, x_3, \ldots, x_{12}]^T \tag{160}$$

where the state variables x_n are defined as,

$$\begin{aligned}
&\phi = x_1 \quad \phi' = \frac{d\phi}{d\tau} = \dot{x}_1 = x_7 \\
&\psi = x_2 \qquad \psi' = x_8 \\
&\theta = x_3 \qquad \theta' = x_9 \\
&Z_1 = x_4 \qquad Z_1' = x_{10} \\
&Z_2 = x_5 \qquad Z_2' = x_{11} \\
&Z_3 = x_6 \qquad Z_3' = x_{12}
\end{aligned} \tag{161}$$

Preparation of the system's state matrix through the usage of Eqns. (82-85) follows,

$$[A] = \begin{bmatrix}
\cdot & \cdot & [0]_{6\times6} & \cdot & \cdot & \cdot & \cdot & [I]_{6\times6} & \cdot & \cdot \\
-4\Omega_z & 0 & 0 & 0 & 0 & 0 & 0 & (\Omega_z - 1) & 0 & \cdot \\
0 & -\Omega_x & 0 & 0 & 0 & 0 & (1+\Omega_x) & 0 & \cdots & \cdot \\
0 & 0 & 3\Omega_y & 0 & 0 & 0 & 0 & \vdots & \cdot & \cdot \\
0 & 0 & 0 & 3-\left(\frac{\omega_1}{\omega_c}\right)^2 & 0 & 0 & & 0 & \cdot & \cdot \\
0 & 0 & 0 & 0 & 3-\left(\frac{\omega_2}{\omega_c}\right)^2 & 0 & & & \cdot & \cdot \\
0 & 0 & 0 & 0 & 0 & 3-\left(\frac{\omega_3}{\omega_c}\right)^2 & 0 & 0 & \cdot & 0
\end{bmatrix} \tag{162}$$

With the substitution of the parameters for the nominal orientation of Case (1), (see Figure 2.1): the principal moment of inertias I_x=2.5x10^8 kgm^2, I_y=I_z=1.25x10^8 kgm^2; the angular velocity ω_c=0.0011162 rad/s; and the modal frequencies ω_1=0.0547 rad/s, ω_2=0.07852 rad/s, and ω_3=0.09773 rad/s, the system's state matrix [A], becomes:

$$[A] = \begin{bmatrix} . & . & [0]_{6x6} & . & . & . & . & [I]_{6x6} & & \\ 4 & 0 & 0 & 0 & 0 & 0 & 0 & -2 & 0 \ \dots & 0 \\ 0 & 0 & 0 & 0 & 0 & 0 & 1 & 0 & \dots & . & 0 \\ 0 & 0 & 3 & 0 & 0 & 0 & 0 & \vdots & \ddots & . & \vdots \\ 0 & 0 & 0 & -2398 & 0 & 0 & \vdots & 0 & . & . & 0 \\ 0 & 0 & 0 & 0 & -4945 & 0 & \vdots & \vdots & . & . & \vdots \\ 0 & 0 & 0 & 0 & 0 & -7663 & 0 & 0 & \dots & . & 0 \end{bmatrix} \quad \textbf{(163)}$$

4.4 - Formulation of the System's Control Vector and Matrix

The system's control effort, [B]{U}, is defined by the matrix multiplication of the system control matrix, [B], and the system control (input) vector, {U}. This term in the state-space equation allows for control feedback for the system. The general control influence matrix, [B], is defined as,

$$B = \begin{bmatrix} [0]_{6x6} \\ [B]_{6x6} \end{bmatrix} \quad \textbf{(164)}$$

where the lower part of the [B] matrix depends on the actuator positions. The control effort, [B]{U}, is formulated as such,

$$[B]\{U\} = \begin{bmatrix} [\vec{T}_p/\omega_c^2]_{3x6} \\ [\vec{E}_n/M_n\ell\omega_c^2]_{3x6} \end{bmatrix} \tag{165}$$

where $\vec{T}_p$ represents the external acceleration due to the $p^{\underline{th}}$ actuator; and $\vec{\bar{E}}_n$ represents the external force on the $n^{\underline{th}}$ mode, their formulation is as follows:

$$\vec{T}_p = \vec{N}_p/J \; ; \quad \vec{N}_p = \sum_j \vec{N}_{p_j} = \sum_j \int \vec{r}_p \times \vec{f}_j \, dm \tag{166}$$

$$\vec{r}_p \times \vec{f}_j = \begin{vmatrix} \hat{i} & \hat{j} & \hat{k} \\ x_p & y_p & z_p \\ f_{x_j} & f_{y_j} & f_{z_j} \end{vmatrix} = \hat{i}(f_{z_j}y_p - f_{y_j}z_p) + \hat{j}(f_{x_j}z_p - f_{z_j}x_p) + \hat{k}(f_{y_j}x_p - f_{x_j}y_p) \tag{167}$$

where $\vec{N}_{pj}$ represents the control torque on the $p^{\underline{th}}$ location due to the $j^{\underline{th}}$ actuator; $\vec{r}_p$ represents the position vector from the origin to the $p^{\underline{th}}$ actuator; and $\vec{f}_j$ represents the control force vector due to the $j^{\underline{th}}$ actuator. For the generic modal equations, the control forces can be transformed into the corresponding modal forces by[16]:

$$\vec{E}_{n_j} = \int \vec{\Phi}(\vec{r}_p)^{(n)} \cdot \vec{f}_j \, dm \tag{168}$$

where $\vec{\Phi}^{(n)}(\vec{r}_p)$ represents the modal shape function at the $p^{\underline{th}}$ location corresponding to the $n^{\underline{th}}$ mode.

To define the system control matrix for the nominal orientation of Case (1), it is necessary to establish the

correct position and force vectors for this system. For the actuator sets, A and A', the general position vectors and force vectors are:

$$\begin{aligned} \vec{R}_{1\text{-}4} &= y\hat{j} - z\hat{k} \; ; \quad \vec{f}_{1\text{-}4} = f_x\hat{i} \\ \vec{R}_{5,6} &= y\hat{j} \; ; \qquad \vec{f}_{5,6} = f_z\hat{k} \end{aligned} \tag{169}$$

The angular acceleration produced by each actuator becomes:

$$\begin{aligned} \vec{T}_{1\text{-}4} &= f_x(z\hat{j}/I_y - y\hat{k}/I_z) \\ \vec{T}_{5,6} &= f_z(y\hat{i})/I_x \end{aligned} \tag{170}$$

The lower half of the system control matrix contains external force terms. A definition of the system's modal deflections at each actuator location is necessary, along with the modal mass. Because the actuators are placed in a symmetrical pattern, the deflections for actuators 1-4 are equal in magnitude but alternate in sign. Since actuators 5 and 6 are located on the side of the plate their deflections are assumed to be zero. Thus the control force terms become:

The system's control effort, [B](U), for both sets of actuator locations, A and A', follows:

$$[B]\{U\}_A = \begin{bmatrix} 0 & 0 & 0 & 0 & -.1605 & .1605 \\ -.1605 & .321 & .1605 & -.321 & 0 & 0 \\ -.321 & -.1605 & .321 & .1605 & 0 & 0 \\ -.2221 & .2221 & -.2221 & .2221 & 0 & 0 \\ -.189 & .189 & -.189 & .189 & 0 & 0 \\ .1842 & .1842 & .1842 & .1842 & 0 & 0 \end{bmatrix} \begin{Bmatrix} f_{1_x} \\ f_{2_x} \\ f_{3_x} \\ f_{4_x} \\ f_{5_x} \\ f_{6_x} \end{Bmatrix} \quad (172)$$

$$[B]\{U\}_{A'} = \begin{bmatrix} 0 & 0 & 0 & 0 & -.1605 & .1605 \\ -.1605 & .214 & .1605 & -.214 & 0 & 0 \\ -.214 & -.1605 & .214 & .1605 & 0 & 0 \\ -.1545 & .1545 & -.1545 & .1545 & 0 & 0 \\ -.0555 & .0555 & -.0555 & .0555 & 0 & 0 \\ .0306 & .0306 & .0306 & .0306 & 0 & 0 \end{bmatrix} \begin{Bmatrix} f_{1_x} \\ f_{2_x} \\ f_{3_x} \\ f \\ f_{5_x} \\ f_{6_x} \end{Bmatrix} \quad (173)$$

CHAPTER 5 - PRESENTATION OF LINEAR QUADRATIC OPTIMUM CONTROL THEORY

The main purpose of linear control theory is to design the correct compensator (gains) for the given system. For this thesis an application of optimum control theory will be implemented to synthesize the control law gains.[18,34]

In this chapter, as an optimum control theory algorithm the linear quadratic regulator (LQR) technique was chosen. Initially, the performance criteria is discussed, the system's linear differential equation is solved, and the LQR technique is stated for a continuous-time system. Finally, the sampling period criteria for the discretization of a continuous-time control system is presented; following the sampling period criteria, an application of the LQR technique to a discrete-time system is performed.

5.1 - Discussion of the Performance Criteria or Cost Function

The dynamic process considered here is characterized by the vector-matrix differential equation

$$\dot{x}(t) = A(t)\,x(t) + B(t)\,u(t) \qquad (174)$$

where the variables have been previously defined in Chapter 4. This chapter will seek to define the linear control law

$$u(t) = G_u(t)\, x(t) \tag{175}$$

where G_u is a suitable gain matrix related to u(t). An attempt will be made to find the optimum gain matrix to minimize the performance criterion, J, (or "cost function") expressed as the integral of the quadratic form in the state error, e(t), plus a second quadratic form in the control, u(t); i.e.,

$$J = \frac{1}{2}\langle e(t_f), Fe(t_f)\rangle + \frac{1}{2}\int_{t_o}^{T_f} [\langle e(t), Q(t)\, e(t)\rangle + \langle u(t), R(t)\, u(t)\rangle]\, dt \tag{176}$$

Initially, there are some assumptions to be made.[31]

a) The terminal time, T_f, is specified.

b) F is a constant mxm positive semidefinite matrix.

c) Q(t) is an mxm positive semidefinite matrix.

d) R(t) is an rxr positive definite matrix.

Previously mentioned was the assumption that the system is completely observable, thus C(t)=I. The error vector is defined by

$$e(t) = z(t) - y(t) \tag{177}$$

where z(t) is assumed to be zero. Therefore,

$$-e(t) = y(t) = x(t) \tag{178}$$

Now the control function, J_1, can be designated as,

$$J_1 = \frac{1}{2}\langle x(T_f), Fx(T_f)\rangle + \frac{1}{2}\int_{t_o}^{T_f} [\langle x(t), Q(t)x(t)\rangle + \langle u(t), R(t)u(t)\rangle]\,dt \tag{179}$$

Before an attempt to find the optimum gain matrix, G_u, is made, some comments about the cost function are in order. With respect to the limits on the integral, the lower limit, t_o, is identified as the present time, and the upper limit, T_f, is the terminal time or final time. The time difference, $T_f - t_o$, is the control interval, or 'time-to-go'. If the terminal, T_f, is finite and fixed, the time-to-go keeps decreasing to zero, at which time the control process ends. However, in the customary case, the terminal time is infinite. In this case we are interested in the behavior of the process 'from now on', including the state.

Attention is now focused on the term: $1/2\langle x(T_f), Fx(T_f)\rangle$. This term is often called the terminal cost; its purpose is to guarantee that the final state is small at the terminal time. This should be included in the final state, if $x(T_f)$ is expected to be particularly large. Otherwise, F can be set to zero and the rest of the cost function can be relied upon to guarantee that the terminal state is not excessively large.

Finally, consider the weighting matrices, Q and R. These are often called the state weighting matrix and the control weighting matrix, respectively. A formula for the control gain matrix, G_u, can be derived such that it involves terms of the weighting matrices and the steady solution to the Ricatti matrix equation. By plugging in the matrices Q and R -along with the matrices, A and B, that define the dynamic process- into the computer routine, ORACLS, G_u can be found.[27] If the process is controllable and Q and R are suitable, the computer finds a suitable G_u. This is not to say that the calculation is a trivial problem -far from it- but only that the problem of determining G_u once A, B, Q, and R are given, is not a control design problem but a problem in numerical analysis.

The question of concern to the control system designer is the selection of the weighting matrices, Q and R. In the cost function defined by Eqn. (179), two terms contribute to the integrated cost of the control: the quadratic form x^TQx, represents a penalty on the deviation of the state x, from the origin (this means that the desired state is at the origin, F=0, not at some other state) and the term u^TRu, represents the 'cost of control'. The physical interpretation of J_1 is this: We wish to keep the state near zero without excessive control-energy expenditure.

The weighting matrix, Q, specifies the importance of various components of the state vector relative to each other. For example, suppose x_1 represents the system error, and $x_2,\ldots,x_k$ represents the successive derivatives, i.e.,[33]

$$\begin{aligned} x_1 &= x \\ x_2 &= \dot{x} \\ x_3 &= \ddot{x} \\ &\vdots \\ x_k &= x^{k-1} \end{aligned} \tag{180}$$

If the error and none of its derivatives are of concern, then one might select a state weighting matrix such as:

$$Q = \begin{bmatrix} 1 & 0 & \cdots & 0 \\ 0 & 0 & \cdots & 0 \\ \vdots & \vdots & \ddots & \vdots \\ 0 & 0 & \cdots & 0 \end{bmatrix} \tag{181}$$

which will yield in the quadratic form

$$x^T q x = x_1^2 \tag{182}$$

But the choice of Eqn. (181) as a state weighting matrix may lead to a control system in which the velocity $x_2=\dot{x}$ is larger than desired. To limit the velocity, the performance integral might include a velocity penalty, i.e.,

$$x^T q x = x_1^2 + c^2 x_2^2 \tag{183}$$

which would result from a state weighting matrix

$$Q = \begin{bmatrix} 1 & 0 & \cdots & 0 \\ 0 & c^2 & \cdots & 0 \\ \vdots & \vdots & \ddots & \vdots \\ 0 & 0 & \cdots & 0 \end{bmatrix} \tag{184}$$

The choice of the state weighting matrix, Q, depends on what the system designer is trying to achieve. The considerations of the above with regard to Q apply to the control weighting matrix, R. The term, u^TRu, in the performance index, J_1, is included in an attempt to limit the magnitude of the control signal, u(t). For this thesis, Q and R are chosen to be constant matrices, where

$$Q = \alpha_Q [I]_{mxm} \tag{185}$$

$$R = \alpha_R [I]_{rxr} \tag{186}$$

The relationships between the weighting matrices, Q and R, and the dynamic behavior of the closed loop system depend on the matrices A and B and are quite complex. It is difficult to predict the effect of a given pair of weighting matrices on the system's closed-loop behavior. A suitable approach for the designer would be to solve for the gain matrices that result from a range of the weighting matrices, Q and R, and calculate (or simulate) the corresponding closed loop response. The gain matrix, G_u, that produces the response closest to meeting the design objectives is the ultimate selection. With the ORACLS software, it is a simple matter to solve for G_u given A, B, Q, and R. In a few hours time, the gain matrices and transient response that result for a dozen or more combinations of Q and R can be determined, and a suitable selection of G_u can be made.

5.1.1 - Solution of the Linear Differential Equations in State-Space Form

Starting with the system differential state equation,

$$\dot{x}(t) = Ax(t) + Bu(t) \tag{187}$$

where the matrices A and B, are considered constant matrices, the simplest form of the general differential equation, Eqn. (186) is the homogeneous, i.e., unforced equation

$$\dot{x}(t) = Ax(t) \tag{188}$$

The solution can be expressed as

$$x(t) = ce^{At} \tag{189}$$

where c is a suitably chosen constant vector. To verify Eqn. (189) the derivative is calculated as

$$\frac{dx(t)}{dt} = cAe^{At} = Ax(t) \tag{190}$$

To evaluate the constant, c, suppose that at some time, τ, the state $x(\tau)$, is given as

$$x(\tau) = ce^{A\tau} \tag{191}$$

Multiplying both sides by the inverse of $e^{A\tau}$ leads to

$$c = (e^{A\tau})^{-1}x(\tau) \tag{192}$$

Substitution into the homogeneous solution leads to

$$x(t) = e^{A(t-\tau)}x(\tau) \tag{193}$$

where the matrix $e^{A(t-\tau)}$ is a special form of the state-transition matrix.

Through the use of 'method of variation of the constant', a particular solution to the nonhomogeneous, or 'forced' differential equation is found. Seeking a solution of the form of Eqn. (187) one can select

$$x(t) = e^{At}c(t) \tag{194}$$

where c(t) is a function of time to be determined. After taking the time derivative of x(t) and substituting into Eqn. (185) the following is obtained

$$Ae^{At}c(t) + e^{At}\dot{c}(t) = Ae^{At}c(t) + Bu(t) \tag{195}$$

Upon cancellation of the terms $Ae^{At}c(t)$ and multiplication of the remainder by e^{-At},

$$\dot{c}(t) = e^{-At}Bu(t) \tag{196}$$

Thus, the desired function c(t), can be obtained by simple integration

$$c(t) = \int_{T}^{t} e^{-A\lambda}Bu(\lambda)\,d\lambda \tag{197}$$

The lower limit, T, on this integral is undefined for now; substitution into the particular solution produces

$$x(t) = e^{At}\int_{T}^{t} e^{-A\lambda}Bu(\lambda)\,d\lambda = \int_{T}^{t} e^{A(t-\lambda)}Bu(\lambda)\,d\lambda \qquad (198)$$

The complete solution to Eqn. (187) is obtained by adding the 'complementary solution', Eqn (193), to the particular solution, Eqn. (198). The result is

$$x(t) = e^{A(t-\tau)}x(\tau) + \int_{T}^{t} e^{A(t-\lambda)}Bu(\lambda)\,d\lambda \qquad (199)$$

The proper value for the lower limit, T, on the integral can now be determined. At $t=\tau$, the complete solution becomes

$$x(t) = x(\tau) + \int_{T}^{\tau} e^{A(\tau-\lambda)}Bu(\lambda)\,d\lambda \qquad (200)$$

The integral in Eqn. (200) must be zero for any u(t); this is only possible if $T=\tau$. Therefore, the complete solution to Eqn. (187), when A and B are constant matrices,

$$x(t) = e^{A(t-\tau)}x(\tau) + \int_{\tau}^{t} e^{A(t-\lambda)}Bu(\lambda)\,d\lambda \qquad (201)$$

5.2 - Discretization of a Continuous-Time Control System

When a continuous-time control system with complex poles is discretized, the introduction of sampling may

impair the controllability and observability of the resulting discretized system. That is, pole-zero cancellation may take place in passing from the continuous-time case to the discrete-time case. Thus, the discretized system may lose controllability and observability.

A system which is completely state controllable and observable in the absence of sampling remains completely state controllable and observable after the introduction of sampling, if and only if, for every eigenvalue of the characteristic equation, the relation

$$Re\,\lambda_i - Re\,\lambda_j \tag{202}$$

implies

$$Im\,(\lambda_i - \lambda_j) \neq \frac{2n\pi}{T_s} \tag{203}$$

where λ_i are the eigenvalues of the continuous-time system matrix A; T_s is the sampling period, and $n=\pm1,\pm2,\ldots$[10]

In addition to the forementioned requirement, two points should be taken into consideration when choosing a sampling period:[17]

a) If the sampling interval is too long, the performance of the sampled data system, tends to deteriorate; this makes signal reconstruction difficult.

b) Implementation of a very short sampling interval may be limited by computer operation times and the expense of

fast A/D and D/A converter devices; thus, overtaxation of the computer system with data may result. Therefore, the sampling time should be as large as possible after the performance of a sampled data system meets the requirements of the design. Using the open-loop eigenvalues calculated by ORACLS a table was developed listing unacceptable sampling periods (see Table 3 and 4).

Table 3
Eigenvalues and Moduli for Continuous-Time Open-Loop System Calculated by ORACLS for Orientation of Case (1)

	Continuous Open Loop		
	Eigenvalues		Moduli
	Real	Imaginary	
1	0	0	0
2	0	0	0
3	1.4142	0	1.4142
4	-1.4142	0	1.4142
5	1.7321	0	1.7321
6	-1.7321	0	1.7321
7	0	49.006	49.006
8	0	-49.006	49.006
9	0	70.346	70.346
10	0	-70.346	70.346
11	0	87.556	87.556
12	0	-87.556	87.556

Table 4
Calculation of Unacceptable Sampling Periods from the System Matrix Eigenvalues

i\j	0	-49.00	+49.00	-70.35	+70.35	-87.55	+87.55
0	0	114.8	-114.8	80.00	-80.00	64.23	-64.23
-49.00	-114.8	0	-57.42	263.7	-47.12	145.9	-41.21
+49.00	114.8	57.42	0	47.12	-263.7	41.21	-145.9
-70.35	-80.00	-263.7	-47.12	0	-39.95	327.4	-35.65
+70.35	80.00	47.12	263.7	*39.95	0	35.65	-327.4
-87.55	-64.23	-145.9	-41.21	-327.4	-35.65	0	-32.07
+87.55	64.23	41.21	145.9	35.65	327.4	32.07	0
	all numbers are multiplied by k,				k=+/-1,2,3..		

i - Ith Imaginary Eigenvalue
j - Jth Imaginary Eigenvalue

5.2.1 - The Linear Quadratic Regulator Technique Applied to a Continuous-Time System

Let's begin by considering the linear time-varying system of Eqn. (202),

$$\dot{x}(t) = A(t)\,x(t) + B(t)\,u(t) \qquad (204)$$

the cost function, J_1, given by Eqn. (205),

$$J_1 = \frac{1}{2}\langle x(t_f), Fx(t_f)\rangle + \frac{1}{2}\int_{t_o}^{T_f} [\langle x(t), Q(t)x(t)\rangle + \langle u(t), R(t)u(t)\rangle]\,dt \qquad (205)$$

and the optimal control u(t), is selected such that the cost function is minimized.[9] It is defined as,

$$u(t) = -R^{-1}(t)\,B^{T}(t)\,K(t)\,x(t) \tag{206}$$

where K(t) is a nxn symmetric matrix and is the unique solution of the Ricatti equation[9]

$$\dot{K}(t) = -K(t)A(t) - A^{T}(t)K(t) + K(t)B(t)R^{-1}(t)B^{T}(t)K(t) - Q(t) \tag{207}$$

which satisfies the boundary condition

$$K(T_f) = F \tag{208}$$

The state of the optimal system is then the solution of the linear differential equation

$$\dot{x}(t) = [A(t) - B(t)R^{-1}(t)B^{T}(t)K(t)]\,x(t) \tag{209}$$

The block-diagram representing the optimal control system is displayed in Figure 10.

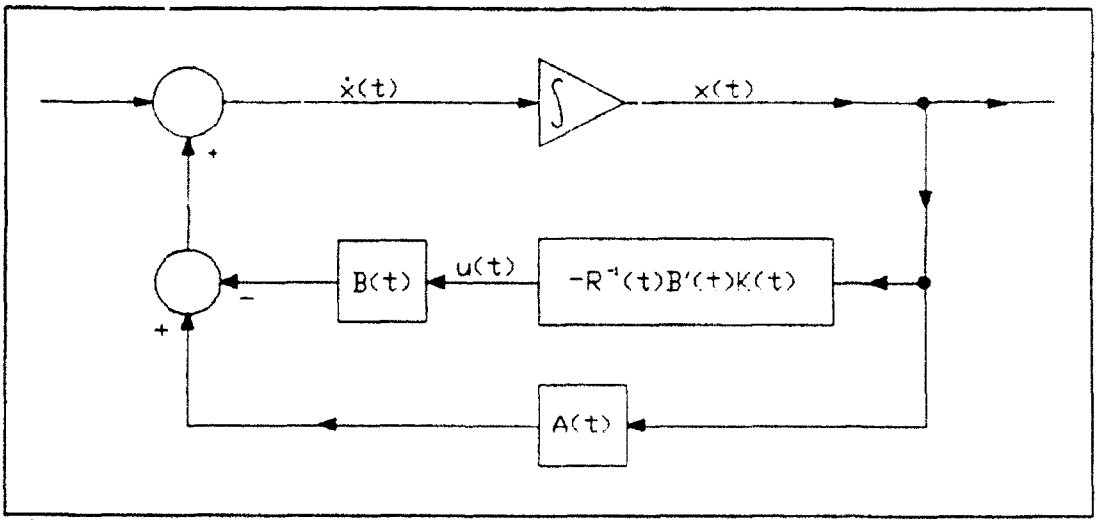

Figure 10. Block Transfer Function of the Optimal Control System

The response, x(t), of the optimal system can now be written as the solution to the differential equation

$$\dot{x}(t) = G(t)\,x(t) \tag{210}$$

where G(t) is an nxn matrix given by

$$G(t) = A(t) - B(t)R^{-1}(t)B^{T}(t)K(t) \tag{211}$$

To find the gain matrix, K(t), a steady state solution of the matrix Ricatti equation (Eqn. (207)) is necessary, when the final time, T_f, approaches infinity; thus, the derivative $\dot{K}(t)=0$, making K(t)=Constant (see boundary conditions, Eqn. (206)). Since the Ricatti equation is nonlinear, closed-form solutions usually cannot be obtained; therefore, K(t) must be computed using a digital computer. For the purposes of this thesis the ORACLS subroutines will be implemented.[27]

ORACLS is a modern control theory design package for constructing controllers and optimal filters for systems modeled by linear time-invariant differential or difference equations. The digital FORTRAN-coded ORACLS system represents an application of some of today's best numerical linear algebra procedures to implement the Linear-Quadratic-Regulator or Guassian methodology of modern control theory. An example of the simulation program which incorporates various ORACLS subroutines has been placed in Appendix D.

One important thing to realize is that the gain matrix, K(t), is independent of the state, so that once the system and the cost, J_1, have been specified, K(t) can be computed before the optimal system starts to operate.

5.2.2 - Formulation of the Linear Quadratic Regulator Technique Subject to a Discrete-Time Domain

Consider the continuous time control system

$$\dot{x}(t) = Ax(t) + Bu(t) \tag{212}$$

subject to

$$J = \frac{1}{2}x^T(t_f)Fx(t_f) + \frac{1}{2}\int_0^T [x^T(t)Qx(t) + u^T(t)Ru(t)]\,dt \tag{213}$$

If the continuous-time control system is approximated by its discrete equivalent, the sampling period T_s, can be represented as

$$\tau = kT_s, \quad k=0,1,2,\ldots,N \tag{214}$$

thus, its discrete equivalent becomes,

$$x((k+1)T_s) = G(T_s)\,x(kT_s) + H(T_s)\,u(kT_s) \tag{215}$$

and the discretized performance index, when the final time $T_f=NT_s$, becomes:[10]

$$\begin{aligned} J = \frac{1}{2}x^T(NT_s)Fx(NT_s) + \frac{1}{2}\sum_{k=0}^{N-1} [x^T(kT_s)Q_1x(kT_s) \\ + 2x^T(kT_s)M_1u(kT_s) + u^T(kT_s)R_1u(kT_s)] \end{aligned} \tag{216}$$

It is noted that the integral term in Eqn. (213) is not replaced by

$$\frac{1}{2}\sum_{k=0}^{N-1}\left[x^T(kT_s)Qx(kT_s)+u^T(kT_s)Ru(kT_s)\right] \qquad (217)$$

but is modified to include a cross term involving $x(kT_s)$ and $u(kT_s)$. Also, matrices Q and R are modified. By considering the discretized quadratic optimal control problem by use of a simple example -similar to the system considered in section 5.1.1- the terms Q_1, M_1, and R_1 are developed.

Consider the continuous-time system defined by

$$\dot{x}(t)=Ax(t)+Bu(t) \qquad (218)$$

where A and B are constant matrices and

$$u(t)=u(kT_s), \quad kT_s\le t\le (k+1)T_s \qquad (219)$$

The performance index to be minimized is

$$J=\frac{1}{2}x^2(NT_s)+\frac{1}{2}\int_0^{NT_s}\left[Qx^2(t)+Ru^2(t)\right]dt \qquad (220)$$

To begin, the system equation and performance index must be transformed to a discrete-time domain; afterwards the discretized quadratic optimal control problem can be formulated. Equation (218) may be discretized as follows:

$$x((k+1)T_s)=G(T_s)\,x(kT_s)+H(T_s)\,u(kT_s) \qquad (221)$$

where,

$$G(T_s) = e^{AT_s} \tag{222}$$

$$H(T_s) = \int_0^{T_s} e^{A(T_s-\tau)} B\,d\tau = \frac{B}{A}\left(e^{AT_s}-1\right) \tag{223}$$

or

$$x((k+1)T_s) = e^{AT_s}x(kT_s) + \frac{B}{A}\left(e^{AT_s}-1\right)u(kT_s) \tag{224}$$

The performance index, J, given by Eqn. (220) may be discretized. First rewrite J as

$$J = \frac{1}{2}x^2(NT_s) + \frac{1}{2}\sum_{k=0}^{N-1}\int_{kT_s}^{(k+1)T_s}\left[Qx^2(t) + Ru^2(t)\right]dt \tag{225}$$

Noting that the solution x(t) for $kT_s \le t \le (k+1)T_s$ can be written as

$$\begin{aligned} x(t) &= e^{A(t-kT_s)}x(kT_s) + \int_{kT_s}^{t} e^{A(t-\tau)}Bu(\tau)\,d\tau \\ &= \xi(t-kT_s)x(kT_s) + \eta(t-kT_s)u(kT_s) \end{aligned} \tag{226}$$

where,

$$\xi(t-kT_s) = e^{A(t-kT_s)} \tag{227}$$

$$\eta(t-kT_s) = \int_{kT_s}^{t}\xi(t-\tau)B\,d\tau = \frac{B}{A}\left[e^{A(t-kT_s)}-1\right] \tag{228}$$

The performance index J_1 can be written as follows

$$\begin{aligned} J = & \frac{1}{2}x^2(NT_s) + \frac{1}{2}\sum_{k=0}^{N-1}\int_{kT_s}^{(k+1)T_s}\{Q[\xi(t-kT_s)x(kT_s) \\ & + \eta(t-kT_s)u(kT_s)]^2 + Ru^2(kT_s)\}dt \\ & - \frac{1}{2}x^2(NT_s) + \frac{1}{2}\sum_{k=0}^{N-1}[Q_1x^2(kT_s) + 2M_1x(kT_s)u(kT_s) + R_1u^2(kT_s)] \end{aligned} \tag{229}$$

where,

$$Q_1 = \int_{kT_s}^{(k+1)T_s} Q\xi^2(t-kT_s)\,dt \tag{230}$$

$$M_1 = \int_{kT_s}^{(k+1)T_s} Q\xi(t-kT_s)\eta(t-kT_s)\,dt \tag{231}$$

$$R_1 = \int_{kT_s}^{(k+1)T_s} [Q\eta^2(t-kT_s) + R]\,dt \tag{232}$$

Notice that Q_1, M_1, and R_1 may be simplified as follows:

$$Q_1 = \int_{kT_s}^{(k+1)T_s} Qe^{2A(t-kT_s)}\,dt = \frac{Q}{2A}[e^{2AT_s} - 1] \tag{233}$$

$$M_1 = \int_{kT_s}^{(k+1)T_s} Qe^{A(t-kT_s)}\frac{B}{A}[e^{A(t-kT_s)} - 1]\,dt = \frac{BQ}{2A^2}(e^{AT_s} - 1)^2 \tag{234}$$

$$\begin{aligned} R_1 = & \int_{kT_s}^{(k+1)T_s}\left[Q\left\{\frac{B}{A}[e^{A(t-kT_s)} - 1]\right\}^2 + R\right]dt \\ & - \frac{B^2Q}{2A^2}[(e^{AT_s} - 3)(e^{AT_s} - 1) + 2AT_s] + RT_s \end{aligned} \tag{235}$$

Summarizing, the present discretized quadratic optimal control problem may be stated as follows. Given the discretized system equation

$$x((k+1)T_s) = G(T_s)\,x(kT_s) + H(T_s)\,u(kT_s) \qquad (236)$$

where,

$$G(T_s) = e^{AT_s} \quad and \quad H(T_s) = \frac{B}{A}(e^{AT_s} - 1) \qquad (237)$$

find the optimal control sequence, $u(0)$, $u(T_s)$,...,$u((N-1)T_s)$ such that the following performance index is minimized

$$J = \frac{1}{2}x^2(NT_s) + \frac{1}{2}\sum_{k=0}^{N-1}\left[Q_1 x^2(kT_s) + 2M_1 x(kT_s)\,u(kT_s) + R_1 u^2(kT_s)\right] \qquad (238)$$

Such a performance index including a cross term involving $x(kT_s)$ and $u(kT_s)$ can be modified to a form that does not include a cross term, and the solution to the discretized quadratic optimal control problem can then be obtained. This subject is presented in the following.

Taking into consideration the quadratic optimal control problem, where the system is given by

$$x(k+1) = Gx(k) + Hu(k) \;, \quad x(0) = c \qquad (239)$$

and the performance index is given by

$$J = \frac{1}{2}x^T(N)\,Fx(N) + \frac{1}{2}\sum_{k=0}^{N-1}\left[x^T(k)\,Q_1 x(k) + 2x^T(k)\,M_1 u(k) + u^T(k)\,R_1 u(k)\right] \qquad (240)$$

where Q_1 and F are nxn positive definite or semidefinite Hermitian matrices, R_1 is an rxr positive definite Hermitian matrix, and M is an nxr matrix such that the matrix

$$\begin{bmatrix} Q_1 & M_1 \\ M_1^T & R_1 \end{bmatrix} \tag{241}$$

is positive definite. This means that

$$\begin{aligned} &[x^T(k) \quad u^T(k)]\begin{bmatrix} Q_1 & M_1 \\ M_1^T & R_1 \end{bmatrix}\begin{bmatrix} x(k) \\ u(k) \end{bmatrix} \\ &= x^T(k)Q_1x(k) + x^T(k)M_1u(k) + u^T(k)M_1^Tx(k) + u^T(k)R_1u(k) \\ &= x^T(k)Q_1x(k) + 2x^T(k)M_1u(k) + u^T(k)R_1u(k) \end{aligned} \tag{242}$$

is positive definite. Note that the performance index, J, of Eqn. (240) includes a cross-term similar to Eqn. (242).

In order to obtain the optimal control vector u(k), let us define

$$\hat{Q} = Q_1 - M_1R_1^{-1}M_1^T \tag{243}$$

and eliminate Q from the performance index J. Then Eqn.(240) becomes

$$\begin{aligned} J &= \frac{1}{2}x^T(N)Fx(N) + \frac{1}{2}\sum_{k=0}^{N-1}\{x^T(k)[\hat{Q}_1 + M_1R_1^{-1}M_1^T]x(k) \\ &\quad + 2x^T(k)M_1u(k) + u^T(k)R_1u(k)\} \\ &= \frac{1}{2}x^T(N)Fx(N) + \frac{1}{2}\sum_{k=0}^{N-1}[x^T(k)\hat{Q}x(k) + x^T(k)M_1R_1^{-1}M_1^Tx(k) \\ &\quad + 2x^T(k)M_1u(k) + u^T(k)R_1u(k)] \\ &= \frac{1}{2}x^T(N)Fx(N) + \frac{1}{2}\sum_{k=0}^{N-1}\{x^T(k)\hat{Q}x(k) \\ &\quad + [x^T(k)M_1R_1^{-1} + u^T(k)]R_1[R_1^{-1}M_1^Tx(k) + u(k)]\} \end{aligned} \tag{244}$$

Define

$$v(k) = R_1^{-1} M_1^T x(k) + u(k) \tag{245}$$

such that

$$J = \frac{1}{2} x^T(N) F x(N) + \frac{1}{2} \sum_{k=0}^{N-1} [x^T(k) \hat{Q} x(k) + v^T(k) R_1 v(k)] \tag{246}$$

Notice that Eqn. (246) no longer involves the cross term; it has been effectively eliminated.

By substituting Eqn. (245) into the system equation, Eqn. (239) becomes

$$\begin{aligned} x(k+1) &= Gx(k) + H[v(k) - R_1^{-1} M_1^T x(k)] \\ &= (G - HR_1^{-1} M_1^T) x(k) + Hv(k) \\ &= \hat{G} x(k) + Hv(k) \end{aligned} \tag{247}$$

where,

$$\hat{G} = G - HR_1^{-1} M_1^T \tag{248}$$

Note that the quadratic optimal control of the system given by Eqn. (239) with the performance index given by Eqn. (240) is equivalent to the quadratic optimal control of the system given by Eqn. (247) with the performance index given by Eqn.(246). Hence, the optimal control vector v(k), that minimizes the performance index given by Eqn. (246) can be given as follows. Defining

$$v(k) = -[R_1 + H^T \hat{P}(k+1) H]^{-1} H^T \hat{P}(k+1) \hat{G} x(k) \tag{249}$$

where $\hat{P}(k)$ is a modified version of the Ricatti Equation.

$$\hat{P}(k) = \hat{Q} + \hat{G}^T \hat{P}(k+1) \left[I + H R_1^{-1} H^T \hat{P}(k+1) \right]^{-1} \hat{G} \qquad (250)$$

$$\hat{P}(N) = F \qquad (251)$$

The optimal control vector, u(k), can then be given by

$$u(k) = v(k) - R_1^{-1} M_1^T x(k) \qquad (252)$$

where v(k) is given in Eqn. (249), Eqn.(252) can be reduced to the following form:

$$u(k) = -\left[R_1 + H^T \hat{P}(k+1) H \right]^{-1} \left[H^T \hat{P}(k+1) G + M_1^T \right] x(k) \qquad (253)$$

5.3 - Solution by the Conventional Minimization Method Using Lagrange Multiplier

In the present optimization problem, the minimization of J given by Eqn. (246), repeated here

$$J = \frac{1}{2} x^T(N) F x(N) + \frac{1}{2} \sum_{k=0}^{N-1} \left[x^T(k) \hat{Q} x(k) + v^T(k) R_1 v(k) \right] \qquad (254)$$

when it is subject to the constraint equation specified by Eqn. (247)

$$x(k+1) = \hat{G} x(k) + H v(k) \qquad (255)$$

with the initial condition on the state vector

$$x(0) = c \tag{256}$$

is considered by using a set of Lagrange multipliers $\lambda(1), \lambda(2), \ldots, \lambda(N)$; the new performance index L can be defined as follows:

$$L = \frac{1}{2} x^T(N) F x(N) + \frac{1}{2} \sum_{k=0}^{N-1} \{ [x^T(k) \hat{Q} x(k) + v^T(k) R_1 v(k)] + \lambda^T(k+1) \cdot [\hat{G} x(k) + H v(k) - x(k+1)] + [\hat{G} x(k) + H v(k) - x(k+1)]^T \lambda(k+1) \} \tag{257}$$

It is a well known fact that minimization of the function L is equivalent to minimization of J when it is subject to the equality defined by Eqn. (255). In order to minimize the function L, one must differentiate L with respect to each component of the vectors x(k), v(k), and λ(k) and set the results equal to zero. Thus we set

$$\frac{\partial L}{\partial x_i(k)} = 0 \qquad i = 1, 2, \ldots, n \; ; \quad k = 1, 2, \ldots, N \tag{258}$$

$$\frac{\partial L}{\partial v_i(k)} = 0 \qquad i = 1, 2, \ldots, r \; ; \quad k = 1, 2, \ldots, N-1 \tag{259}$$

$$\frac{\partial L}{\partial \lambda_i(k)} = 0 \qquad i = 1, 2, \ldots, n \; ; \quad k = 1, 2, \ldots, N \tag{260}$$

Dropping the subscript for simplicity, Eqns. (258), (259), and (260) may be obtained as follows:

$$\frac{\partial L}{\partial x(k)} = 0 \qquad \hat{Q} x(k) + \hat{G}^T \lambda(k+1) - \lambda(k) = 0 \quad k = 1, 2, \ldots, N-1 \tag{261}$$

$$\frac{\partial L}{\partial x(N)} = 0 \qquad Fx(N) - \lambda(N) = 0 \tag{262}$$

$$\frac{\partial L}{\partial v(k)} = 0 \qquad R_1 v(k) + H^T \lambda(k+1) = 0 \qquad k = 0, 1, \ldots, N-1 \tag{263}$$

$$\frac{\partial L}{\partial \lambda(k)} = 0 \qquad \hat{G}x(k-1) + Hv(k-1) - x(k) = 0 \qquad k = 1, 2, \ldots, N \tag{264}$$

After the simplification of the equations just obtained, there results,

$$\lambda(k) = \hat{Q}x(k) + \hat{G}^T \lambda(k+1) \qquad k = 1, 2, \ldots, N-1 \tag{265}$$

with the final condition

$$\lambda(N) = Fx(N) \tag{266}$$

Rearrangement of the terms of Eqn. (263) leads to the solution of v(k)

$$v(k) = -R_1^{-1} H^T \lambda(k+1) \tag{267}$$

The last partial differential Eqn. (264) is simply the state equation (see Eqn. (255)). Substitution of Eqn. (267) into Eqn. (255) results in

$$x(k+1) = \hat{G}x(k) - HR_1^{-1} H^T \lambda(k+1); \qquad x(0) = c \tag{268}$$

In order to obtain the solution to the minimization problem we need to solve Eqns. (265) and (268) simultaneously. Notice for the system equation, Eqn. (268), the initial condition is specified, while for the Lagrange multiplier equation, Eqn. (265), the final condition is specified. Thus the problem here becomes a two-point boundary value problem

(TPBVP). If the TPBVP is solved, then the optimal values for the state vector and Lagrange multiplier vector may be determined and the optimal control vector, v(k) may be obtained in the open-loop form. However, if one employs the Ricatti transformation, the optimal control vector, v(k), can be obtained in the following closed-loop or feedback form:

$$v(k) = -G_u(k)\,x(k) \tag{269}$$

where $G_u(k)$ is the rxn feedback matrix.

Under the assumption that $\lambda(k)$ can be written in the following form

$$\lambda(k) = \hat{P}(k)\,x(k) \tag{270}$$

where $\hat{P}(k)$ is an nxn Hermitian matrix (see Eqn. (250)). Substitution of Eqn. (270) into Eqn. (261) results in

$$\hat{P}(k)\,x(k) = \hat{Q}x(k) + G^T\hat{P}(k+1)\,x(k+1) \tag{271}$$

and substitution of Eqn. (270) into Eqn. (268) gives

$$x(k+1) = \hat{G}x(k) - HR_1^{-1}H^T\hat{P}(k+1)\,x(k+1) \tag{272}$$

Notice that Eqns. (271) and (272) do not involve $\lambda(k)$ and thus $\lambda(k)$ has been effectively eliminated. The transformation process employed here is called the Ricatti transformation. It is of extreme importance in solving such a TPBVP. From Eqn. (272)

$$[I+HR_1^{-1}H^T\hat{P}(k+1)]\,x(k+1)=\hat{G}x(k) \tag{273}$$

because of the existence of the inverse matrix, Eqn.(273) can be written as

$$x(k+1)=[I+HR_1^{-1}H^T\hat{P}(k+1)]^{-1}\hat{G}x(k) \tag{274}$$

By substituting Eqn. (274) into Eqn. (271) one obtains

$$\hat{P}(k)=\hat{Q}+\hat{G}^T\hat{P}(k+1)\,[I+HR_1^{-1}H^T\hat{P}(k+1)]^{-1}\hat{G} \tag{275}$$

Equation (275) is the same as Eqn. (250), it may be modified to

$$\hat{P}(k)=\hat{Q}+\hat{G}^T\hat{P}(k+1)\hat{G}-\hat{G}^T\hat{P}(k+1)H[R_1+H^T\hat{P}(k+1)H]^{-1}H^T\hat{P}(k+1)\hat{G} \tag{276}$$

Equation (276) is called the Ricatti equation. Referring to Eqn. (262) notice at k=N

$$\begin{aligned}&\hat{P}(N)x(N)=\lambda(N)=Fx(N)\\ &\therefore\\ &\hat{P}(N)=F\end{aligned} \tag{277}$$

Hence, Eqns. (275) and (276) can be solved uniquely backward from k=N to k=0. So one can obtain P(N), P(N-1),..., P(0) starting from P(N) which is known. By referring to Eqns. (270) and (274), the optimal control vector, v(k) given by Eqn. (267) now becomes

$$\begin{aligned}v(k)&=-R_1^{-1}H^T\hat{P}(k+1)x(k+1)\\ &=-R_1^{-1}H^T\hat{P}(k+1)\,[I+HR_1^{-1}H^T\hat{P}(k+1)]^{-1}\hat{G}x(k)\end{aligned} \tag{278}$$

A modified form of the optimal control vector, v(k) can be given by

$$v(k) = -[R_1 + H^T \hat{P}(k+1)\, H]^{-1} H^T \hat{P}(k+1)\, \hat{G} x(k) \qquad (279)$$

the same as Eqn. (249)

5.3.1 - Evaluation of the Minimum Performance Index

Evaluation of the minimum performance index given by Eqn. (254) follows

$$J_{min} = \min \left\{ \frac{1}{2} x^T(N) F x(N) + \frac{1}{2} \sum_{k=0}^{N-1} [x^T(k) \hat{Q} x(k) + v^T(k) R_1 v(k)] \right\} \qquad (280)$$

Premultiplying both sides of Eqn. (271) by $x^T(k)$ gives

$$x^T(k) \hat{P}(k) x(k) = x^T(k) \hat{Q} x(k) + x^T(k) G^T \hat{P}(k+1)\, x(k+1) \qquad (281)$$

Substituting Eqn. (273) and arranging terms leads to

$$x^T(k) \hat{P}(k) x(k) - x^T(k) \hat{Q} x(k) + x^T(k+1) [I + \hat{P}(k+1) H R_1^{-1} H^T] \hat{P}(k+1) x(k+1) \qquad (282)$$

Hence,

$$x^T(k) \hat{Q} x(k) = x^T(k) \hat{P} x(k) - x^T(k+1) \hat{P}(k+1) x(k+1) + - x^T(k+1) \hat{P}(k+1) H R_1^{-1} H^T \hat{P}(k+1) x(k+1) \qquad (283)$$

Similarly, from Eqn. (278)

$$v(k) = -R_1^{-1} H^T \hat{P}(k+1) x(k+1) \qquad (284)$$

Hence,

$$v^T(k) R_1 v(k) = [-x^T(k+1)\hat{P}(k+1)HR_1^{-1}]\, R_1\, [-R_1^{-1}H^T\hat{P}(k+1)x(k+1)] - x^T(k+1)\hat{P}(k+1)HR_1^{-1}H^T\hat{P}(k+1)x(k+1) \quad (285)$$

By adding Eqns. (283) and (285)

$$x^T(k)\hat{Q}x(k) + v^T(k)R_1 v(k) - x^T(k)\hat{P}x(k) - x^T(k+1)\hat{P}(k+1)x(k+1) \quad (286)$$

By substituting Eqn. (286) into Eqn. (280) one obtains

$$\begin{aligned} J_{min} &= \frac{1}{2}x^T(N)Fx(N) + \frac{1}{2}\sum_{k=0}^{N-1}[x^T(k)\hat{P}(k)x(k) - x^T(k+1)\hat{P}(k+1)x(k+1)] \\ &= \frac{1}{2}x^T(N)Fx(N) + \frac{1}{2}[x^T(0)\hat{P}(0)x(0) - x^T(1)\hat{P}(1)x(1) + x^T(1)\hat{P}(1) \\ &\quad - x^T(2)\hat{P}(2)x(2) + \ldots + x^T(N-1)\hat{P}(N-1)x(N-1) - x^T(N)\hat{P}(N)x(N)] \\ &= \frac{1}{2}x^T(N)Fx(N) + \frac{1}{2}x^T(0)\hat{P}(0)x(0) - \frac{1}{2}x^T(N)\hat{P}(N)x(N) \end{aligned} \quad (287)$$

Notice from Eqn. (277) $\hat{P}(N)=F$. Hence, Eqn. (287) becomes

$$J_{min} = \frac{1}{2}x^T(0)\hat{P}(0)x(0) \quad (288)$$

Thus, the minimum value of the performance index J is given by Eqn. (280). It is a function of $\hat{P}(0)$ and the initial state, x(0).

CHAPTER 6 - RESULTS AND DISCUSSION

For this thesis three different comparisons have been analyzed for the nominal orientation of Case (1). The first is a comparison of two sets of actuator locations (see Fig. 8), this will provide the most effective placement of the actuators. The second is a parametric study involving the state penalty matrix and the control penalty matrix (see Eqns. (185) and (186)), this will yield the best choice of penalty matrices under the given conditions. The last comparison is also a parametric study, through the variance of the sampling period (see Section 5.2) a display of its effect on the system performance will be produced. Together these three comparisons will result in the design of the optimum control system.

For each comparison three different system characteristics will be analyzed. The first characteristic is the discretized open and/or closed loop system eigenvalue and their moduli. In a z-domain the system's eigenvalues or moduli should display the following characteristics:

a) the magnitude should be less than 1 to ensure stability of the system.

b) the magnitude should be as small as possible. The system with the smaller eigenvalues usually displays the better system response.

The second analysis is the tabulation of the calculated optimum cost function (see Section 5.3.1). The optimum cost function -also known as the minimum performance index- is calculated through the minimization of the cost function, therefore, the obvious selection for an optimum system is the smallest possible value of $x_o^T P_o x_o$.

The transient time response of the rotational angles, modal amplitudes, and the control forces of each actuator is the third system characteristic investigated. A transient response refers to the process generated in going from an initial state to the final state.[35] Consideration is giving to several elements of the transient response, they are:

a) the maximum overshoot or undershoot which is directly related to the robustness of the system. In the case of the modal amplitudes, the response is due to an initial normalized deflection of 0.01, which corresponds to a 1 meter deflection. If the response overshoot or undershoot is too high, internal stresses may reach a maximum resulting in fracture or failure of the structure. In reference to the forces, a large initial overshoot is associated with the maximum amplitude of the control force

b) the area under the response curves is being investigated. When comparing the rotational angle response there is no overshoot or undershoot. The

system is subjected to an initial angular deflection of 0.01 radian. The area under this response and the tangential envelopes created by the other responses is proportional to the control energy dissipated; therefore, the overshoot and the area should be as small as possible.

c) the rise time is the time required for the response initially to reach the equilibrium value during the first cycle of the response.

d) the peak time is the time it takes the response to reach the first peak of an overshoot or undershoot.

e) the settling time is an important characteristic to take into consideration. The settling time is the point in time when the response curve reaches and stays within 5% of the equilibrium value of the system's response. Hence, one would prefer this duration of time to be as short as possible.

f) the signal reconstruction is one other system characteristic which is especially important in the comparison of the sampling periods. The transient time response should appear as smooth as possible, thus exhibiting a proper signal reconstruction.

In the subsequent sections of Chapter 6, three comparative studies will be discussed.

6.1 - Comparison of Actuator Positions

For the comparison of the actuator locations, two sets have been chosen, Set A and A' (see Fig. 8). The nominal orientation of Case (1), with a sampling period of 5 seconds, and the set of penalty matrices Sq=0.5 and $Sr=1.0x10^{-10}$ is selected as the standard system.

The system's closed-loop eigenvalues and optimum cost functions are displayed in Table 5. Notice that the minimum modulus and the overall average modulus of Set A eigenvalues are smaller than those for Set A'. The optimum cost function is smaller for Set A than Set A'.

Upon inspection of the transient time responses, it is seen that the response for the rotational angles are exactly the same (see Figs. 11 and 12). The responses for the first and second modal amplitude are quite different. On the other hand, the third mode's amplitudal responses are exactly the same (see Fig. 13). Set A' first mode has a higher overshoot and a much larger settling time than that of Set A. Similarly, the second mode has a larger overshoot, undershoot, curve area, rise time, peak time, and settling time for Set A' than for Set A. The same follows for the transient responses of the forces for actuators 1-4 (see Figs. 14 and 15). The actuators 5 and 6 are in the same

position for both sets; thus, there isn't any difference in transient time response for the two actuator forces (see Fig. 16). Also, notice the symmetry of response for the actuator groups 1 & 3, 2 & 4, and 5 & 6. This is due to the fact that the actuators are placed in a symmetrical pattern around the center of the plate (origin).

The choice between actuator location sets is an easy one. Obviously, the system of Set A exhibits the best characteristics. This is an expected result for a couple of reasons. The first is: the torque arm is a maximum for Set A, thus, reducing the maximum force needed to control its rigid rotational motion. The second is: Most of the Set A' actuators are placed in the vicinity of the nodal lines -for the first three modes included in the system model- thus, possibly reducing their overall effect.

Table 5
The Effect of Different Actuator Locations on the Closed-Loop System Eigenvalues and Moduli

	Set A			**Set A'**		
	Eigenvalues		Moduli	Eigenvalues		Moduli
	Real	Imag.		Real	Imag.	
1	0.20871	0	0.20871	0.20872	0	0.20872
2	0.20873	.00177	0.20873	0.20873	.00174	0.20874
3	0.20873	-.00177	0.20873	0.20873	-.00174	0.20874
4	0.22710	0	0.22710	0.22273	0	0.22273
5	0.25698	0	0.25698	0.26381	0	0.26381
6	0.79820	0	0.79820	0.79575	0	0.79575
7	0.92454	0	0.92454	0.93528	0	0.93528
8	0.88714	.36217	0.9452	0.89757	.36118	0.96752
9	0.88714	-.36217	0.9452	0.89757	-.36118	0.96752
10	0.99443	0	0.99443	0.99443	0	0.99443
11	0.99443	0	0.99443	0.99443	0	0.99443
12	0.99443	0	0.99443	0.99443	0	0.99443
	$X_o^T P_o X_o$=0.0086919			$X_o^T P_o X_o$=0.018983		

$X_o^T P_o X_o$ - Optimum Cost Function

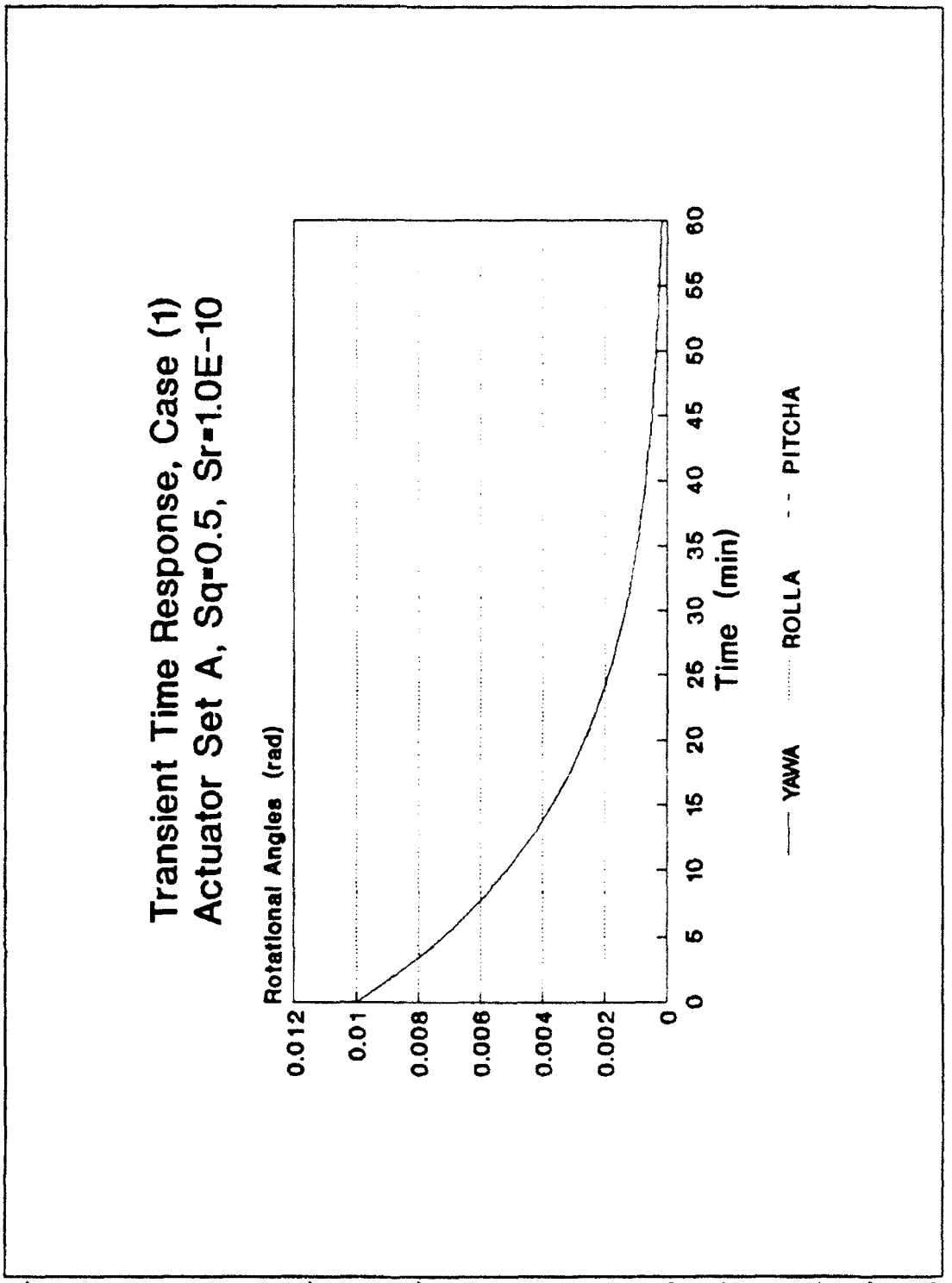

Figure 11. Transient Time Response Of the Rotational Angles' for Comparison of Actuator Positioning, Set A

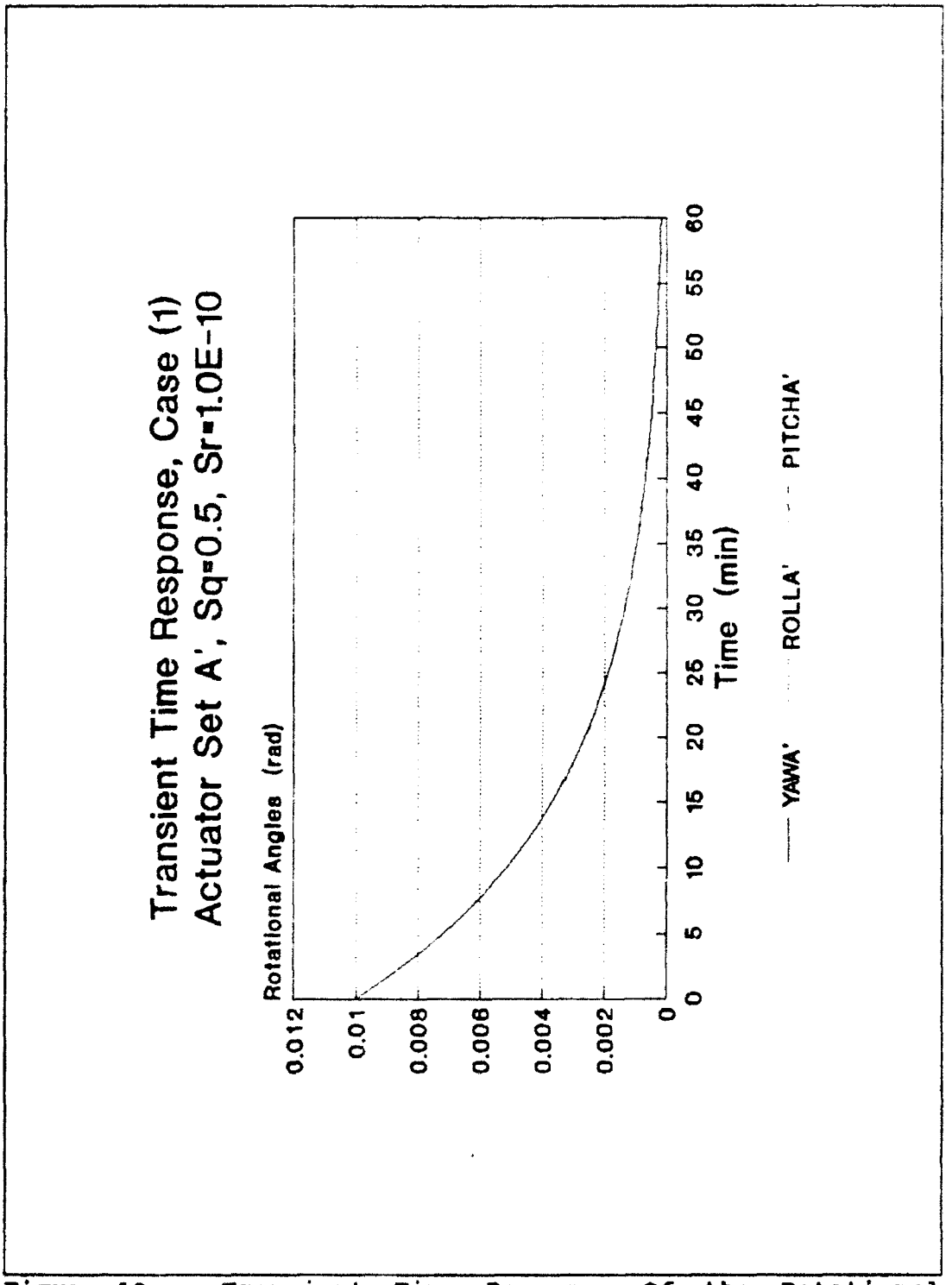

Figure 12. Transient Time Response Of the Rotational Angles' for Comparison of Actuator Positioning, Set A'

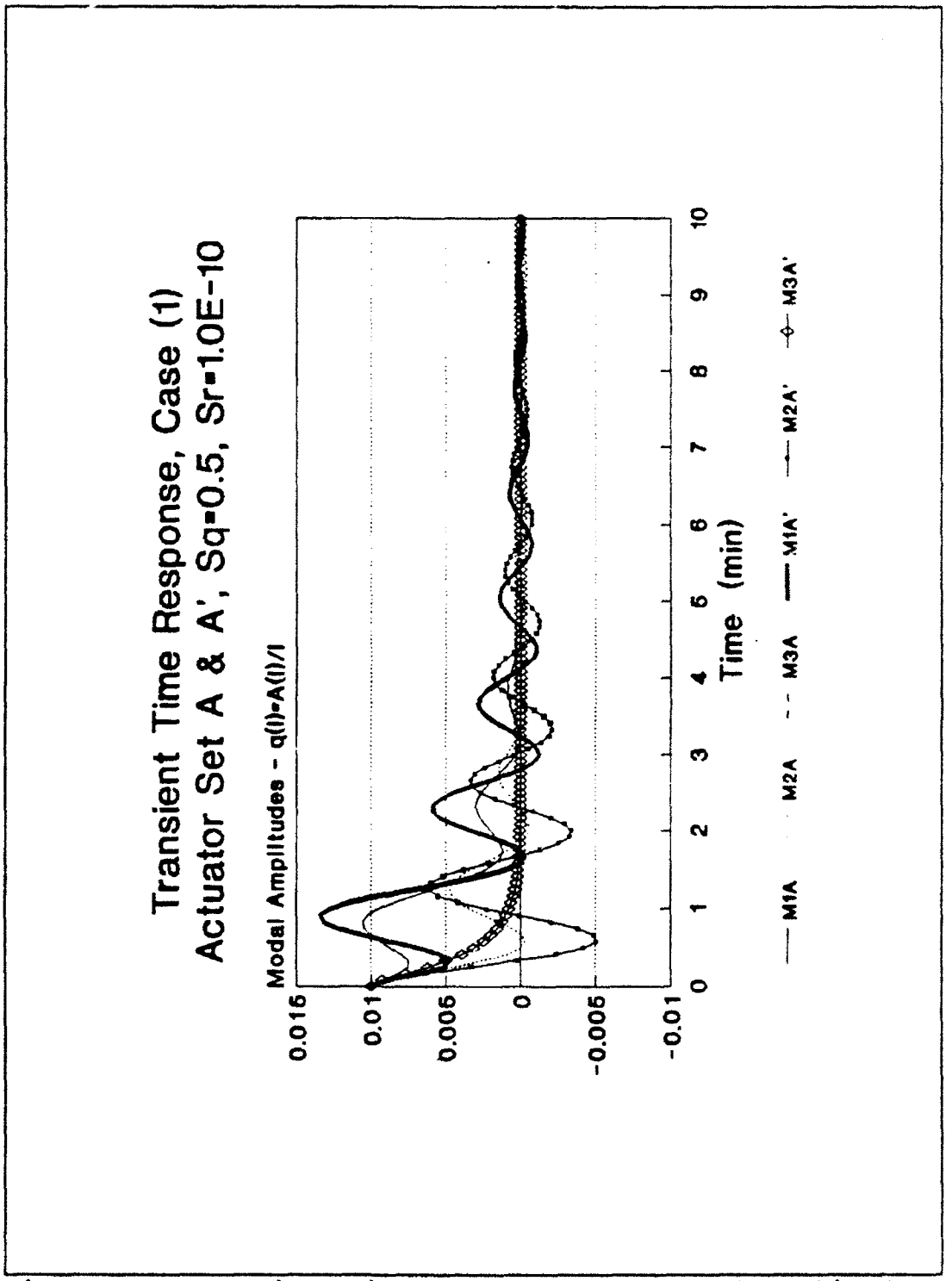

Figure 13. Transient Time Response Of the Modal Amplitudes' for Comparison of Actuator Positioning, Set A & A'

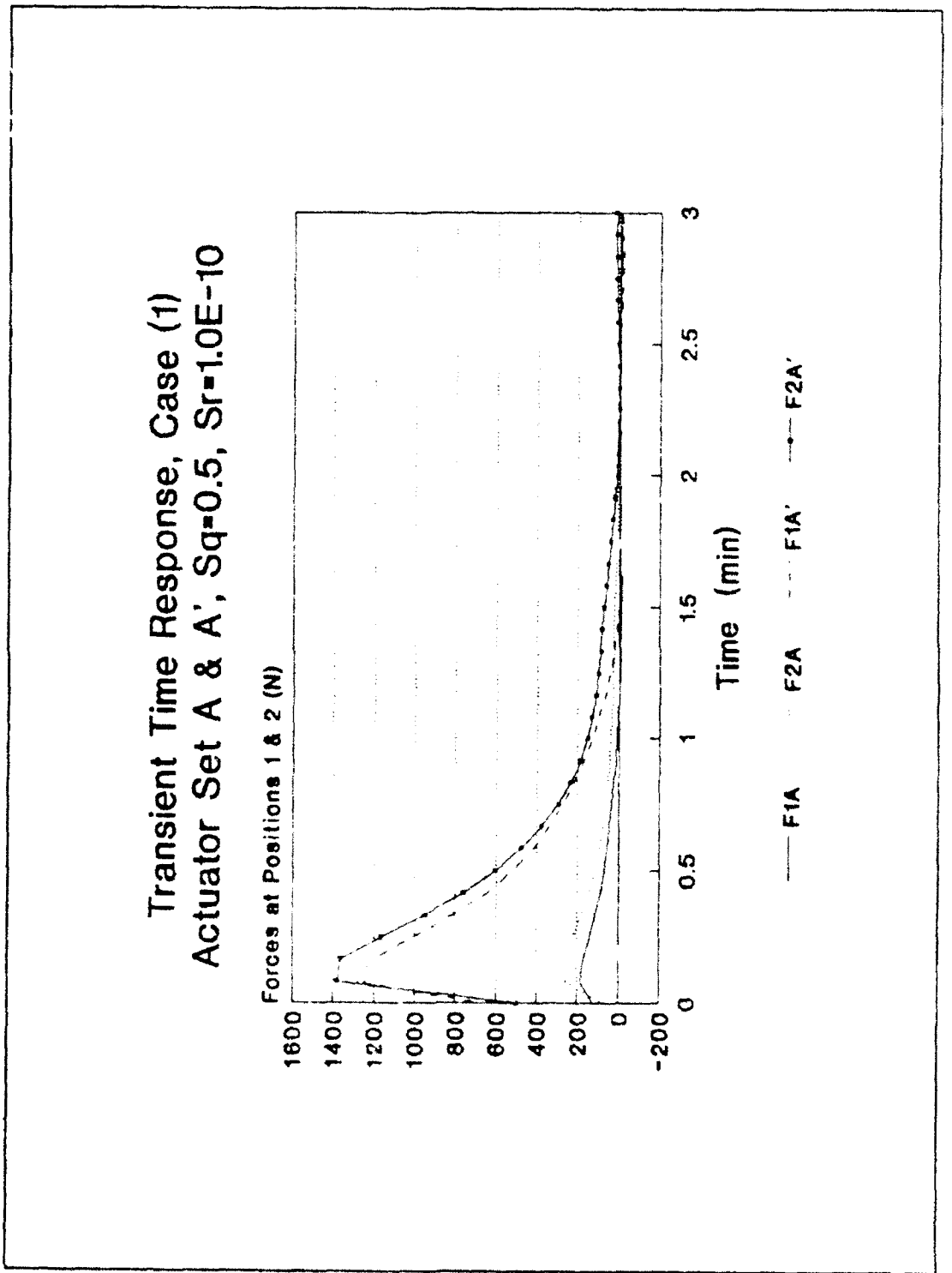

Figure 14. Transient Time Response of the Actuator Force At 1 & 2 for Comparison of Actuator Positioning, Set A & A'

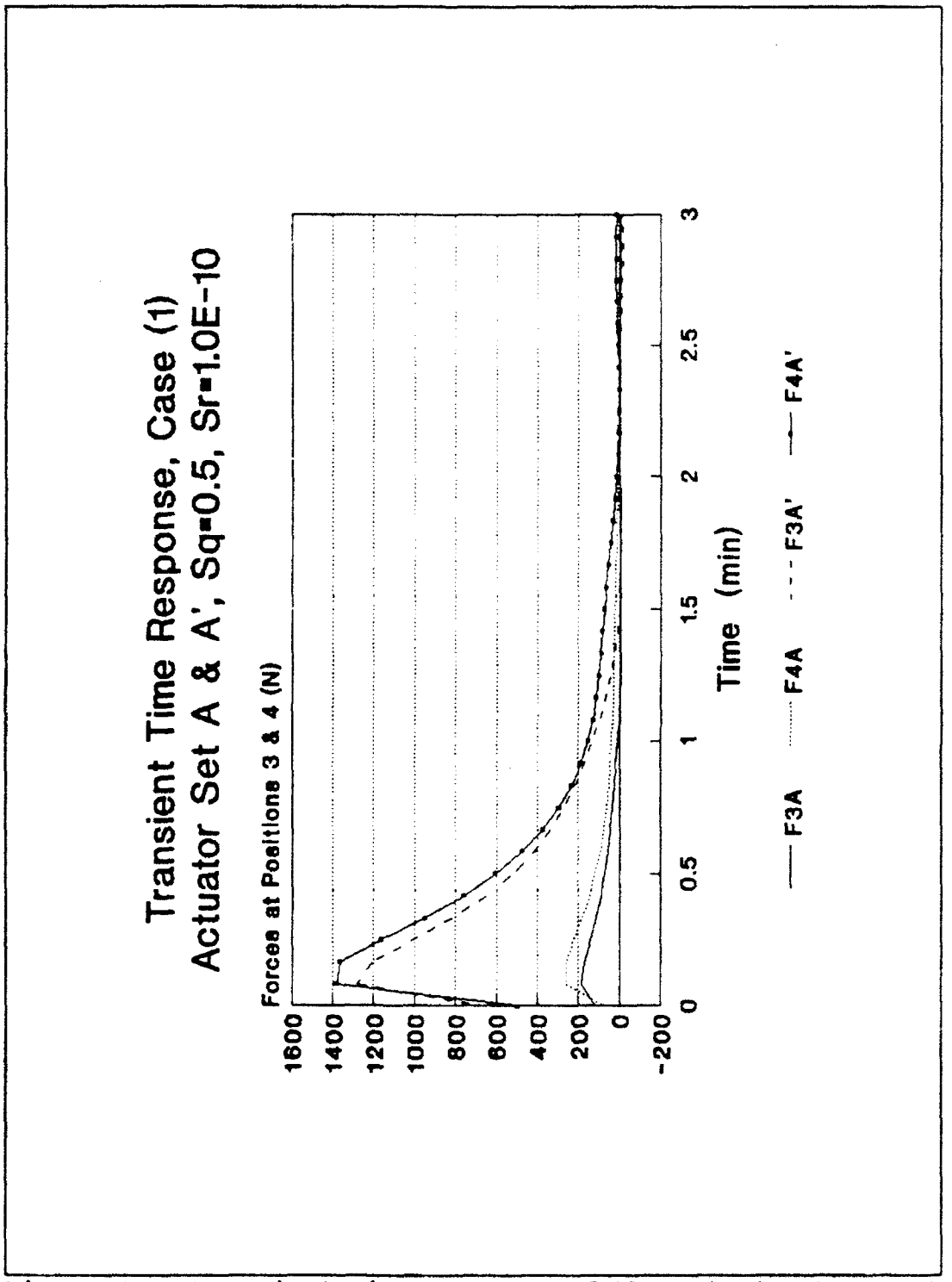

Figure 15. Transient Time Response of the Actuator Force At 3 & 4 for Comparison of Actuator Positioning, Set A & A'

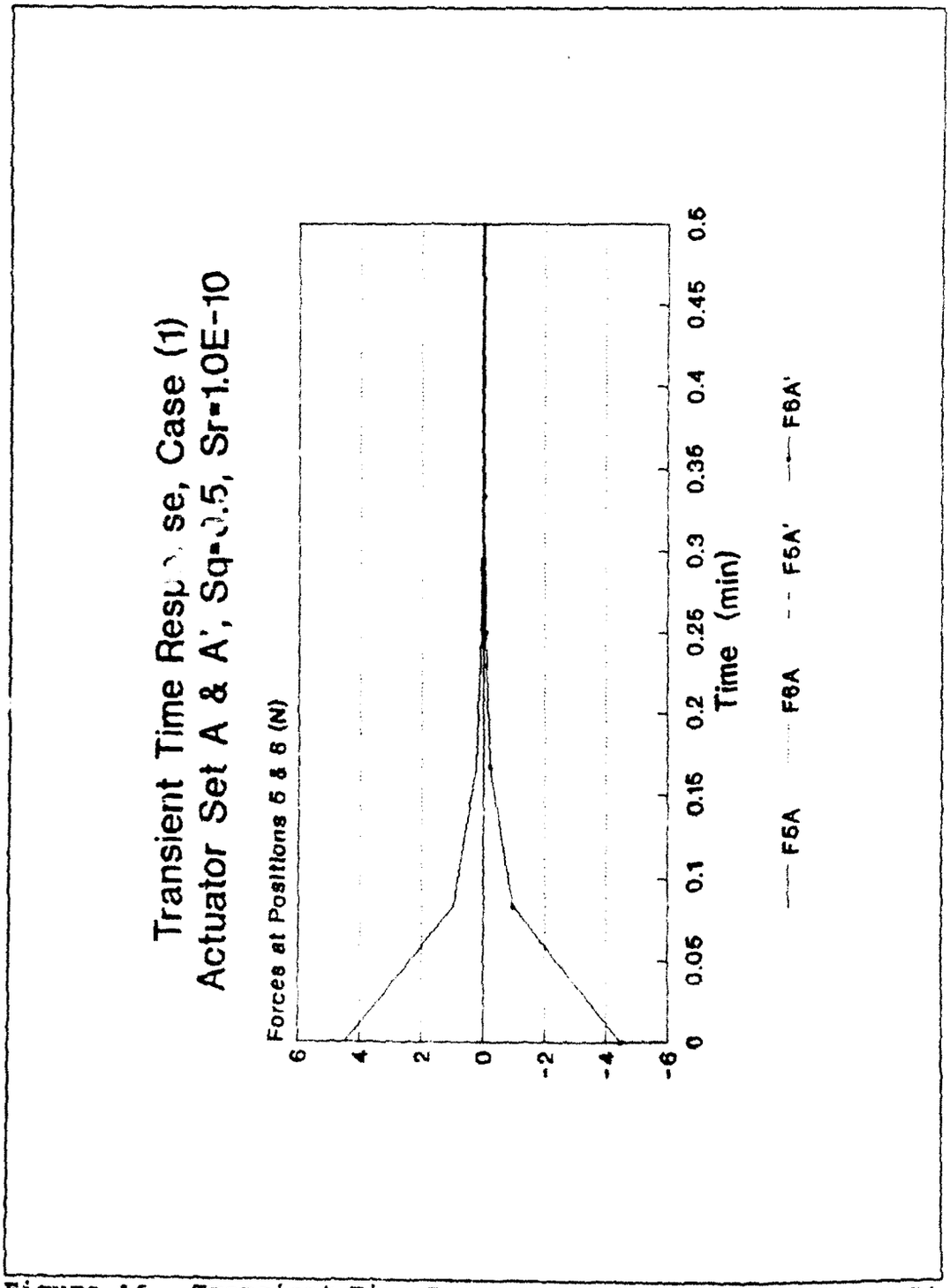

Figure 16. Transient Time Response of the Actuator Force At 5 & 6 for Comparison of Actuator Positioning, Set A & A'

6.2 - Comparison of Penalty Matrices

For the parametric study of the penalty matrices, several system variables were kept constant; they were chosen as: the nominal orientation of Case (1), Set A for the actuator locations, and a sampling period of 5.0 seconds. The variance of the system penalty matrices is handled by changing the control penalty matrix while holding the state penalty matrix constant, and vice-versa. The penalty matrices are defined by Eqns. (185) and (186) where, α_Q=Sq and α_R=Sr. The sets of penalty matrices are:

a) Set 1 - Sq_1=0.5, Sr_1=1.0x10^{-10}

b) Set 2 - Sq_1=0.5, Sr_2=1.0x10^{-12}

c) Set 3 - Sq_2=0.001, Sr_1=1.0x10^{-10}

d) Set 4 - Sq_2=0.001, Sr_1=1.0x10^{-12}

Note that in this study only block diagonal penalty matrices -where all the elements are the same- are considered.

The eigenvalues, moduli, and optimum cost function for each set are displayed in Table 6. The eigenvalues and moduli of Sets 1, 2, and 4 are very close, whereas, the first modulus of Set 3's eigenvalues is noticeably larger. This helps to narrow the system comparison down to the three sets 1, 2, and 4. After taking a second look at their eigenvalues, it is noticed that the moduli of Set 4's eigenvalues are slightly larger than those of the two other

sets; but the optimum cost function for Set 4 is smaller than those for Sets 1 and 2.

For a complete comparison the transient response is viewed. The responses for the system's rotational angles pictured in Figure 17 show no appreciable difference regardless of the penalty matrices used. In addition, there is no significant difference between the yaw, pitch, and roll responses. The transient response of the modal amplitudes show a slight variation as a function of the penalty matrices used. For the first and second mode there is virtually no difference in responses for all combinations of penalty matrices (see Figs. 18 and 19). The third mode responses display a deviation towards a better response for Set 4 (see Fig. 20). Similarly, all the actuator force responses (see Figs. 21-26) exhibit better characteristics for the case of Set 4 penalty matrices.

The determination of the best combination of the state penalty matrix and control matrix is a little more difficult than the previous choice of positioning. After taking into consideration the system characteristics, Set 4 (Sq=0.001, and $Sr=1.0x10^{-12}$) was chosen. Even though the Set 4 system eigenvalues are not the smallest ones considered, its optimum cost function is the least and its response is the best.

Table 6

The Effect of Different Penalty Matrix Combinations on the Closed-Loop System Eigenvalues and Moduli

	Set 1:Sq=0.5,Sr=1.0E-10			Set 2:Sq=0.5,Sr=1.0E-12		
	Eigenvalues		Moduli	Eigenvalues		Moduli
	Real	Imag.		Real	Imag.	
1	0.20871	0	0.20871	0.20870	0	0.20870
2	0.20873	.00177	0.20873	0.20870	.00174	0.20870
3	0.20873	-.00177	0.20873	0.20870	-.00174	0.20870
4	0.22710	0	0.22710	0.22709	0	0.22709
5	0.25698	0	0.25698	0.25679	0	0.25679
6	0.79820	0	0.79820	0.79827	0	0.79827
7	0.92454	0	0.92454	0.92454	0	0.92454
8	0.88714	.36217	0.94520	0.88714	.36217	0.94520
9	0.88714	-.36217	0.94520	0.88714	-.36217	0.94520
10	0.99443	0	0.99443	0.99443	0	0.99443
11	0.99443	0	0.99443	0.99443	0	0.99443
12	0.99443	0	0.99443	0.99443	0	0.99443
	$X_o^T P_o X_o$=0.0086919			$X_o^T P_o X_o$=0.0086915		
	Set 3:Sq=.001,Sr=1.0E-10			**Set 4:Sq=.001,Sr=1.0E-12**		
	Eigenvalues		Moduli	Eigenvalues		Moduli
	Real	Imag.		Real	Imag.	
1	0.21375	0	0.21375	0.20875	0	0.20875
2	0.21394	0	0.21394	0.20885	.00174	0.20886
3	0.23154	0	0.23154	0.20885	-.00174	0.20886
4	0.23262	0	0.23262	0.22713	0	0.22713
5	0.34728	0	0.34728	0.25776	0	0.25776
6	0.76206	0	0.76206	0.79792	0	0.79792
7	0.92394	0	0.92394	0.92454	0	0.92454
8	0.88712	.36218	0.94519	0.88714	.36217	0.9452
9	0.88712	-.36218	0.94519	0.88714	-.36217	0.9452
10	0.99443	0	0.99443	0.99443	0	0.99443
11	0.99443	0	0.99443	0.99443	0	0.99443
12	0.99443	0	0.99443	0.99443	0	0.99443
	$X_o^T P_o X_o$=1.7823E-5			$X_o^T P_o X_o$=1.7388E-5		

$X_o^T P_o X_o$ - Optimum Cost Function

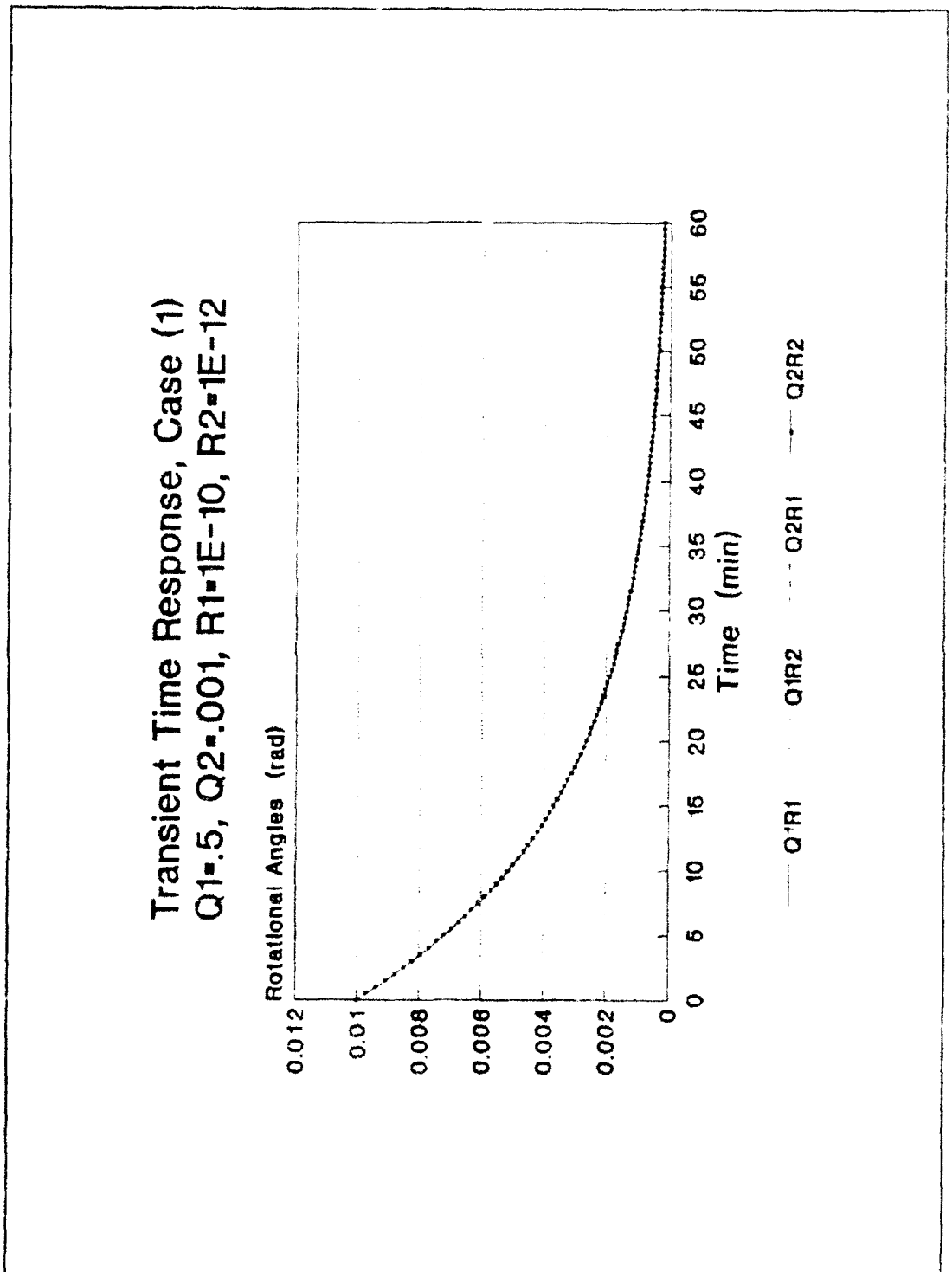

Figure 17. Transient Time Response of the Rotational Angles' for Comparison of Penalty Matrices

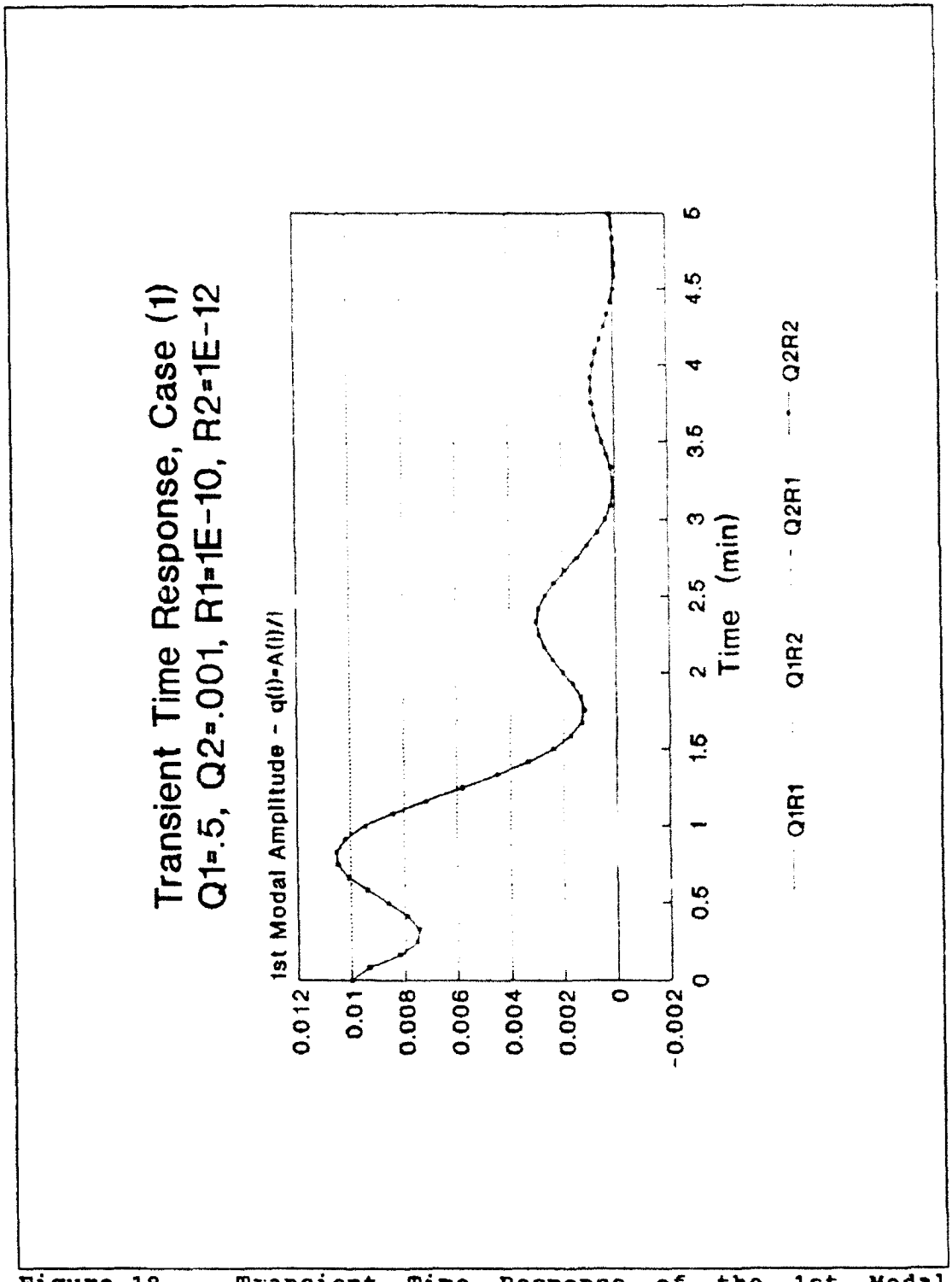

Figure 18. Transient Time Response of the 1st Modal Amplitudes' for Comparison of Penalty Matrices

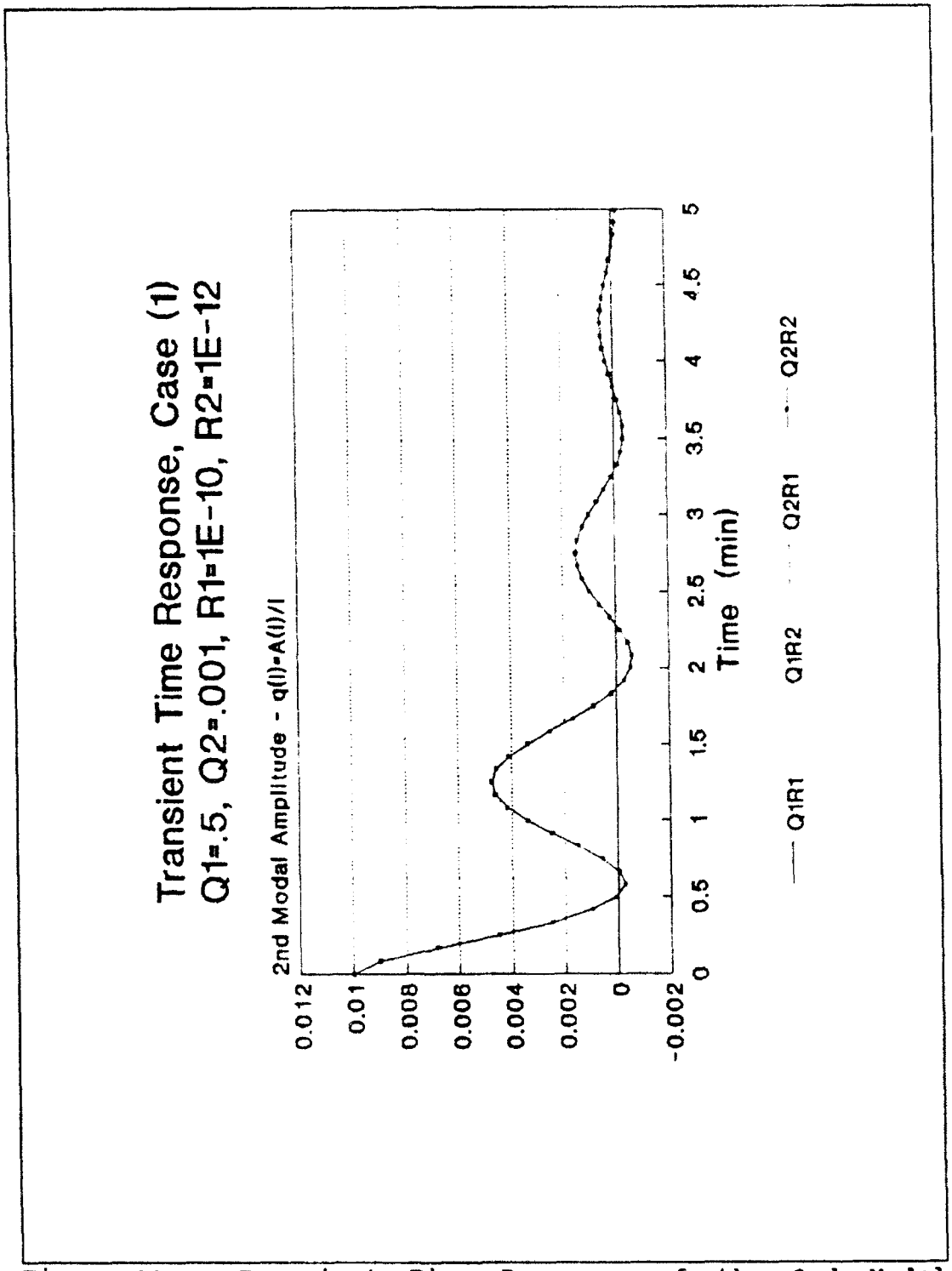

Figure 19. Transient Time Response of the 2nd Modal Amplitudes' for Comparison of Penalty Matrices

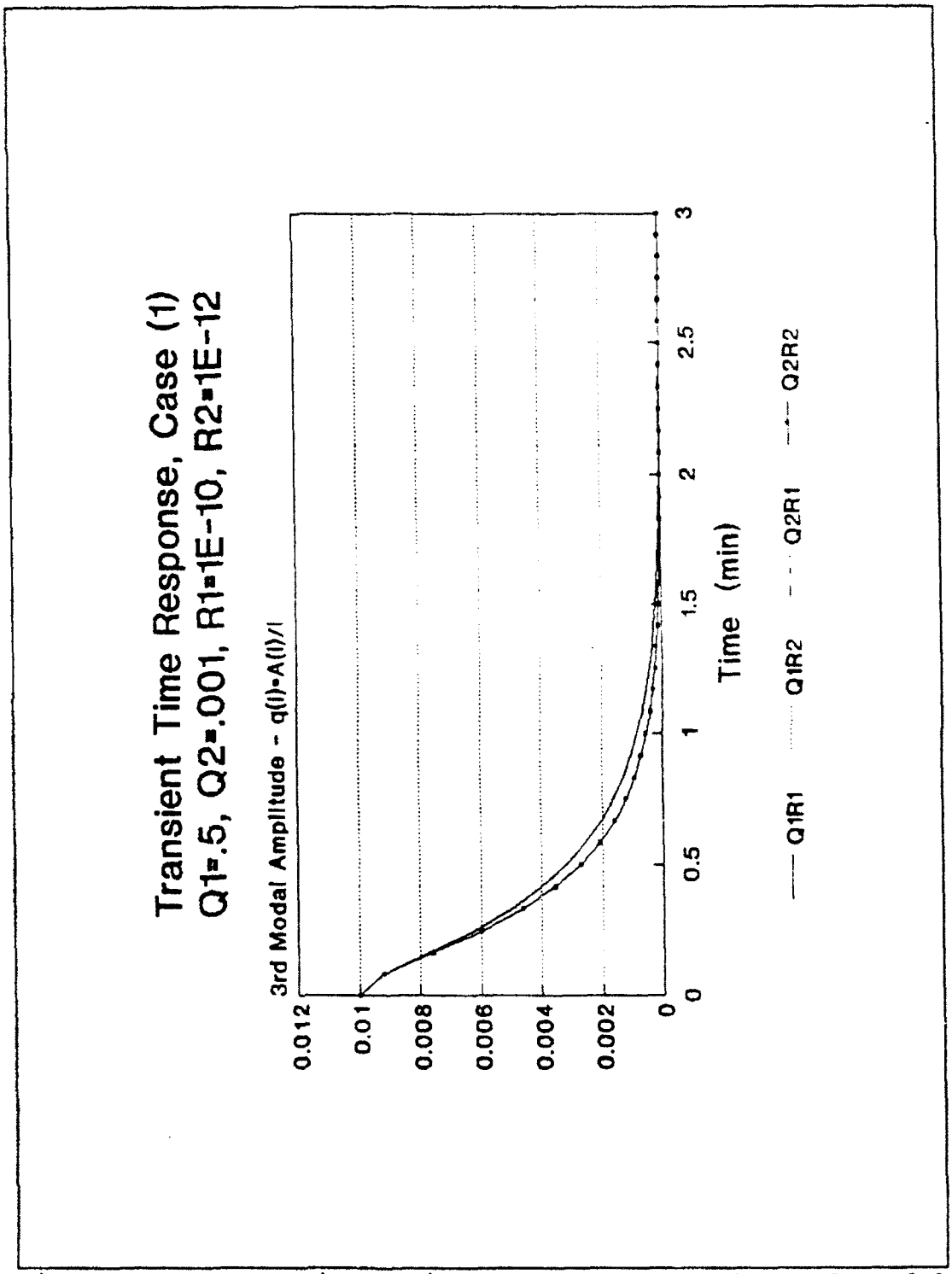

Figure 20. Transient Time Response of the 3rd Modal Amplitudes' for Comparison of Penalty Matrices

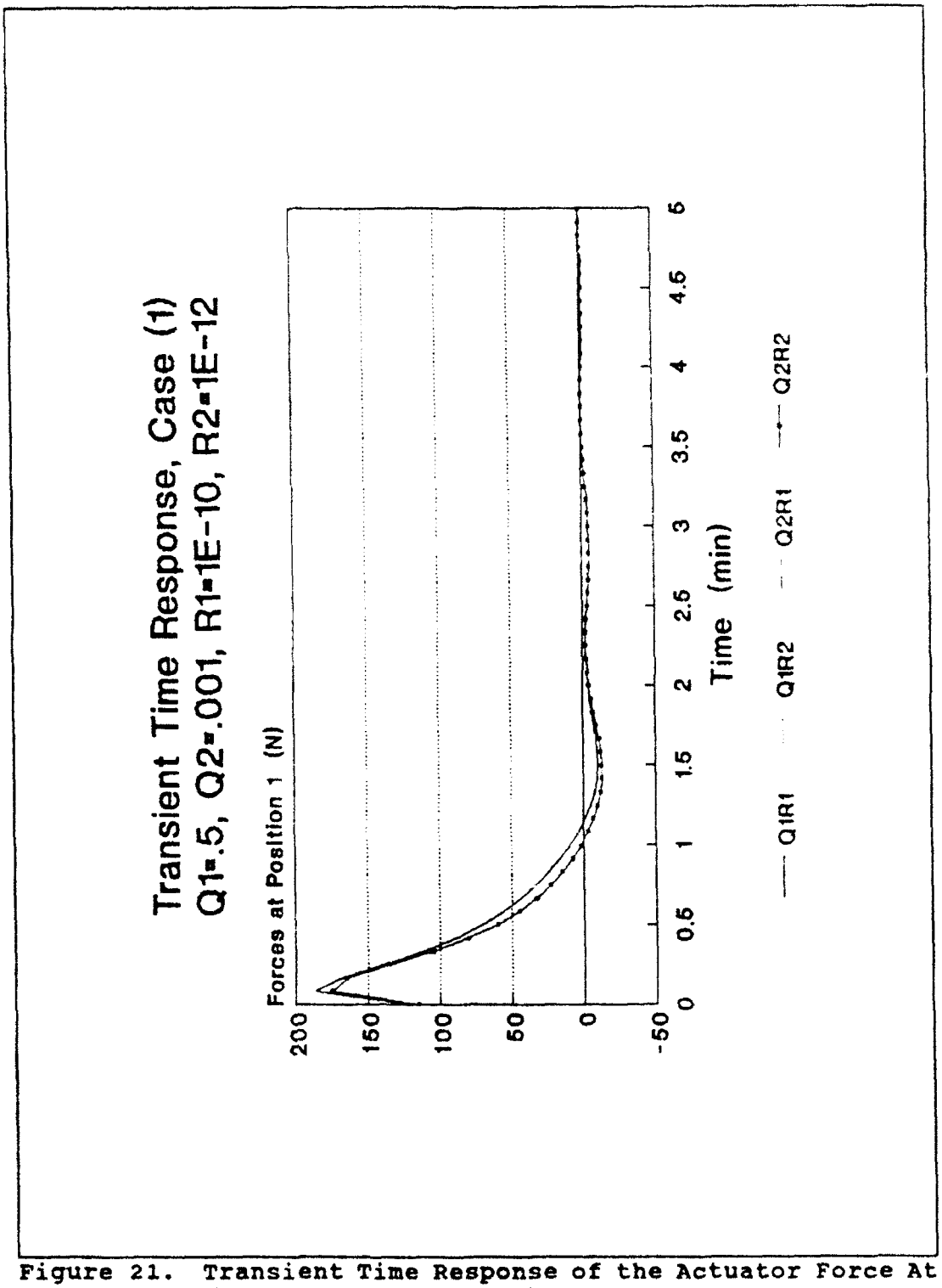

Figure 21. Transient Time Response of the Actuator Force At 1 for Comparison of Penalty Matrices

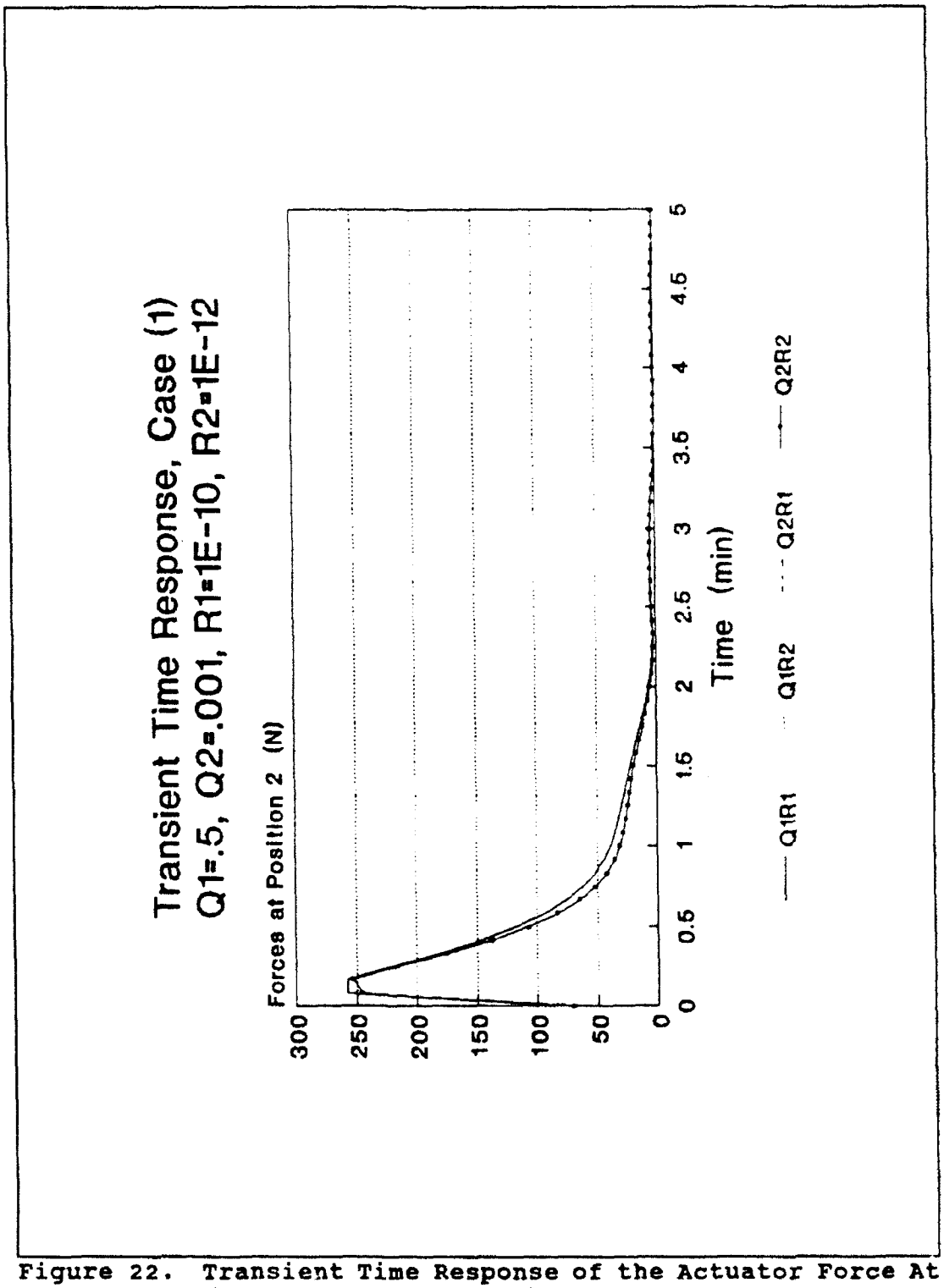

Figure 22. Transient Time Response of the Actuator Force At 2 for Comparison of Penalty Matrices

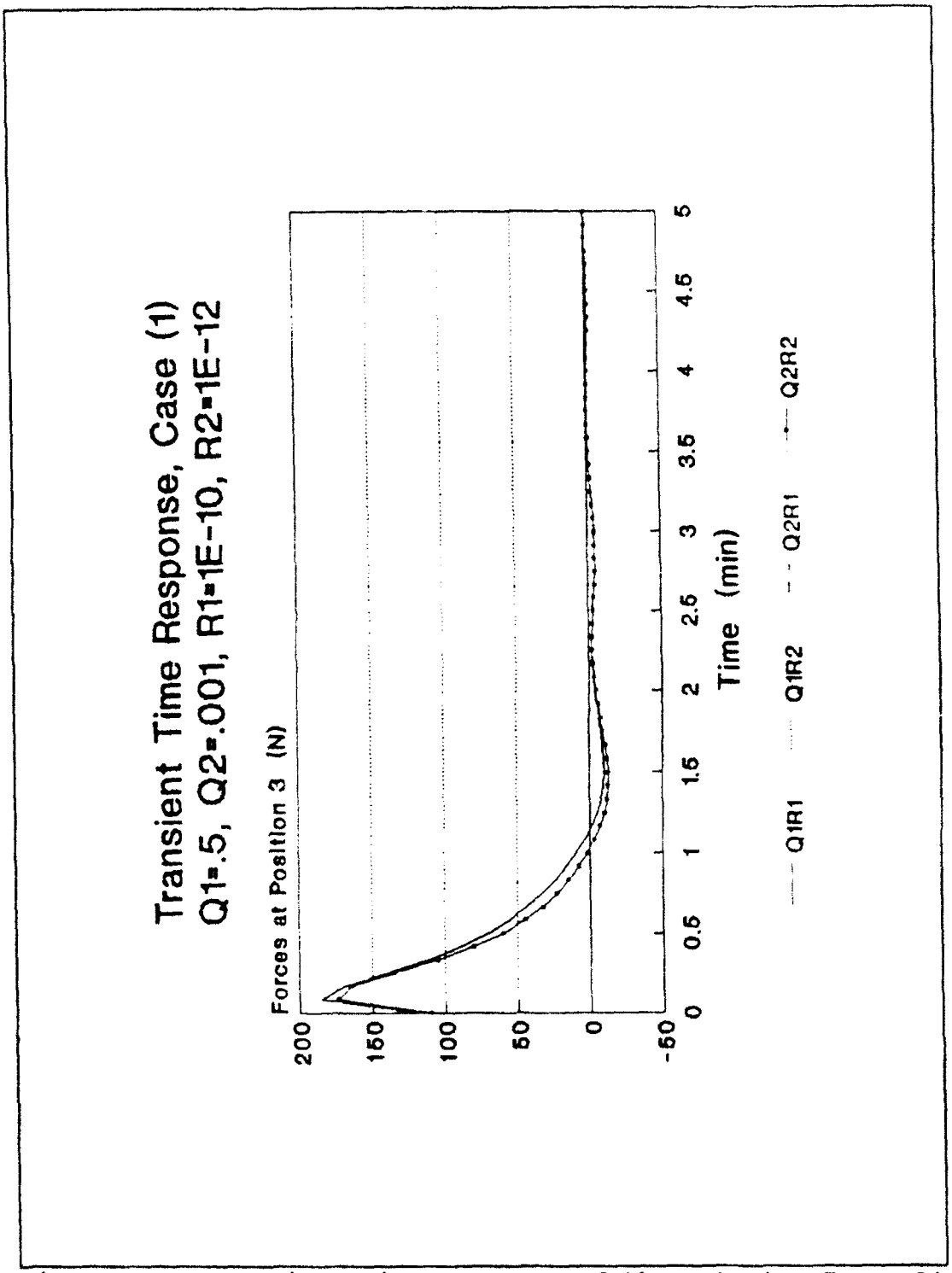

Figure 23. Transient Time Response of the Actuator Force At 3 for Comparison of Penalty Matrices

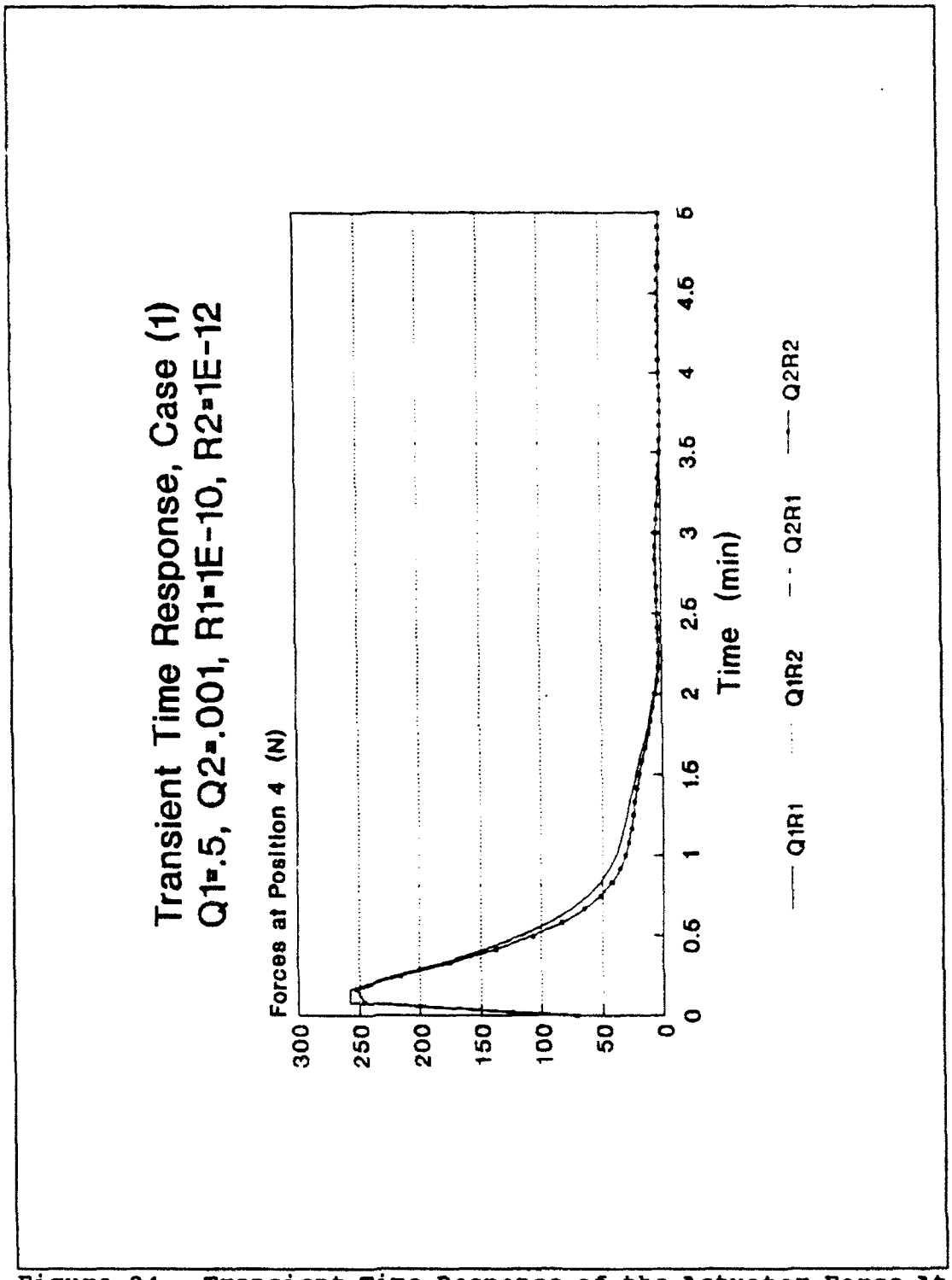

Figure 24. Transient Time Response of the Actuator Force At 4 for Comparison of Penalty Matrices

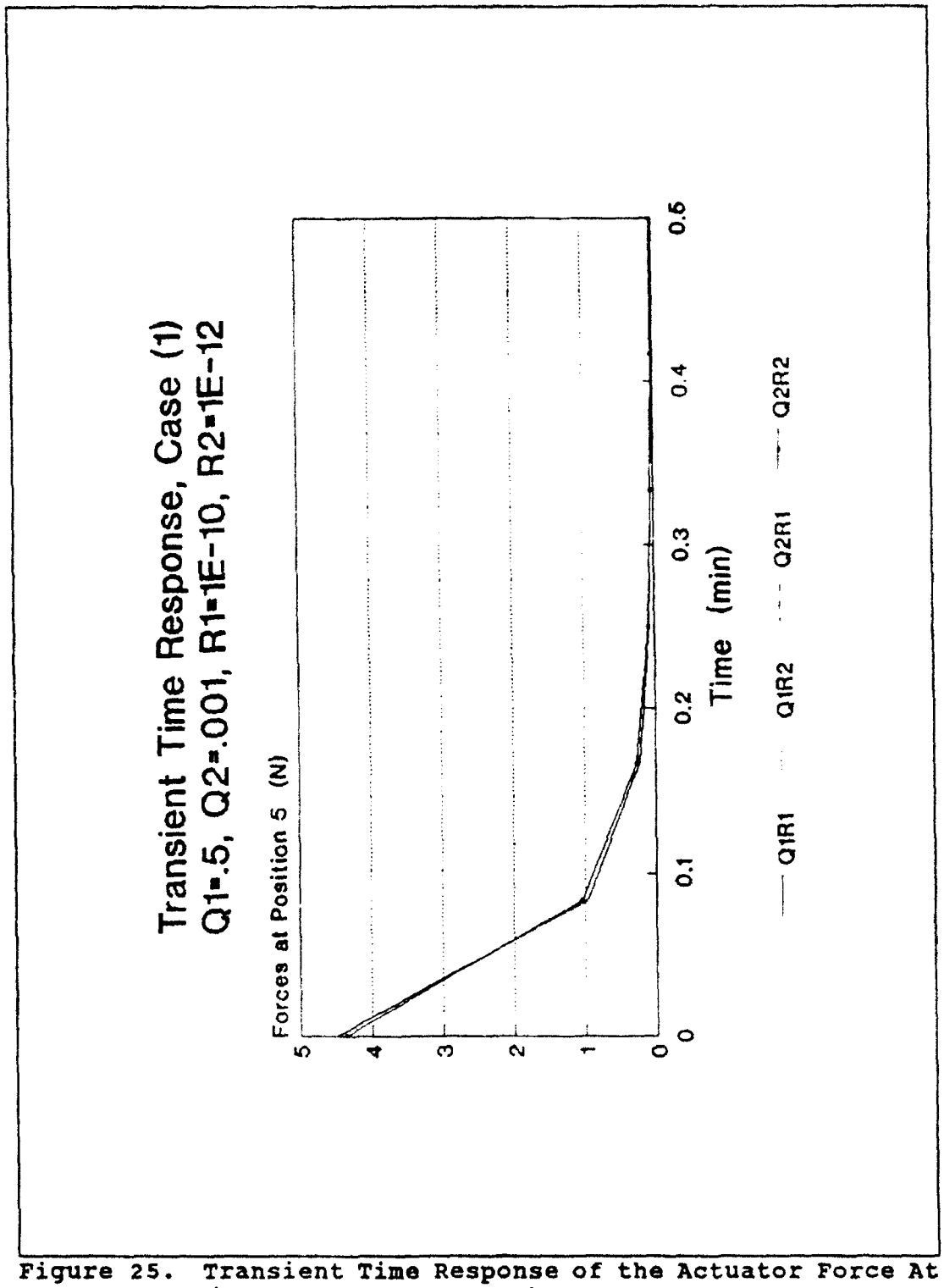

Figure 25. Transient Time Response of the Actuator Force At 5 for Comparison of Penalty Matrices

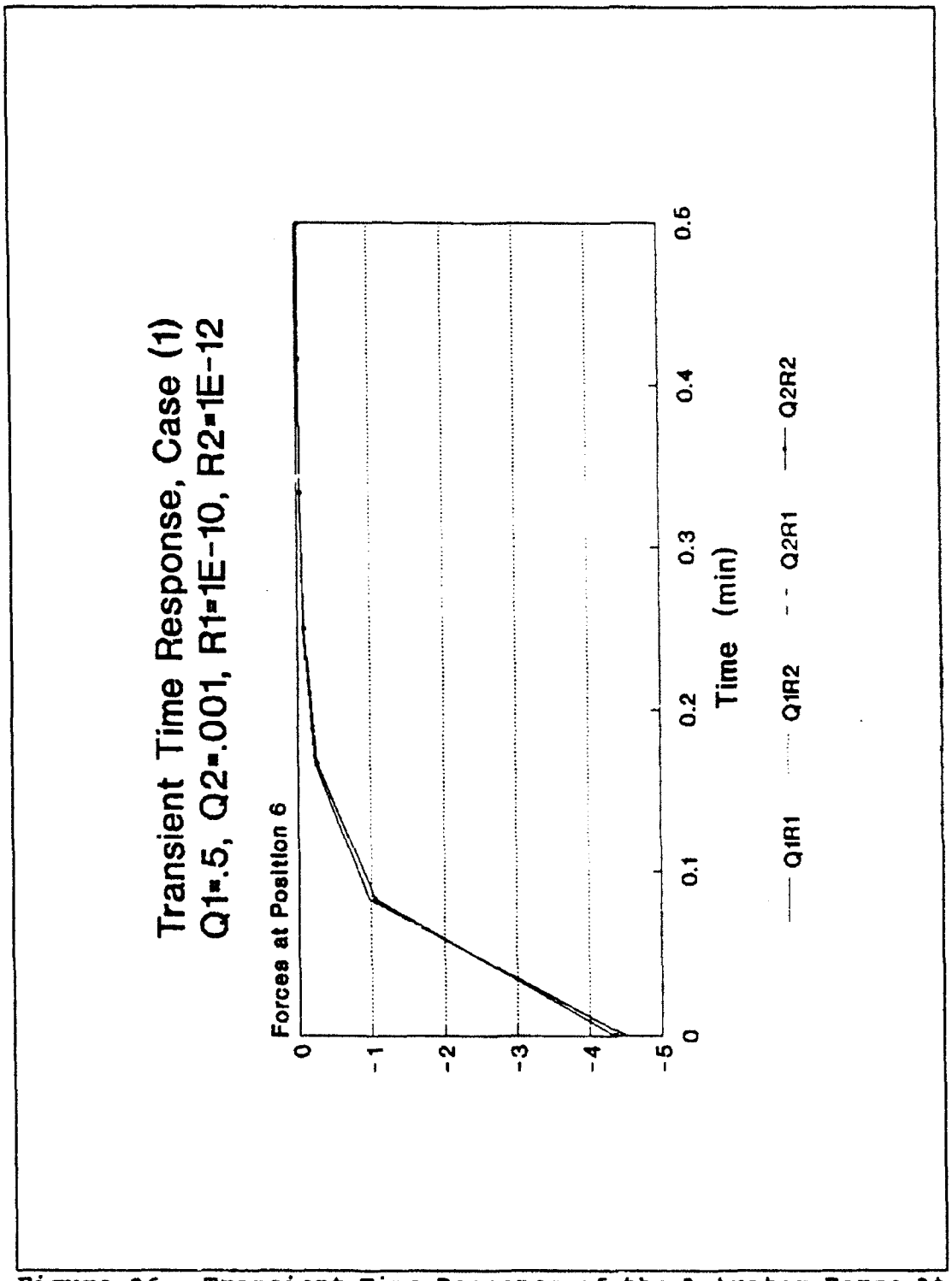

Figure 26. Transient Time Response of the Actuator Force At 6 for Comparison of Penalty Matrices

6.3 - Comparison of Sampling Period

For the comparison of sampling periods, several system characteristics kept constant were chosen to be: the nominal orientation of Case (1), the actuator placement of Set A, and the penalty matrices of Set 1. The different sampling periods chosen for the comparison were 2.5, 5.0, 10.0, and 40.0 seconds, respectively. The latter was an approximate value chosen from Table 4 (see 39.95 seconds) as a representation of system degradation.

Each set's discretized open and closed loop system eigenvalues and moduli and their optimum cost functions are shown in Table 7. The open-loop eigenvalues of all four sampling periods show signs of instability by containing moduli greater than 1. This is a confirmation that the uncontrolled (local horizontal) orientation of Case (1) is unstable. When the closed-loop eigenvalues of each sampling period are examined, an unexpected result surfaces. Almost all the moduli of the 40.0 second eigenvalues are slightly smaller than those for the other sampling periods. This results from the fact that the calculated unacceptable sampling period is 39.95 seconds and not 40.0 seconds, i.e., roundoff error. The sampling period of 40.0 seconds was employed to provide an equivalent final time period with the other sampling periods, in other words, 2.5, 5.0, 10.0 are

multiplies of 40.0. The moduli of the last eigenvalue of Set IV is very close to the limit of 1, thus exhibiting a trend towards degradation. Comparison of the optimum cost function indicates a minimum for the 2.5 second sampling period.

The transient time response for the rotation angles are the same for all the sampling periods (see Fig. 27). When the transient response of the modal amplitude are considered the first mode's maximum overshoot decreases, its undershoot increases, as the sampling period increases (see Figs. 28-31). The same relationship holds for the response of the second mode. The third mode's response displays an undershoot for the 10.0 and 40.0 seconds sampling periods, a characteristic not shown before in this study. The entire modal responses for the 40.0 second sampling period represent a degradation in comparison with the modal responses for the other sampling periods. For the case of the transient force responses, the maximum overshoot decreases as the sampling period increases (see Figs. 31-35). For the 40.0 second case there is no overshoot but a large undershoot and a very choppy response, again associated with system performance degradation.

Initially, the selection of the sampling period can be reduced to just three periods, 2.5, 5.0, and 10.0 seconds,

for the obvious reason that the sampling period of 40 seconds is associated with performance degradation. However, it is not an easy task to decide on the best sampling period from the three other sampling periods. Effectively, 2.5 seconds can be released from consideration due to the larger moduli of the eigenvalues and overshoot. The decision between the last two sampling periods is a more difficult one. The sampling period of 5.0 seconds has a higher overshoot, a smaller undershoot, a smaller optimum cost function, and a smooth response curve. The sampling period of 10.0 seconds displays a lower overshoot, a larger undershoot, smaller eigenvalues, and a choppy response. Finally, taken into consideration that signal reconstruction is very important, the sampling period of 5.0 seconds can be chosen.

Table 7
The Effect of Different Sampling Periods on the Open and Closed Loop System Eigenvalues and Moduli

	Set I: Delta=2.50 sec						Set II: Delta=5.0 sec					
	Open Eigenvalue		Moduli	Closed Eigenvalue		Moduli	Open Eigenvalue		Moduli	Closed Eigenvalue		Moduli
	Real	Imag.		Real	Imag.		Real	Imag.		Real	Imag.	
1	.99518	0	.99518	.20875	0	.20875	.99038	0	.99038	.20871	0	.20871
2	.99606	0	.99606	.20883	.000869	.20883	.99214	0	.99214	.20873	.00177	.20873
3	.97030	.24190	1	.20883	.000869	.20883	.88297	.46943	1	.20873	-.00177	.20873
4	.97030	-.24190	1	.21302	0	.21302	.88297	-.46943	1	.22710	0	.22710
5	.98079	.19504	1	.21906	0	.21906	.92392	.38259	1	.25698	0	.25698
6	.98079	-.19504	1	.95088	0	.95088	.92392	-.38259	1	.79820	0	.79820
7	.99066	.13632	1	.95745	.17032	.97249	.96283	.27010	1	.92454	0	.92454
8	.99066	-.13632	1	.95745	-.17032	.97249	.96283	-.27010	1	.88714	.36217	.94520
9	1	0	1	.9812	0	.98120	1	0	1	.88714	-.36217	.94520
10	1	0	1	.99721	0	.99721	1	0	1	.99443	0	.99443
11	1.0040	0	1.0040	.99721	0	.99721	1.0079	0	1.0079	.99443	0	.99443
12	1.0048	0	1.0048	.99721	0	.99721	1.0097	0	1.0097	.99443	0	.99443
				$X_o^T P_o X_o$=0.0059678						$X_o^T P_o X_o$=. 08692		

Table 7
continued

	Set III: Delta=10.0 sec						Set IV: Delta=40.0 sec					
	Open Eigenvalue		Moduli	ClosedEigenvalue		Moduli	Open Eigenvalue		Moduli	ClosedEigenvalue		Moduli
	Real	Imag.		Real	Imag.		Real	Imag.		Real	Imag.	
1	.98085	0	.98085	.20866	0	.20866	.92558	0	.92558	.20790	0	.20790
2	.98434	0	.98434	.20866	.00349	.20869	.93881	0	.93881	.20773	.01387	.20819
3	.55926	.82899	1	.20866	-.00349	.20869	-.71957	.69441	1	.20773	-.01387	.20819
4	.55926	.82899	1	.32154	0	.32154	-.71957	-.69441	1	-.2722	.20635	.34157
5	.70725	.70697	1	.32247	.29996	.44041	-1	.00079	1	-.2722	-.20635	.34157
6	.70725	-.70697	1	.32247	-.29996	.44041	-1	-.00079	1	.38995	0	.38995
7	.85409	.52013	1	.66539	0	.66539	-.57876	.81550	1	.42418	.31937	.53097
8	.85409	-.52013	1	.67643	.57747	.88940	-.57876	-.81550	1	.42418	-.31937	.53097
9	1	0	1	.67643	-.57747	.88940	1	0	1	.95572	0	.95572
10	1	0	1	.98887	0	.98887	1	0	1	.95618	0	.95618
11	1.0159	0	1.0159	.98887	0	.98887	1.0652	0	1.0652	.95670	0	0.9567
12	1.0195	0	1.0195	.98893	0	.98893	1.0804	0	1.0804	-.9992	0	.99921
				$X_o^T P_o X_o$=0.01397						$X_o^T P_o X_o$=0.03024		

Delta - Sampling Period, $X_o^T P_o X_o$ - Optimum Cost Function

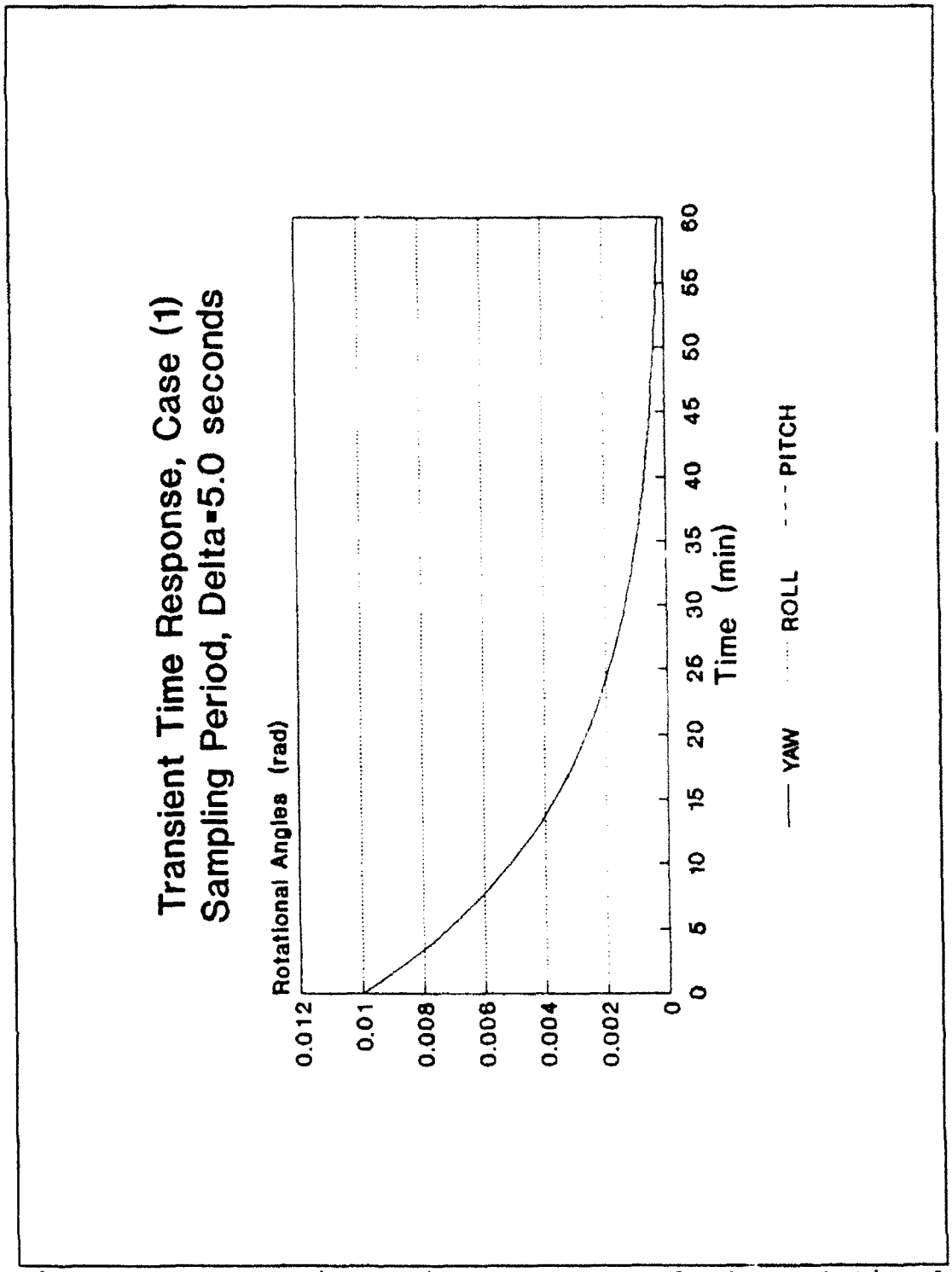

Figure 27. Transient Time Response of the Rotational Angles' for Comparison of Sampling Period, 5.0 seconds

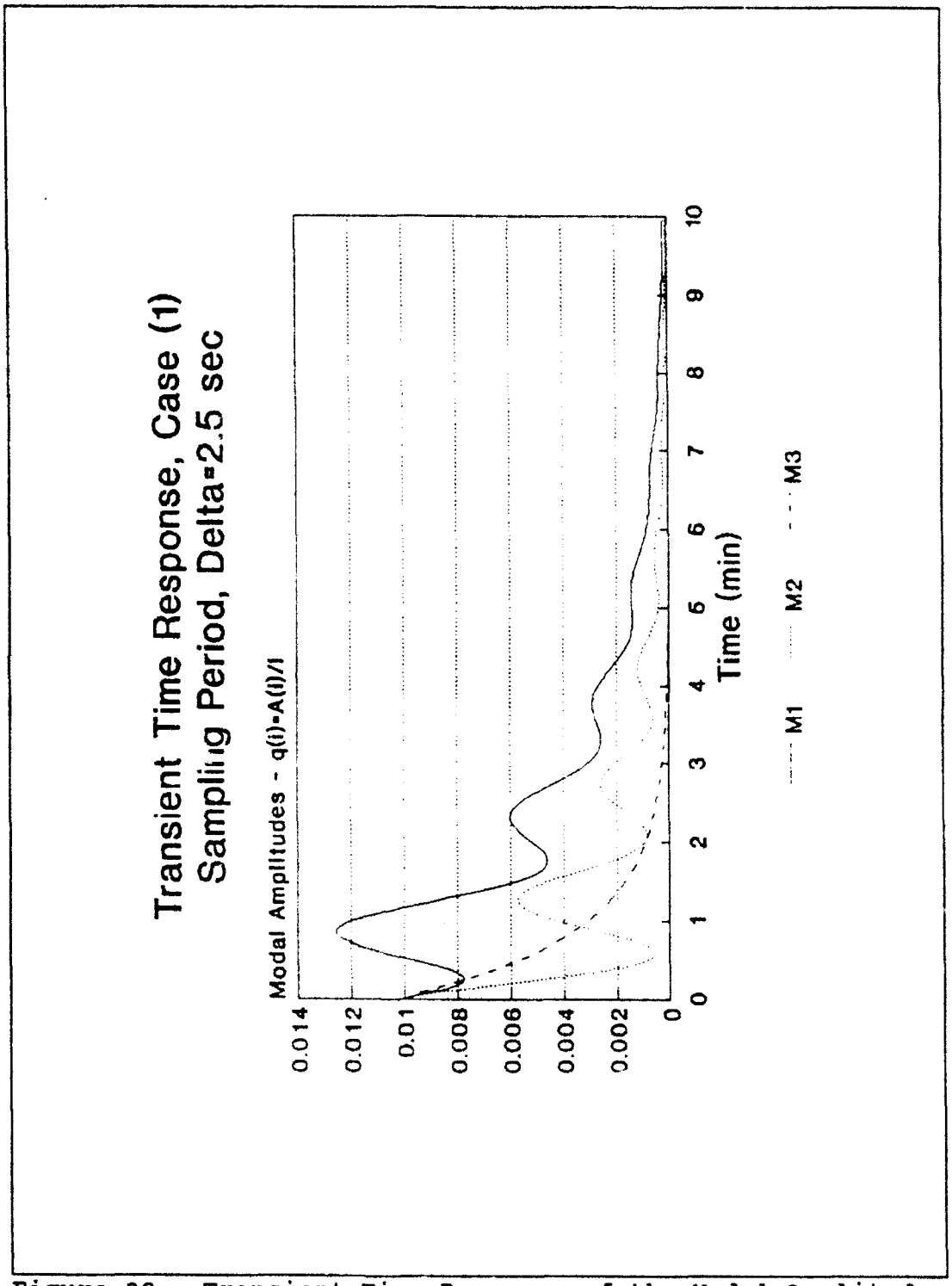

Figure 28. Transient Time Response of the Modal Amplitudes for Comparison of Sampling Period, 2.5 seconds

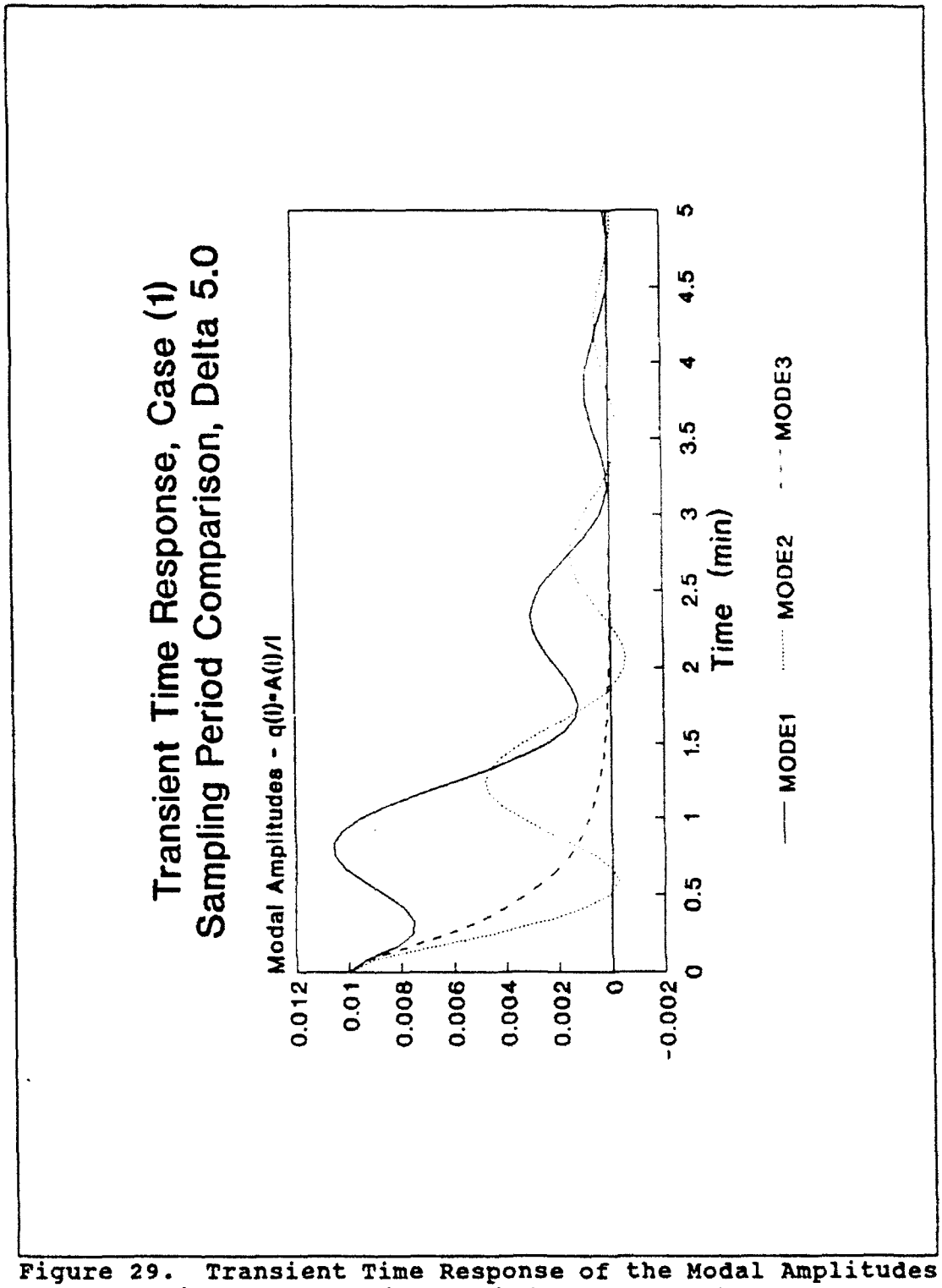

Figure 29. Transient Time Response of the Modal Amplitudes for Comparison of Sampling Period, 5.0 seconds

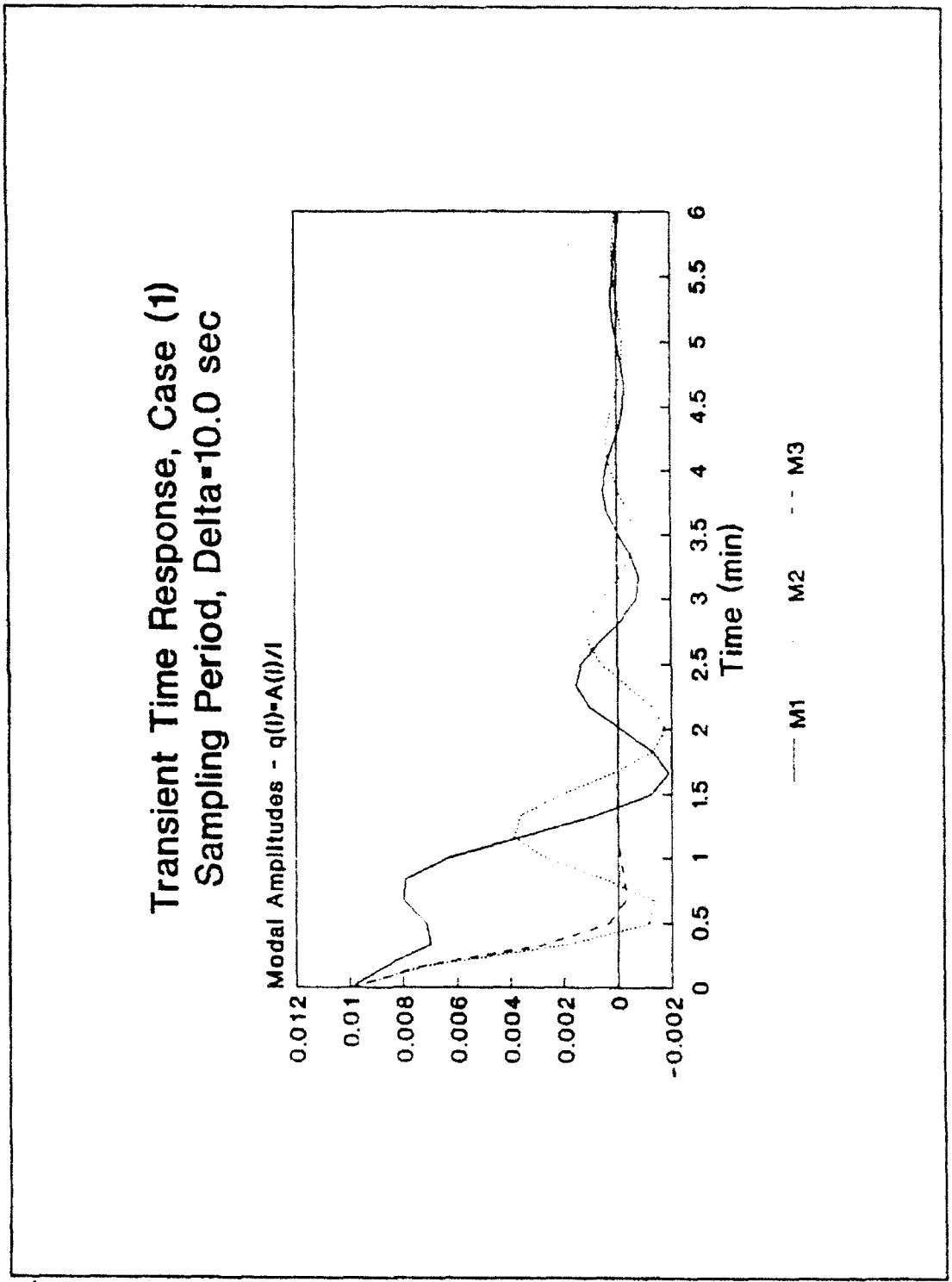

Figure 30. Transient Time Response of the Modal Amplitudes for Comparison of Sampling Period, 10.0 seconds

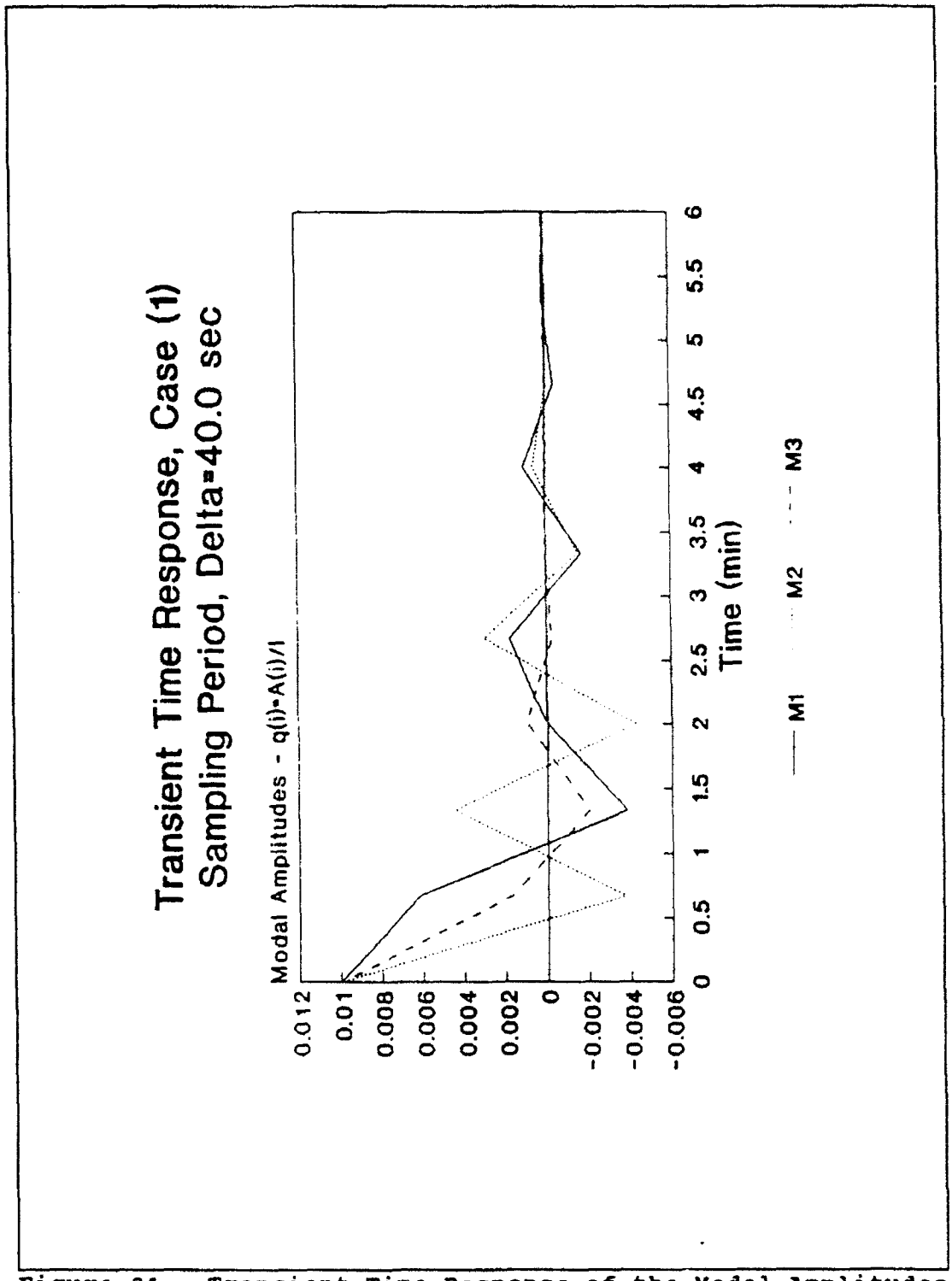

Figure 31. Transient Time Response of the Modal Amplitudes for Comparison of Sampling Period, 40.0 seconds

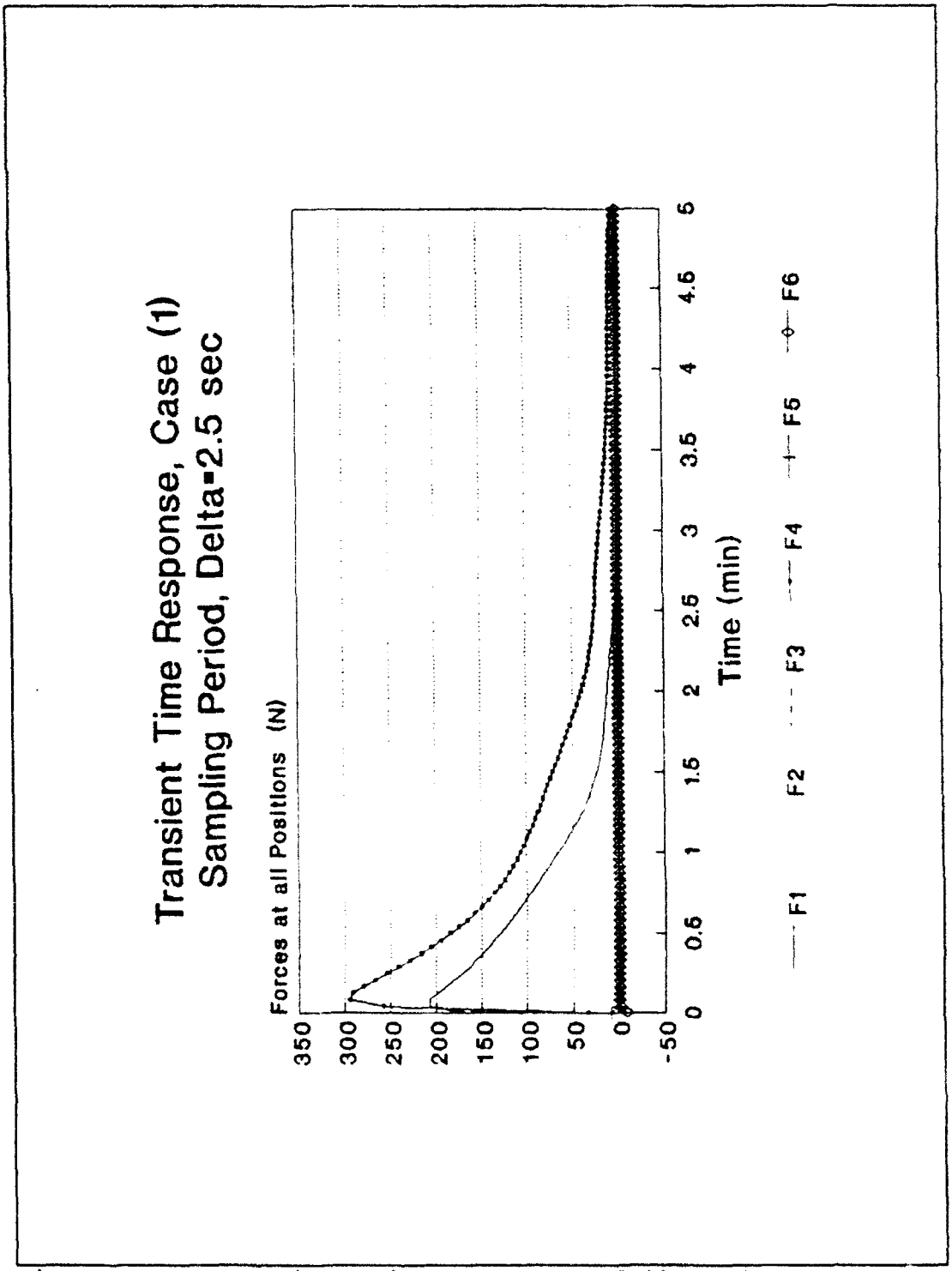

Figure 32. Transient Time Response of the Actuator Forces At All Positions for Comparison of Sampling Period, 2.5 seconds

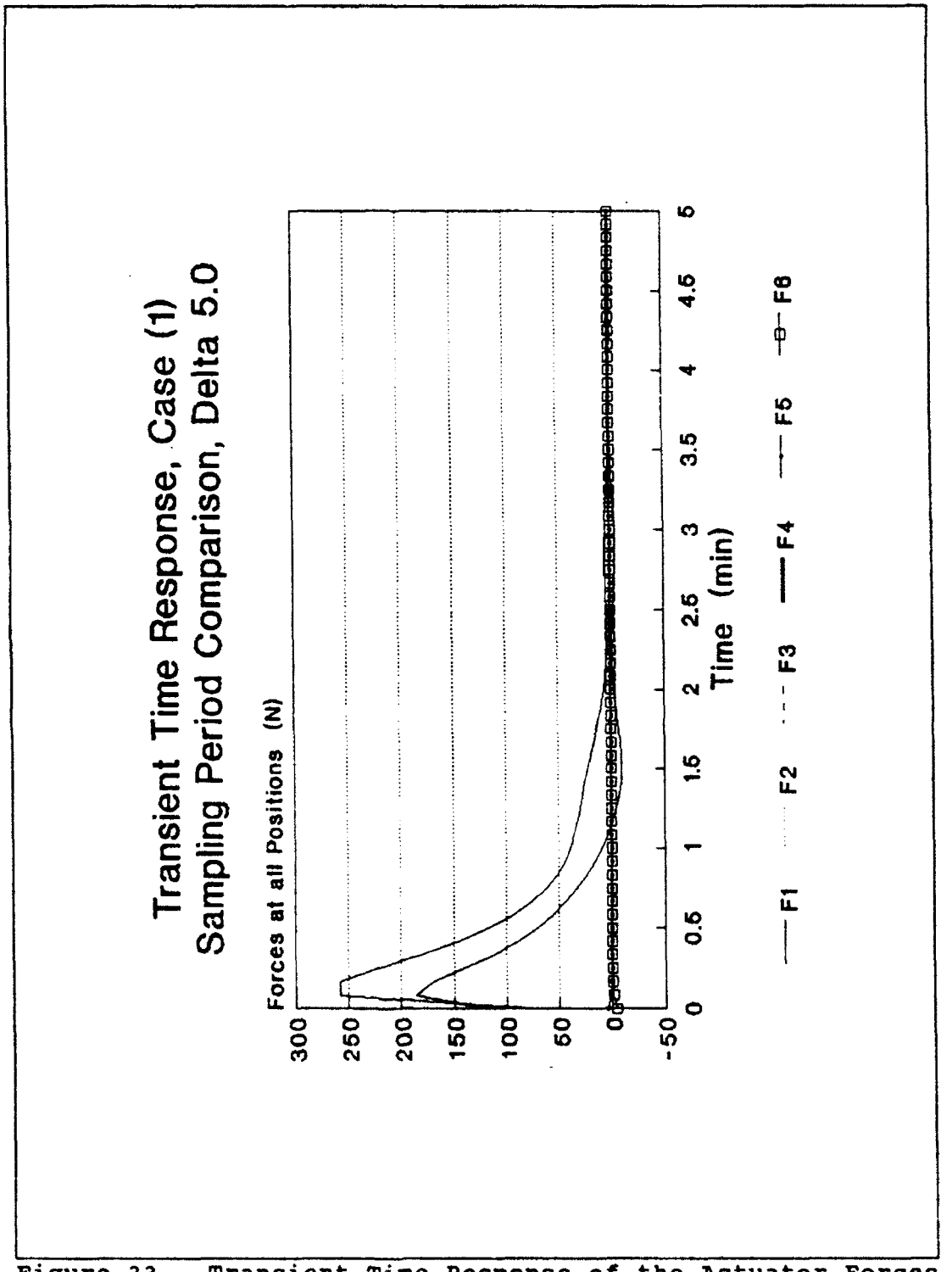

Figure 33. Transient Time Response of the Actuator Forces for Comparison of Sampling Period, 5.0 seconds

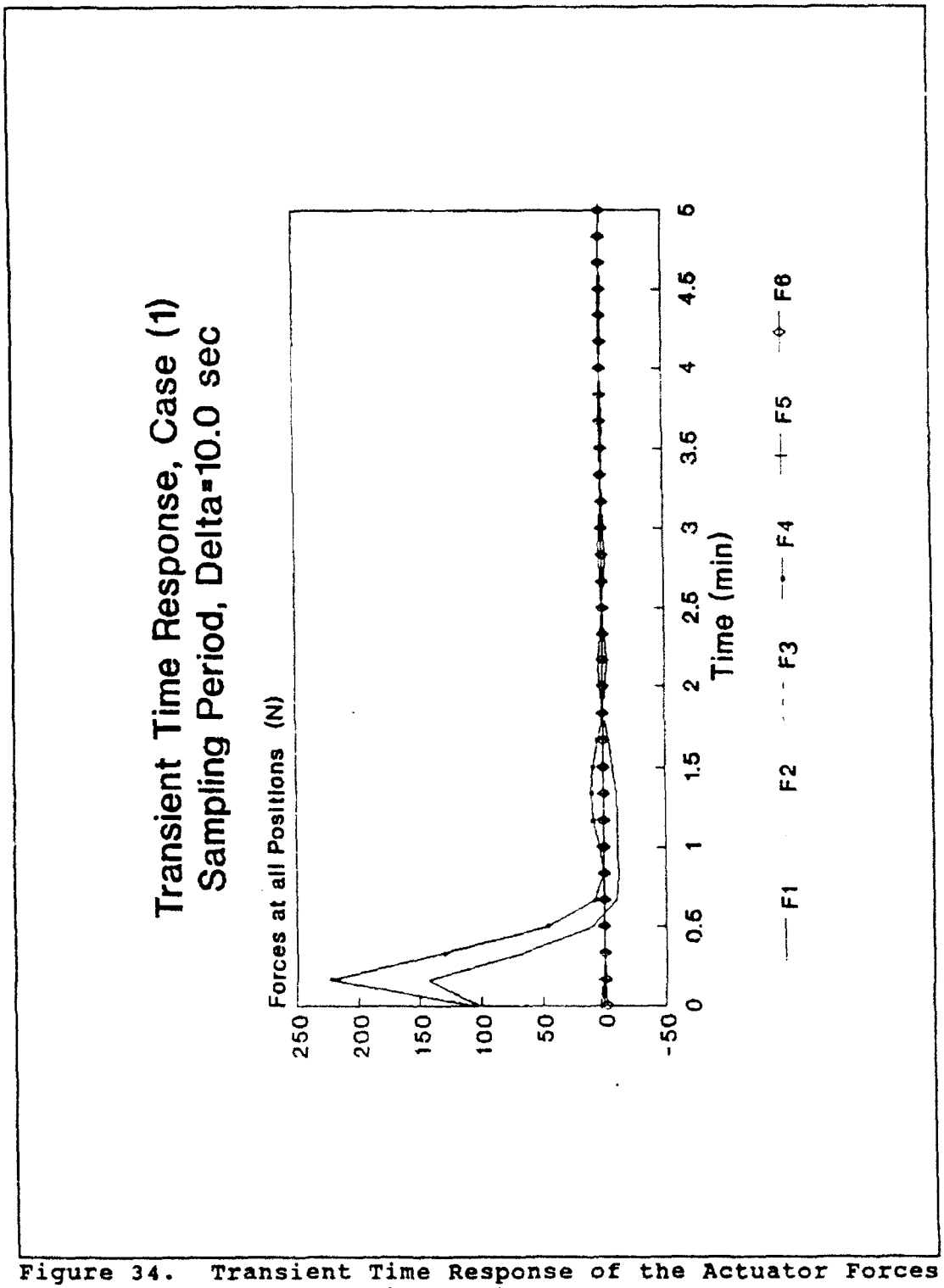

Figure 34. Transient Time Response of the Actuator Forces for Comparison of Sampling Period, 10.0 seconds

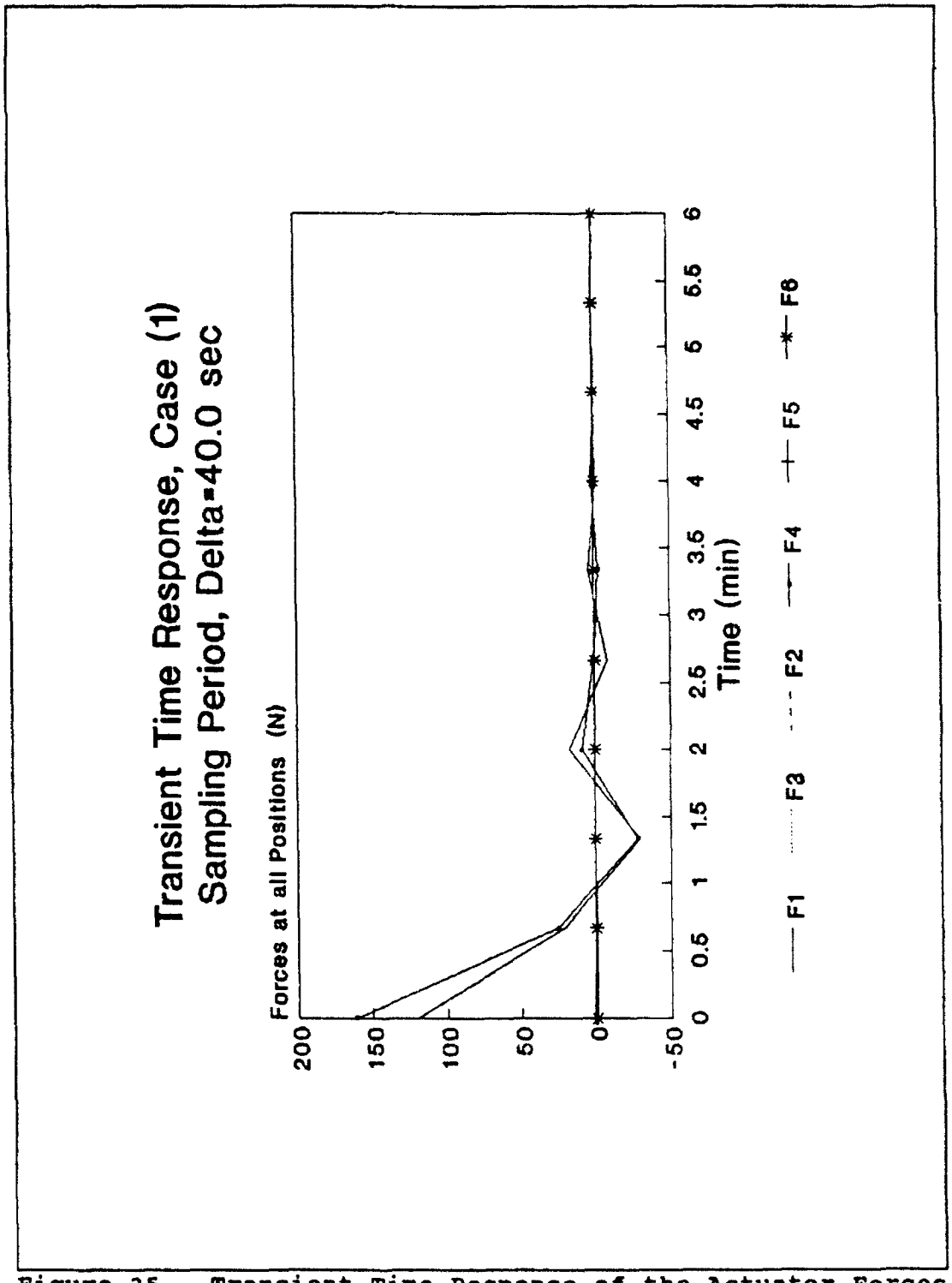

Figure 35. Transient Time Response of the Actuator Forces for Comparison of Sampling Period, 40.0 seconds

CHAPTER 7 - CONCLUSIONS

A mathematical model to predict the dynamics of a flexible orbiting platform was developed. Under the assumption that the linear system is completely observable, the optimal control laws are developed for the case where the observational data is collected on a sampled basis, i.e., a discrete time data system.

Attitude and shape control of the platform was assumed to be provided by the placement of point thrust actuators perpendicular to the main surface and the edge of the plate. Their effects on the system's motion were modeled to the first order. Controllability for the system was verified for two sets of actuator locations. An application of the linear quadratic regulator (LQR) technique in a discrete-time domain yields the optimum control law feedback gains.

A comparison of the performance of the different sets of actuator locations resulted in the best choice of actuator positioning. Two parametric studies were conducted to show the effect of varying the state penalty matrix and the control penalty matrix, and the effect of changing the sampling period on the transient performance of the system.

Generally, when comparing all of the system

characteristics, one must search for the system with the maximum number of positive characteristics. Unfortunately, it is not always a clear cut decision as to which combination of characteristics designate the best system. Often a system may exhibit some value tradeoffs, it may possess several minimum values along with several maximum values. In this thesis particular emphasis is placed on the quality of the transient response. With this in mind the following conclusions have been made.

When deciding upon the best placement of the actuators on the main surface, two items should be kept in mind. The first is that the actuators should be placed such that there is the maximum distance between the origin and the actuator locations. This creates a maximum torque arm which reduces the maximum force needed to control the system's rigid body motions. The second is that the actuators should be placed as far away as possible from the nodal lines of the fundamental and lower frequency elastic modes (with which most of the elastic energy is associated).

For the determination of the best choice of the penalty matrices, one usually chooses a large state penalty matrix and a small control penalty matrix within the limits of control saturation levels. These matrices should be chosen such that they optimize the performance index and produce

the best transient time response.

Since the sampling period is directly related to discretization and the signal reconstruction of the system, careful consideration should be given to its choice. Initially, when deciding upon a sampling period, one should take into consideration the sampling period theorem which involves the use of the open-loop system eigenvalues to calculate the unacceptable sampling periods for which the system is not controllable. Any sampling period values near the values of the unacceptable periods should not be utilized, for they can lead to system performance degradation. The sampling period should be chosen such that the sampling period is not too small to avoid excessive handling and accumulation of data for the onboard computer system. On the other hand, the sampling period should not be too large, otherwise the system's transient time response will appear choppy, thus, failing to provide a good example of signal reconstruction.

CHAPTER 8 - SUGGESTIONS

In terms of new actuator positioning, different locations for the actuators placed on the edge of the plate should be investigated. In addition, the number of actuators could be varied, in an effort to improve system performance. There are some system tradeoffs to consider in the event that the number of actuators is increased or decreased. If the number of actuators are decreased there may be some loss in system controllability and robustness. On the other hand, if the number of actuators are increased, the system's total mass will then be increased, thus, creating an increase in the system's operational costs.

One other possible improvement to actuator modeling would be incorporation of lumped masses to represent the actuator mass at its particular location. Implementation of GTSTRUDL or similar finite element methods for the recalculation of modal frequency and deflections could than be performed.

When considering possible improvements in the choice of penalty matrices, a more indepth comparison should be performed. The split weighting penalty matrix approach could be applied, with a possible variance of each individual matrix element. This could result in a smaller optimum cost

function.

For this thesis the system considered was assumed to be completely observable and deterministic, it is an inadequate assumption. To improve system modeling the observer matrix should be developed and the system should be considered stochastic (i.e., experience external disturbances and/or noise). The linear quadratic Gaussian (LQG) technique can be applied to provide the control law and estimator for a stochastic system with a Kalman filter to act as a screen.

One last improvement to the system corresponds to the initial assumptions about the material properties of composite graphite. For this thesis the material is assumed to be isotropic. This is an questionable assumption for reinforced composite graphite. Generally, the material is composed of graphite fibers bonded by a resin epoxy. Even if the fibers were aligned with a 90°, 0°, or 45° orientation, the material at best can be assumed to be orthotropic.[35] The system's various material constants would then need to be redefined. These material properties affect the stress-strain relationship of Eqn. (125) and create cross terms in the plate vibrational equation, thus affecting the values of the natural frequency. The new values for Young's Modulus, Poisson's ratio, and/or Shear Modulus, (i.e., E_x, E_y, E_z, ν_{xy}, etc.) could then be submitted to GTSTRUDL for recalculation

of the modal frequencies and deflections.

The results of the present study could then be compared to the previous LQG results with the thin flat plate and the shallow spherical shell for corresponding actuator positions.[26,17]

Appendix A - The Elements of the Stiffness Matrix [K], for 'BPR' Element

For a thin rectangular plate element with the dimensions axbxh, the stiffness matrix $[K]^e$, can be represented as

$$[K]^{(e)} = \frac{D}{15ab}[k]^{(e)} \quad \textbf{(A.1)}$$

where, a and b represents the length of the side, 100.0 m; h represents the thickness, 0.01 m; and the values of the elements of [k] are shown below.

$$D = \frac{Eh^3}{12(1-\nu^2)} = 25,256.41 \quad \textbf{(A.2)}$$

where, υ represents the Poisson's ratio, 0.3; and a/b=r=1.

Elements of [k]

$$k_{11} = 20a^2 + 4b^2(1-\nu) = 2.28x10^5$$
$$k_{21} = -15ab = -1.5x10^5$$
$$k_{22} = 20b^2 + 4a^2(1-\nu) = 2.28x10^5$$
$$k_{31} = -30ar - 15b\nu - 3b(1-\nu) = -3,660$$
$$k_{32} = 30b/r + 15a\nu + 3a(1-\nu) = 3,660$$
$$k_{33} = 60/r^2 + 60r^2 + 30\nu + 42(1-\nu) = 158.4$$
$$k_{41} = 10a^2 - b^2(1-\nu) = 9.3x10^4$$
$$k_{42} = k_{51} = k_{72} = k_{\square} = k_{81} = k_{84} = 0$$
$$k_{43} = -30b^2 - 3b(1-\nu) = 300,210$$
$$k_{44} = 20a^2 + 4b^2(1-\nu) = 2.28x10^5$$
$$k_{52} = 10b^2 - 4b^2(1-\nu) = 7.2x10^4$$
$$k_{53} = 15b/r - 15a\nu - 3a(1-\nu) = 840$$
$$k_{54} = 15ab\nu = 4.5x10^4$$
$$k_{55} = 20b^2 + 4a^2(1-\nu) = 2.28x10^5$$

Elements of [k] continued:

$$k_{61} = 30ar + 3b(1-\nu) = 3,210$$
$$k_{62} = 15b/r - 15a\nu + 3a(1-\nu) = 840$$
$$k_{63} = 30/r^2 - 60r^2 - 30\nu + 42(1-\nu) = -68.4$$
$$k_{64} = 30ar - 15b\nu + 3b(1-\nu) = 2,760$$
$$k_{65} = 30b/r + 15a\nu + 3a(1-\nu) = 3,660$$
$$k_{66} = 60/r^2 + 60r^2 + 30\nu + 42(1-\nu) = 158.4$$
$$k_{71} = 10a^2 - 4b^2(1-\nu) = 7.2x10^4$$
$$k_{73} = -15ra + 15b\nu + 3b(1-\nu) = -840$$
$$k_{74} = 5a^2 + b^2(1-\nu) = 5.3x10^4$$
$$k_{76} = 15ar - 3b(1-\nu) = 1,290$$
$$k_{77} = 20a^2 + 4b^2(1-\nu) = 2.28x10^5$$
$$k_{82} = 10b^2 - a^2(1-\nu) = 9.3x10^4$$
$$k_{83} = 30b/r - 3a(1-\nu) = -3,210$$
$$k_{85} = 5b^2 + a^2(1-\nu) = 5.7x10^4$$
$$k_{86} = 15b/r - 3a(1-\nu) = 1,290$$
$$k_{87} = 15ab = 1.5x10^5$$
$$k_{88} = 20b^2 + 4a^2(1-\nu) = 2.28x10^5$$
$$k_{91} = -15ar + 15b\nu - 3b(1-\nu) = -840$$
$$k_{92} = -30b/r - 3a(1-\nu) = -3,210$$
$$k_{93} = 60/r^2 + 30r^2 - 30\nu - 42(1-\nu) = 51.6$$
$$k_{94} = -15a/r + 3b(1-\nu) = -1,290$$
$$k_{95} = -15b/r - 15a\nu = -1,290$$
$$k_{96} = -30/r^2 - 30r^2 + 30\nu + 42(1-\nu) = -21.6$$
$$k_{97} = -30ar - 15b\nu - 3b(1-\nu) = -3,660$$
$$k_{98} = -30b/r - 15a\nu - 3a(1-\nu) = -3,660$$
$$k_{99} = 15b/r - 15a\nu - 3a(1-\nu) = 840$$

Elements of [k] continued:

$$k_{10,1} = 5a^2 + b^2(1-\nu) = 5.7x10^4$$
$$k_{10,3} = -15ar + 3b(1-\nu) = 1,290$$
$$k_{10,4} = 10a^2 - 4b^2(1-\nu) = 7.2x10^4$$
$$k_{10,6} = 15ar - 15b\nu - 3b(1-\nu) = 840$$
$$k_{10,7} = 10a^2 - b^2(1-\nu) = 9.3x10^4$$
$$k_{10,9} = -30ar - 3b(1-\nu) = -3,210$$
$$k_{10,10} = 20a^2 + 4b^2(1-\nu) = 2.28x10^5$$
$$k_{10,2} = k_{10,5} = k_{10,8} = k_{11,1} = k_{11,4} = k_{11,7} = 0$$
$$k_{11,2} = 5b^2 + a^2(1-\nu) = 5.7x10^4$$
$$k_{11,3} = 15b/r^2 - 3a(1-\nu) = 1,290$$
$$k_{11,5} = 10b^2 - a^2(1-\nu) = 9.3x10^4$$
$$k_{11,6} = 30b/r + 15a\nu + 3a(1-\nu) = 3,660$$
$$k_{11,8} = 10b^2 - 4a^2(1-\nu) = 7.2x10^4$$
$$k_{11,9} = -15b/r + 15a\nu + 3a(1-\nu) = -840$$
$$k_{11,10} = -15ab\nu = -1.5x10^5$$
$$k_{11,11} = 20b^2 + 4a^2(1-\nu) = 2.28x10^5$$
$$k_{12,1} = 15a/r - 3b(1-\nu) = 1,290$$
$$k_{12,2} = -15b/r + 3a(1-\nu) = -1,260$$
$$k_{12,3} = -30/r^2 - 30r^2 + 30\nu + 42(1-\nu) = -21.6$$
$$k_{12,4} = 15ar - 15b\nu + 3a(1-\nu) = 840$$
$$k_{12,5} = -30b/r - 3a(1-\nu) = -3,210$$
$$k_{12,6} = 60/r^2 + 30r^2 - 30\nu - 42(1-\nu) = 51.6$$
$$k_{12,7} = 30ar + 3b(1-\nu) = 3,210$$
$$k_{12,8} = -15b/r + 15a\nu - 3a(1-\nu) = -840$$
$$k_{12,9} = 30/r^2 - 30r^2 - 30\nu - 42(1-\nu) = -38.4$$
$$k_{12,10} = 30ar + 15b\nu + 3b(1-\nu) = 3,660$$
$$k_{12,11} = -30b/r - 15a\nu - 3a(1-\nu) = -3,660$$
$$k_{12,12} = 15b/r - 15a\nu - 3a(1-\nu) = 840$$

Appendix B - GTSTRUDL Program and a Summary of the Implemented Commands for the Calculation of Modal Frequencies and Shape Patterns

Because the model being considered is a free-free structure, GTSTRUDL recognizes the generated stiffness matrix as a representation of an unstable structure. Consequently, it will not formulate a complete dynamic modal analysis. For a calculation of the modal frequency values, the command, 'COMPUTE RIGID BODY MODES', must be implemented. Since the rigid body modes must be computed, this eliminates using the eigenproblem solver, 'SUBSPACE ITERATION', for it can not calculate those modes. There are two other eigenproblem solution methods available: 'TRIADIAGONALIZATION' and 'GTLANCZOS'. Triadiagonalization can not make the correct calculations, because it incorporates the Inverse Iteration method, which inverts the matrix resulting in problems with singularity. Therefore, for the solution of the eigenvalues the GTLANCZOS method must be used; it uses the Lanczos eigenvalue solver method.

The eigenvalues are obtained by using two GTSTRUDL commands, 'PERFORM EIGEN ANALYSIS' and 'LIST EIGENVALUES'. The final values for the frequencies are approximated graphically. By using the 'LIST EIGENVECTORS' command the eigenvectors can be computed. This gives the normalized

deflections at each node. The modal shape patterns are acquired through the combination of the 'LIST EIGENVECTORS' and 'PLOT PLANE MODE SHAPE #XZ PROJECTION' commands. The second command plots a diagram of the normalized deflections of the XZ plane. The YZ plane was another plane orientation viewed; for this orientation the Z axis is perpendicular to the major surface. Table 3 represents the modal shape patterns derived from GTSTRUDL.

In addition to the previous commands, there are some others that check the performance criteria and calculation values: 'ORTHOGONALITY', 'STURM SEQUENCE', and 'ERROR ESTIMATE'. The ORTHOGONALITY check has been previously mentioned in Section 3.4.5. The STURM SEQUENCE check determines whether the correct number of modes are within a specified range. This calculation requires the decomposition of a matrix that has an order and banding equal to the system stiffness matrix. Since the stiffness matrix for this system is very large, it was assumed this check would need too much memory space and could not be afforded. Similarly, was the situation with the ERROR ESTIMATE process. This command computes an error for each mode as follows:

$$\varepsilon_i = \frac{|[K]\{\Phi_i\} - \omega_i^2[M]\{\Phi_i\}|}{|[K]\{\Phi_i\}|} \quad \text{(B.1)}$$

The ERROR ESTIMATE command compares this calculate value, ε_i, to the set 'TOLERANCE' value -default of 1.0×10^{-6}- to determine whether the percentage of error is within a reasonable range. For most situations the default value is appropriate, but may be changed; this may have a major effect on solution time.

Appendix C - The System Matrices for the Nominal Orientations of Case (2) and Case (3)

Case (2) - Ix=Iy=Iz/2

State Matrix, [A]:

$$[A]_2 = \begin{bmatrix} . & . & [0]_{6x6} & . & . & . & . & [I]_{6x6} & & \\ 0 & 0 & 0 & 0 & 0 & 0 & 0 & 1 & 0 \ldots & 0 \\ 0 & 1 & 0 & 0 & 0 & 0 & -2 & 0 & \ldots . & 0 \\ 0 & 0 & -3 & 0 & 0 & 0 & 0 & \vdots & \ddots . & \vdots \\ 0 & 0 & 0 & -2402 & 0 & 0 & \vdots & 0 & . . & 0 \\ 0 & 0 & 0 & 0 & -4919.5 & 0 & \vdots & \vdots & . . & \vdots \\ 0 & 0 & 0 & 0 & 0 & -7667 & 0 & 0 & \ldots . & 0 \end{bmatrix} \quad \text{(C.1)}$$

Control Effort Matrix, [B](U):

$$[B]\{U\}_{2,A} = \begin{bmatrix} .1605 & -.321 & -.1605 & .321 & 0 & 0 \\ .321 & .1605 & -.321 & -.1605 & 0 & 0 \\ 0 & 0 & 0 & 0 & -.1605 & .1605 \\ -.2221 & .2221 & -.2221 & .2221 & 0 & 0 \\ -.189 & .189 & -.189 & .189 & 0 & 0 \\ .1842 & .1842 & .1842 & .1842 & 0 & 0 \end{bmatrix} \begin{Bmatrix} f_{1_x} \\ f_{2_x} \\ f_{3_x} \\ f_{4_x} \\ f_{5_x} \\ f_{6_x} \end{Bmatrix} \quad \text{(C.2)}$$

$$[B]\{U\}_{2,A'} = \begin{bmatrix} .1605 & -.214 & -.1605 & .214 & 0 & 0 \\ .214 & .1605 & -.214 & -.1605 & 0 & 0 \\ 0 & 0 & 0 & 0 & -.1605 & .1605 \\ -.1545 & .1545 & -.1545 & .1545 & 0 & 0 \\ -.05556 & .05556 & -.05556 & .05556 & 0 & 0 \\ .0306 & .0306 & .0306 & .0306 & 0 & 0 \end{bmatrix} \begin{Bmatrix} f_{1_x} \\ f_{2_x} \\ f_{3_x} \\ f_{4_x} \\ f_{5_x} \\ f_{6_x} \end{Bmatrix} \quad \text{(C.3)}$$

Case (3) - Ix=Iz=Iy/2

State Matrix, [A]:

$$[A]_3 = \begin{bmatrix} . & . & [0]_{6x6} & . & . & . & . & [I]_{6x6} & & \\ -4 & 0 & 0 & 0 & 0 & 0 & 0 & \cdots & 0 \cdots & 0 \\ 0 & -1 & 0 & 0 & 0 & 0 & \vdots & 0 & \cdots \; . & 0 \\ 0 & 0 & 0 & 0 & 0 & 0 & 0 & \vdots & \ddots \; . & \vdots \\ 0 & 0 & 0 & -2401 & 0 & 0 & \vdots & 0 & . \; . & 0 \\ 0 & 0 & 0 & 0 & -4948.5 & 0 & \vdots & \vdots & . \; . & \vdots \\ 0 & 0 & 0 & 0 & 0 & -7666 & 0 & 0 & \cdots \; . & 0 \end{bmatrix} \quad \text{(C.4)}$$

Control Effort Matrix, [B](U):

$$[B]\{U\}_{3,A} = \begin{bmatrix} .1605 & -.321 & -.1605 & .321 & 0 & 0 \\ 0 & 0 & 0 & 0 & -.1605 & .1605 \\ -.321 & -.1605 & .321 & .1605 & 0 & 0 \\ -.2221 & .2221 & -.2221 & .2221 & 0 & 0 \\ -.189 & .189 & -.189 & .189 & 0 & 0 \\ .1842 & .1842 & .1842 & .1842 & 0 & 0 \end{bmatrix} \begin{Bmatrix} f_{1_x} \\ f_{2_x} \\ f_{3_x} \\ f_{4_x} \\ f_{5_x} \\ f_{6_x} \end{Bmatrix} \quad \text{(C.5)}$$

$$[B]\{U\}_{3,A'} = \begin{bmatrix} .1605 & -.214 & -.1605 & .214 & 0 & 0 \\ 0 & 0 & 0 & 0 & -.1605 & .1605 \\ -.214 & -.1605 & .214 & .1605 & 0 & 0 \\ -.1545 & .1545 & -.1545 & .1545 & 0 & 0 \\ -.05556 & .05556 & -.05556 & .05556 & 0 & 0 \\ .0306 & .0306 & .0306 & .0306 & 0 & 0 \end{bmatrix} \begin{Bmatrix} f_{1_x} \\ f_{2_x} \\ f_{3_x} \\ f_{4_x} \\ f_{5_x} \\ f_{6_x} \end{Bmatrix} \quad \text{(C.6)}$$

REFERENCES

1) Pioneering The Space Frontier - The Report of the National Commission on Space, Bantam Book, New York, N.Y., May 1986.
2) Cuneo, W.J., Jr., and Williams, D.P., III, "Space Platforms for NASA - Opportunity or Pitfall", Advances in the Astronautical Sciences, Space Shuttle: Dawn of an Era, American Astronautical Society, Vol.41, Part I, San Diego, CA, 1980, pp.118.
3) Bowman, R., "Large Platforms in Space - The Needs", Advances in the Astronautical Sciences, Space Shuttle: Dawn of an Era, American Astronautical Society, Vol.41, Part I, San Diego, CA, 1980, pp 111-124, AAS 79-263.
4) Zoller, L.K., and Brown, R.L., "Commercial Use of Materials Processing in Space", Advances in the Astronautical Sciences, Space Shuttle: Dawn of an Era, American Astronautical Society, Vol.41, Part I, San Diego, CA, 1980, pp 101-107, AAS 79-239.
5) Farrell, R.M., Rumuel, J.A., and Schilling, T.C., "Experiments for Dedicated Life Sciences Missions", Advances in the Astronautical Sciences, Space Shuttle: Dawn of an Era, American Astronautical Society, Vol.41, Part I, San Diego, CA 1980,pp 691-708, AAS 79-251.
6) Stamminger, R., "The Future in Commercial Satellite Communications", Advances in the Astronautical Sciences, Space Shuttle: Dawn of an Era, American Astronautical Society, Vol.41, Part I, San Diego, CA, 1980, pp 75-82, AAS 79-235.
7) Nangen, R.H., and Johnson, O.E., "Economic Aspects of Energy from Space", Abstract, Advances in the Astronautical Sciences Space Shuttle: Dawn of an Era, American Astronautical Society, Vol.41, Part I, San Diego, CA 1980, pp 83, AAS 79-236.
8) Kumar, V.K., "Attitude Dynamics and Stability of Large Flexible Structures in Orbit", Doctor of Philosophy Dissertation Submitted to the Faculty of the Graduate School of Howard University, Department of Mechanical Engineering, Washington, DC, September 1981.
9) Athans, M., and Falb, P.L., Optimal Control: An Introduction to the Theory and Its Applications, McGraw-Hill Book Co., New York, 1966.
10) Ogata, K., Discrete-Time Control Systems, Prentice Hall, Inc., New Jersey, 1987.
11) Santini, P., "Stability of Flexible Spacecrafts", Acta Astronautica, Vol.3, 1977, pp 685-713.
12) Bainum, P.M., and Kumar, V.K., "The Dynamics and Control of Large Flexible Space Structures", Part B: Development of Continuum Model and Computer Simulation, NASA Grant NSG-1414, 1978.
13) Bainum, P.M., James, P.K., Kumar, V.K., and Krishna, R., "The Dynamics and Control of Large Flexible Space

Structures -II", Part B: Model Development and Computer Simulation, NASA Grant NSG-1414, 1979.

14) Bainum, P.M., and Reddy, A.S.S.R., "Decoupling Control of a Long Flexible Beam in Orbit", AAS/AIAA Astrodynamics Specialist Conference, Provincetown, MA, June 25-27, 1979, AAS 79-158.

15) Bainum, P.M., and Kumar, V.K., "Dynamics of a Flexible Body in Orbit", AIAA Astrodynamics Conference, Palo Alto, CA, August 7-9, 1978, AAS 78-1418; also, Journal of Guidance and Control, Vol. 3, No. 1, January-February 1980, 90-92.

16) Bainum, P.M., and Reddy, A.S.S.R., "On the Controllability of a Long Flexible Beam in Orbit", pp 145-160.

17) Xing, G.Q., and Bainum, P.M., "The Optimal Control of Orbiting Large Flexible Beams with Discrete-Time Observational Data and Random Measurement Noise", AAS/AIAA Astrodynamics Conference, Kalispell, MT, August 10-12, 1987, AAS 87-418, also, The Journal of Astronautical Sciences, Vol.37, No.1, January-March 1989, pp 59-79.

18) Reddy, A.S.S.R., Bainum, P.M., Krishna, R., and Hamer, H.A., "Control of Large Flexible Platform in Orbit", Journal of Guidance and Control, Vol.4, No.6, November-December 1981, pp 642-649.

19) Bainum, P.M., Reddy, A.S.S.R., Krishna, R., and James, P.K., "The Dynamics and Control of Large Flexible Space Structures -III", Final Report, NASA Grant NSG-1414, Suppl.2, Part A: Shape and Orientation Control of a Platform in Orbit Using Point Actuators, Howard University, June 1980.

20) "GTSTRUDL User's Manual", GTICES Systems Laboratory, Georgia Institute of Technology, Altanta, GA, Rev.J, April 1978.

21) Ericsson, A.J., "Determination of Frequencies and Mode Shapes for Thin Flexible Free-Free Plate Using GTSTRUDL", Unpublished Term Project Report for the Course CE234-513: 'Matrix Structural Analysis', Howard University, Deptartment of Civil Engineering, November, 1988.

22) Warburton, G.B., "Vibration of Rectangular Plates", Proceeds Institute of Mechanical Engineers, Vol.168, No.12, 1954, pp 371-394.

23) Warburton, G.B., "Response Using the Raleigh-Ritz Method", Earthquake Engineering and Structural Dynamics, Vol.7, 1979, pp 327-334.

24) Leissa, A.W., "Vibration of Plates", NASA SP-160, NASA, Washington, DC, 1969, pp 87-110.

25) Logcher, R.D., Connor, J.J., Jr., and Nelson, M.F., "ICES-STRUDL-II, Engineering Users Manual, Vol. 2", 2nd Edition, Massachusetts Institute of Technology, December 1973.

26) Tan, Z., and Bainum, P.M., "The Optimal LQG Digital Control of An Orbiting Large Flexible Platform", Offered for Presentation at the International Conference on Dynamics, Vibration and Control, Beijing, China, July 3-7, 1990.
27) Armstrong, E.S., "ORACLS- A System for Linear-Quadratic-Gaussian Control Law Design", NASA TP1106, April 1978.
28) Ashton, J.E., Halphin, J.C., and Petit, P.H., Primer on Composite Materials: Analysis, Technomic Publishing Co., Inc., Westport, CT, 1969.
29) Williams, D.G., and Alami, B., Thin Plate Design for In-Plane Loading, John-Wiley & Sons, New York, 1979.
30) Weaver, W., Jr., and Johnston, P.R., Finite Elements for Structural Analysis, Prentice-Hall, Inc., New Jersey, 1984.
31) Shames, I.H., and Dyn, C.L., Energy and Finite Element Methods in Structural Mechanics, Hemisphere Publishing Corp., New York, 1985.
32) Craig, R.R., Jr., Structural Dynamics, John Wiley & Sons, New York, 1981.
33) Friedland, B., Control System Design - An Introduction to State-Space Methods, McGraw-Hill Book Co., Inc., New York, 1986.
34) Hurty, W.C., and Rubenstein, M.F., Dynamics of Structures, Prentice-Hall, Inc., New Jersey, 1964.
35) Ogata, K., System Dynamics, Prentice-Hall, Inc., New Jersey, 1978.
36) Jones, R.M., Mechanics of Composite Materials, Scripta Book Co., Washington, DC, 1975.